

On the Spectral Evolution of Helium-Atmosphere White Dwarfs Showing Traces of Hydrogen

B. Rolland, P. Bergeron & G. Fontaine

*Département de Physique, Université de Montréal, C.P. 6128, Succ. Centre-Ville,
Montréal, Québec H3C 3J7, Canada*

rolland@astro.umontreal.ca, bergeron@astro.umontreal.ca,
fontaine@astro.umontreal.ca

ABSTRACT

We present a detailed spectroscopic analysis of 115 helium-line (DB) and 28 cool, He-rich hydrogen-line (DA) white dwarfs based on atmosphere fits to optical spectroscopy and photometry. We find that 63% of our DB population show hydrogen lines, making them DBA stars. We also demonstrate the persistence of pure DB white dwarfs with no detectable hydrogen feature at low effective temperatures. Using state-of-the-art envelope models, we next compute the total quantity of hydrogen, M_{H} , that is contained in the outer convection zone as a function of effective temperature and atmospheric H/He ratio. We find that some $(T_{\text{eff}}, M_{\text{H}})$ pairs cannot physically exist as a homogeneously mixed structure; such combination can only occur as stratified objects of the DA spectral type. On that basis, we show that the values of M_{H} inferred for the bulk of the DBA stars are too large and incompatible with the convective dilution scenario. We also present evidence that the hydrogen abundances measured in DBA and cool, helium-rich white dwarfs cannot be globally accounted for by any kind of accretion mechanism onto a pure DB star. We suggest that cool, He-rich DA white dwarfs are most likely created by the convective mixing of a DA star with a thin hydrogen envelope; they are not cooled down DBA's. We finally explore several scenarios that could account for the presence of hydrogen in DBA stars.

Subject headings: stars: abundances — stars: evolution — stars: fundamental parameters — white dwarfs

1. INTRODUCTION

The extreme chemical purity of white dwarf atmospheres can be attributed to the intense gravitational field present at the surface of these stars, causing all the heavy elements to

sink rapidly out of sight (Schatzman 1945). This gravitational settling process should thus produce white dwarf atmospheres that are completely dominated by hydrogen — or DA stars. However, it is well known that a significant fraction of the white dwarf population is hydrogen-deficient — e.g., PG 1159, DO, DB, DQ, DZ, and some DC stars (Wesemael et al. 1993) — and a very small fraction even have carbon-dominated atmospheres (Dufour et al. 2007b). More importantly, the relative number of white dwarfs of a given spectral type varies considerably as a function of effective temperature, indicating that there exist several physical mechanisms that compete with gravitational settling to alter the chemical composition of the outer layers of white dwarfs as they evolve along the cooling sequence. Such physical mechanisms include convective mixing, convective dredge-up from the core, accretion from the interstellar medium or circumstellar material, radiative levitation, and stellar winds. Understanding the so-called *spectral evolution of white dwarf stars* has always remained a fundamental topic of research in the white dwarf field, in particular with the large number of new discoveries in the Sloan Digital Sky Survey (SDSS; see, e.g., Kleinman et al. 2013).

Probably the most significant evidence for the spectral evolution of white dwarfs, discussed at length in Fontaine & Wesemael (1987), is the existence of a “DB-gap”, a range in effective temperature between $T_{\text{eff}} \sim 30,000$ K and 45,000 K where only DA stars are found, while helium-atmosphere white dwarfs exist both above (the DO stars) and below (the DB stars) the gap. One model proposed by Fontaine & Wesemael to account for this gap starts with hot white dwarf progenitors with hydrogen-deficient atmospheres (PG 1159 or DO stars) containing only minute amounts of hydrogen thoroughly diluted within the stellar envelope. As these stars cool off, hydrogen would gradually float up to the surface, thus building an atmosphere enriched with hydrogen. The fact that all white dwarfs turn into DA stars by the time they reach $T_{\text{eff}} \sim 45,000$ K imposes a lower limit on the total amount of hydrogen present in the hot progenitors, of the order of $M_{\text{H}} \sim 10^{-16} M_{\odot}$. Hybrid white dwarfs with thinner hydrogen layers floating in diffusive equilibrium on top of the helium envelope would appear as DAO stars, bearing the signature of chemically stratified atmospheres (see Manseau et al. 2016 and references therein).

Below the red edge of the gap ($T_{\text{eff}} \lesssim 30,000$ K), the reappearance in large numbers of helium-atmosphere white dwarfs — DB stars in this case — has been interpreted in terms of the dilution of a thin, superficial hydrogen *radiative* layer ($M_{\text{H}} \sim 10^{-15} M_{\odot}$) by the underlying and more massive convective helium envelope (Fontaine & Wesemael 1987). In this paper, we refer to this mechanism as the *convective dilution scenario* (see also MacDonald & Vennes 1991). Even though the large number of white dwarfs discovered in the SDSS has unveiled the existence of many hot DB stars in the gap, the fraction of DB white dwarfs within the gap remains significantly lower than that found at lower temperatures, and we are thus dealing with a DB deficiency rather than a true gap. Nevertheless, the

float-up model and convective dilution scenario discussed above must occur for a significant fraction of white dwarfs, perhaps of the order of $\sim 20\%$ (Bergeron et al. 2011).

Another important signature of the spectral evolution of white dwarfs, also discussed in Fontaine & Wesemael (1987), is the spectacular increase in the ratio of non-DA to DA stars below $T_{\text{eff}} \sim 10,000$ K, which jumps from a value around 25% above this temperature to a value near unity below it. This sudden increase in the number of non-DA stars (i.e., DQ, DZ, DC) in this temperature range has been interpreted as the result of the mixing of the superficial *convective* hydrogen layer with the deeper and much more massive convective helium envelope (Koester 1976; Vauclair & Reisse 1977; Dantona & Mazzitelli 1979). We will refer to this mechanism as the *convective mixing scenario*, as opposed to the *convective dilution scenario* discussed above, in which the hydrogen superficial layer is purely radiative.

One way to further our understanding of the spectral evolution of helium-atmosphere white dwarfs below $T_{\text{eff}} \sim 30,000$ K is to determine the hydrogen abundance in these stars, often present as a trace element, and to study the hydrogen abundance pattern as a function of effective temperature. Indeed, a large fraction of DB white dwarfs shows traces of hydrogen — the DBA stars — if observed at sufficiently high signal-to-noise ratio (S/N). Koester & Kepler (2015) even suggested, based on their analysis of the DB stars in the DR10 and DR12 of the SDSS, that perhaps *all* DB white dwarfs would show hydrogen if the resolution and S/N were high enough. The origin of hydrogen in DBA stars has remained a mystery, and the subject of controversy as well. While it seems reasonable to assume that the presence of hydrogen in these stars has a residual origin — the leftovers from the convective dilution scenario discussed above — the total mass of hydrogen inferred in those stars, which is homogeneously mixed in the convective stellar envelope, lies in the range $M_{\text{H}} = 10^{-13}$ to $10^{-10} M_{\odot}$ (Voss et al. 2007; Bergeron et al. 2011; Koester & Kepler 2015). The problem with these estimates is that DA progenitors with such thick hydrogen layers would easily survive the convective dilution process, and thus never turn into DB stars in the first place (MacDonald & Vennes 1991). The most common way around this problem is to assume that the DA progenitors have hydrogen layers thin enough (of the order of $M_{\text{H}} \sim 10^{-15} M_{\odot}$) to allow the DA-to-DB transition below $T_{\text{eff}} \sim 30,000$ K, and that significant amounts of hydrogen are then accreted onto the DB star from external sources such as the interstellar medium, disrupted asteroids, small planets, and even comets (MacDonald & Vennes 1991; Bergeron et al. 2011; Koester & Kepler 2015; Gentile Fusillo et al. 2017). These accretion scenarios can easily account for the observed hydrogen abundances in DBA stars, assuming reasonable accretion rates.

Also of key interest is the presence of hydrogen in much cooler ($T_{\text{eff}} \lesssim 10,000$ K) helium-atmosphere white dwarfs, the prototypes of which are the DZA stars L745-46A and

Ross 640 (see, e.g., Figure 14 of Giammichele et al. 2012), which show broad and shallow $H\alpha$ absorption features resulting from van der Waals broadening in a helium-dominated atmosphere. Traces of hydrogen have now been detected in many DZ stars from the SDSS (Dufour et al. 2007a). The origin of hydrogen in these objects, whether it has a residual origin — cooled off DBA stars or convectively mixed DA stars — or has been accreted from external bodies, remains an open question.

In this paper, we revisit the problem of the spectral evolution of helium-atmosphere white dwarfs below $T_{\text{eff}} \sim 30,000$ K, by studying the hydrogen abundance pattern in these stars as a function of effective temperature. We first present in Section 2 a detailed model atmosphere analysis of relatively bright DB and DBA white dwarfs, as well as cool He-rich DA stars drawn from the SDSS. In Section 3, we describe our stellar envelope models with stratified and homogeneous chemical compositions appropriate for these stars, which are then used in Section 4 to explore and test various scenarios that could account for the observed hydrogen abundance pattern, and discuss possible evolutionary channels that could produce DB, DBA, and cool He-rich DA and DZA stars. Our conclusions follow in Section 5.

2. HYDROGEN ABUNDANCE PATTERN IN HELIUM-ATMOSPHERE WHITE DWARFS

2.1. Hydrogen in DBA stars

2.1.1. Spectroscopic Observations

Our sample of bright, helium-line DB and DBA stars is based on an extension of the 108 DB white dwarfs analyzed in detail in Bergeron et al. (2011). In particular, high S/N spectra of 6 additional DB stars, selected from the electronic version of the Catalogue of Spectroscopically Identified White Dwarfs¹ (McCook & Sion 1999, hereafter WD Catalog), have been secured with the Steward Observatory 2.3 m Bok Telescope equipped with the Boller & Chivens spectrograph. The 4"5 slit together with the 600 line mm^{-1} grating blazed at 3568 Å in first order provides a spectral coverage from about 3500 to 5250 Å at a resolution of ~ 6 Å FWHM (see also Bergeron et al. 2015). Also included are 1919–362² from Subasavage et al. (2017), as well as the 4 new DB stars discovered by Limoges et al. (2015, see their Figure 15) in the course of their spectroscopic survey of the SUPERBLINK proper

¹<http://www.astronomy.villanova.edu/WDCatalog/index.html>

²We omit in the remainder of this paper the WD prefix for conciseness.

motion catalog. We also secured a new optical spectrum for PG 1654+160 using the same setup. These additional optical spectra are displayed in Figure 1 in order of decreasing effective temperature; the other blue spectra in our sample have already been displayed in Figure 5 of Bergeron et al. (2011). Note the particular strength of the hydrogen lines in PB 8252 (0025–032).

Because we are mostly interested here in studying the hydrogen abundance pattern in helium-atmosphere white dwarfs, we also improved the sample of DB stars from Bergeron et al. (2011) by acquiring 54 high signal-to-noise $H\alpha$ spectra missing from our original data set (see also Bergeron et al. 2015). These spectra have been obtained with the NOAO Mayall 4-m telescope; the adopted configuration allows a spectral coverage of $\lambda\lambda 3800\text{--}6700$, at an intermediate resolution of ~ 6 Å FWHM. These spectra are displayed in Figure 2. Note how the strength of $H\alpha$ varies considerably from object to object, and how it is particularly strong for PB 8252 (0025–032) and Lan 143 (0258+683). Hydrogen is now detected in 63% of the DB stars in our sample, a value somewhat lower than the estimated 75% fraction of DBA white dwarfs obtained by Koester & Kepler (2015) using their best spectra. Four objects in our sample still lack $H\alpha$ spectroscopic data — L715–34 (0308–565), BPM 17731 (0418–539), L151-81A (1454–630.1), and GD 27 (0220+480) — and these are excluded from our analysis for homogeneity purposes. Our final sample thus includes 115 DB white dwarfs, among which 73 are DBA stars.

A significant advantage of our extended sample is its homogeneity, both in terms of wavelength coverage and S/N. Even though its size is modest in comparison to the SDSS sample (Koester & Kepler 2015), the quality of our spectra is superior in terms of S/N. Indeed, because the exposure time of a given SDSS spectrum is constant for all targets on a given plate, the corresponding S/N is necessarily a function of the magnitude of the star, resulting in typical sensitivity between $S/N \sim 5$ and 20. In comparison, the majority of our spectra have S/N well above 50, with an average around 80.

2.1.2. Model Atmosphere Analysis

Our model atmospheres and synthetic spectra are identical to those described at length in Bergeron et al. (2011) and references therein. These models are built from the LTE model atmosphere code described in Tremblay & Bergeron (2009) and references therein, in which the improved Stark profiles of neutral helium of Beauchamp et al. (1997) have been incorporated. These detailed profiles of more than 20 neutral helium lines take into account the transition from the impact to the quasistatic regime for electrons, the transition from quadratic to linear Stark broadening, as well as forbidden components. We also include in the cooler

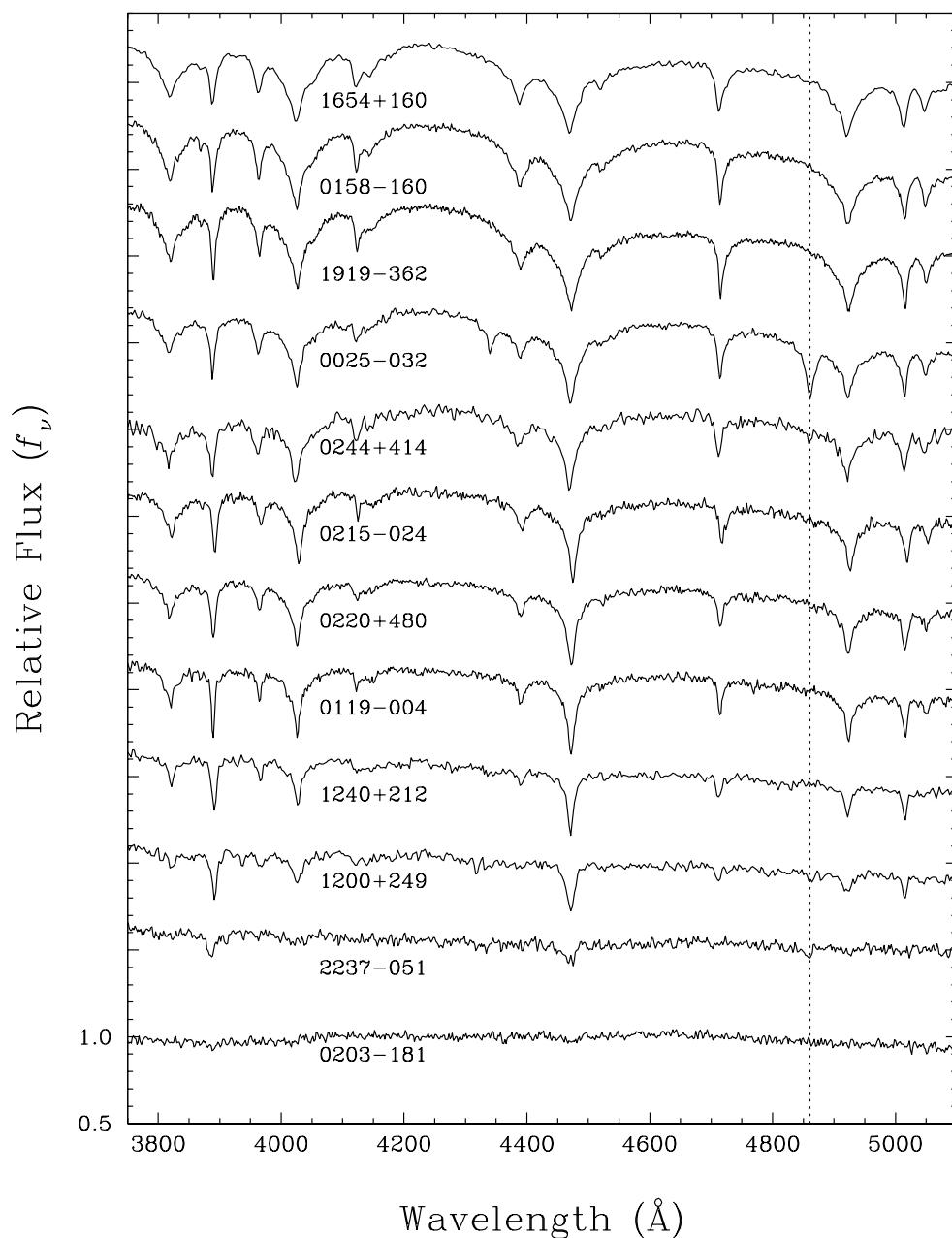


Fig. 1.— Optical (blue) spectra for the 11 new DB stars included in our extended sample, as well as a new spectrum for PG 1654+160; the remaining spectra used in our analysis are displayed in Figure 5 of Bergeron et al. (2011). The spectra are normalized at 4500 Å and shifted vertically from each other by a factor of 0.5 for clarity. The effective temperature decreases from top to bottom. The location of H β is shown by a dotted line.

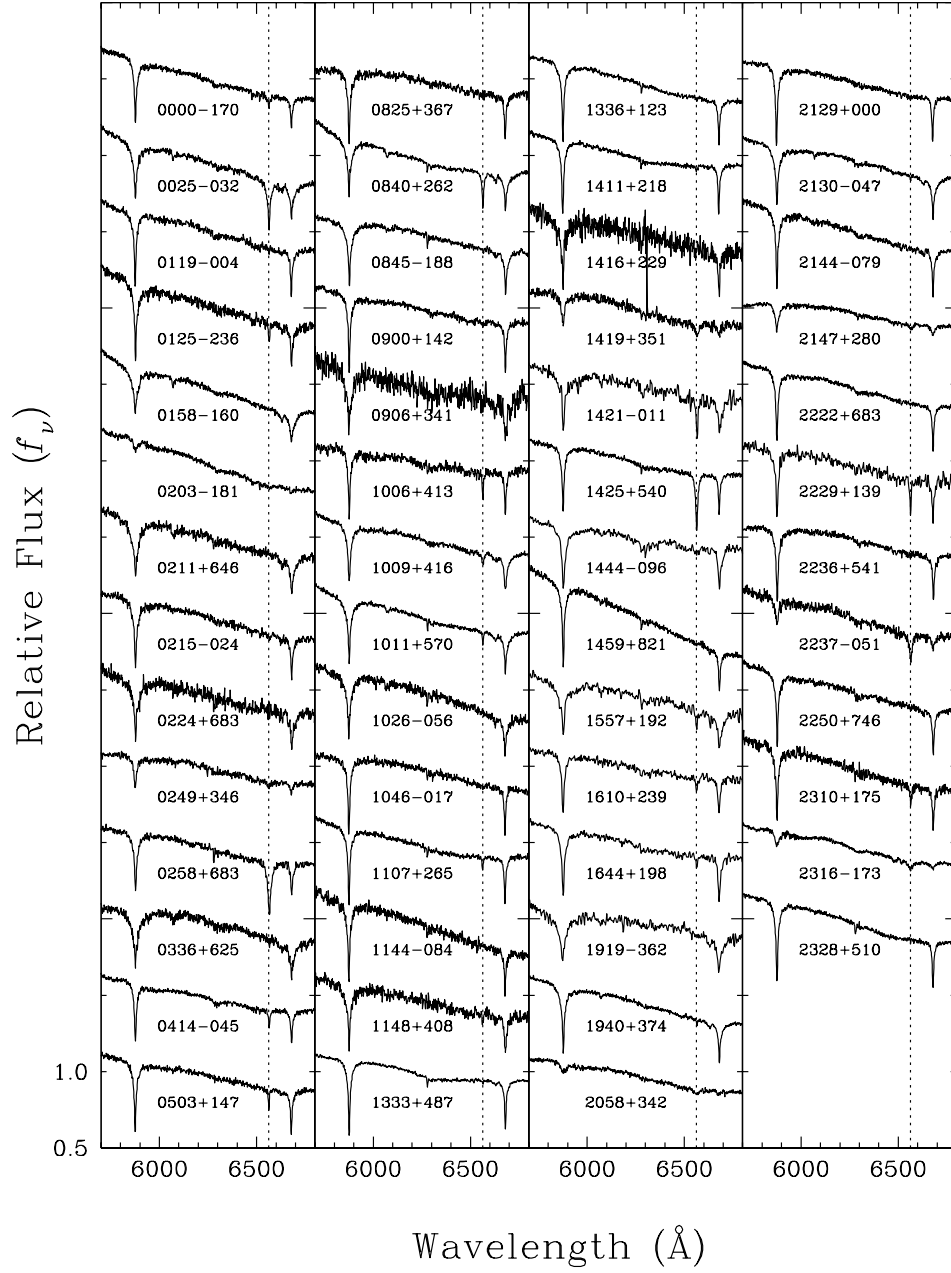


Fig. 2.— New spectra near the H α region for 54 DB and DBA stars in our extended sample, together with the DB star from Subasavage et al. (2017, 1919–362). The spectra are shown in order of right ascension, normalized at 6200 \AA , and shifted vertically from each other by a factor of 0.5 for clarity. The location of H α is shown by a dotted line.

models van der Waals broadening following the treatment of Deridder & van Renspergen (1976). For the treatment of the hydrogen lines, we rely on the improved calculations for Stark broadening of Tremblay & Bergeron (2009), as well as resonance broadening and non-resonant broadening for the Balmer lines in the cooler models, as also described in Tremblay & Bergeron. Convective energy transport is treated within the ML2 version of the mixing-length theory with a value of $\alpha = \ell/H$ — the ratio of the mixing length to the pressure scale height — set to 1.25, following the prescription of Bergeron et al. (2011). All hydrogen and helium level populations are computed using the occupation probability formalism of Hummer & Mihalas (1988), which is also included in the calculations of the corresponding bound-bound, bound-free, and pseudo-continuum opacities. Our model grid has been extended to the regime of cool, He-rich DA stars, and now covers a range of effective temperature between $T_{\text{eff}} = 40,000$ K and 6000 K by steps of 1000 K, while $\log g$ ranges from 7.0 to 9.0 by steps of 0.5 dex. In addition to pure helium models, we also calculated models with $\log \text{H}/\text{He} = -7.0$ to -1.5 by steps of 0.5. Illustrative spectra are displayed in Figure 1 of Bergeron et al. (2011) for various values of effective temperatures, surface gravities, and convective efficiencies, while we show in Figure 3 synthetic spectra at $\log g = 8$ for various effective temperatures — including our extension to low temperatures — and hydrogen-to-helium abundance ratios. Note that for the largest hydrogen abundance shown in this plot ($\text{H}/\text{He} = 10^{-2}$), the star would appear as a normal DB white dwarf at high effective temperatures, but as a pure DA star below $T_{\text{eff}} \sim 12,000$ K, when the helium lines vanish.

Because of the complexity and degeneracy of the atmospheric parameter space for DB stars, the values derived from various studies for T_{eff} , $\log g$, and H/He can differ significantly, as illustrated, for instance, by Voss et al. (2007, see their Figures 3 and 4) who compare the results of the SPY survey with those of independent studies (Beauchamp et al. 1999; Friedrich et al. 2000; Castanheira et al. 2006). One major reason for these discrepancies is the lack of sensitivity of the neutral helium lines to effective temperature in hotter DB stars. Indeed, for a given set of H/He , $\log g$, and α , the equivalent width of He I $\lambda 4471$ reaches a plateau between 20,000 K and 30,000 K (see Figure 2 of Bergeron et al. 2011); a similar behavior can be observed in our model spectra displayed in Figure 3. As a result, two solutions exist for a given DB star, one on each side of the maximum strength of He I $\lambda 4471$. As discussed by Bergeron et al. (2011), this degeneracy can be lifted with the use of spectroscopic observations at $\text{H}\alpha$, which add an additional constraint to the solution.

Our fitting procedure is similar to that described at length in Bergeron et al. (2011). Since in most cases our $\text{H}\alpha$ spectra are independent of our blue data, we first fit the blue spectrum with pure helium models to obtain an estimate of T_{eff} and $\log g$. The $\text{H}\alpha$ spectrum is then used to determine the hydrogen abundance — or upper limits on H/He — at these particular values of T_{eff} and $\log g$. The procedure is then repeated iteratively until an internal

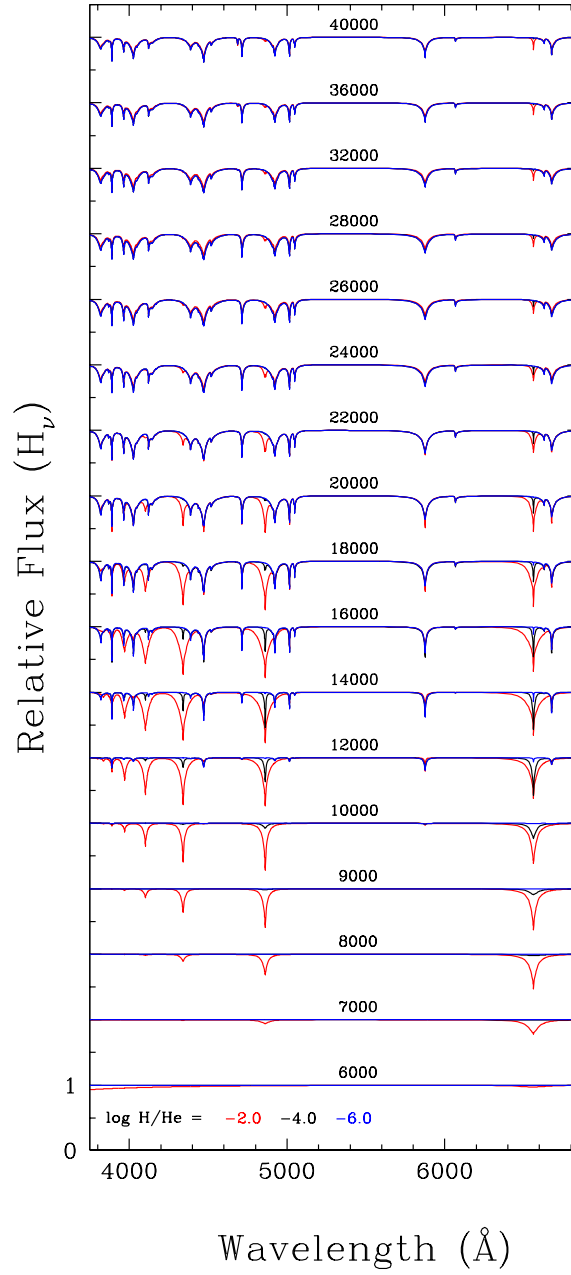


Fig. 3.— Synthetic spectra of homogeneous H/He models at $\log g = 8$ for various effective temperatures and hydrogen abundances of $\text{H}/\text{He} = 10^{-6}$ (blue), 10^{-4} (black), and 10^{-2} (red). All spectra are normalized to a continuum set to unity and offset from each other by a factor of 1.0 for clarity.

consistency is reached. An example of our solution for PB 8252 (0025–032, HE 0025–0317) — a new object added to the sample of Bergeron et al. (2011) — is displayed in Figure 4. The H α absorption feature shown in the inset serves as an important constraint on the hydrogen abundance. This fitting procedure is reliable when the H α absorption line is present in the optical spectrum. When no feature is visible, only upper limits on the hydrogen abundance can be determined. We adopt a detection limit of 200 mÅ for the equivalent widths of H α based on the S/N of our DB spectra. For high S/N spectra with no detectable hydrogen feature, the value of H/He is set to the appropriate upper limit for the corresponding temperature. In cases where the spectrum is noisier, however, our fitting procedure may find an upper limit to the hydrogen abundance that is larger than that inferred from this upper limit.

2.1.3. Selected Results

Because of the inclusion of additional objects and new H α spectroscopic data to our sample of bright DB stars, we present here an update of the relevant results from Bergeron et al. (2011). The atmospheric parameters for all 115 DB and DBA white dwarfs in our enlarged sample are provided in Table 1; pure DB stars in this table correspond to the objects where only an upper limit on the hydrogen abundance is given. For completeness, we also include the four objects listed in Section 2.1.1 that still lack H α data (these are noted in the table). For each star we give the stellar mass (M) and white dwarf cooling age ($\log \tau$) obtained from evolutionary models similar to those described in Fontaine et al. (2001) but with C/O cores, $q(\text{He}) \equiv M_{\text{He}}/M_{\star} = 10^{-2}$ and $q(\text{H}) = 10^{-10}$, which are representative of helium-atmosphere white dwarfs³. The absolute visual magnitude (M_V) and luminosity (L) are determined using the improved calibration of Holberg & Bergeron (2006), while the distance D is obtained by combining M_V with the magnitude V , also given in the table. Since the presence or not of hydrogen features is crucial to our understanding of the origin of DB stars, we provide as online material our spectroscopic fits for all white dwarfs in our sample, where the left panels show the blue portion of our spectroscopic fits, while the right panels show the corresponding region near H α .

The hydrogen abundances as a function of effective temperature for all DB stars in our sample, but with H α spectra available to us, are displayed in Figure 5. Also shown are the upper limits on the hydrogen abundance for DB stars, as determined from the absence of H α . In general, the pure DB stars are aligned on these observational limits but as discussed

³See <http://www.astro.umontreal.ca/~bergeron/CoolingModels>.

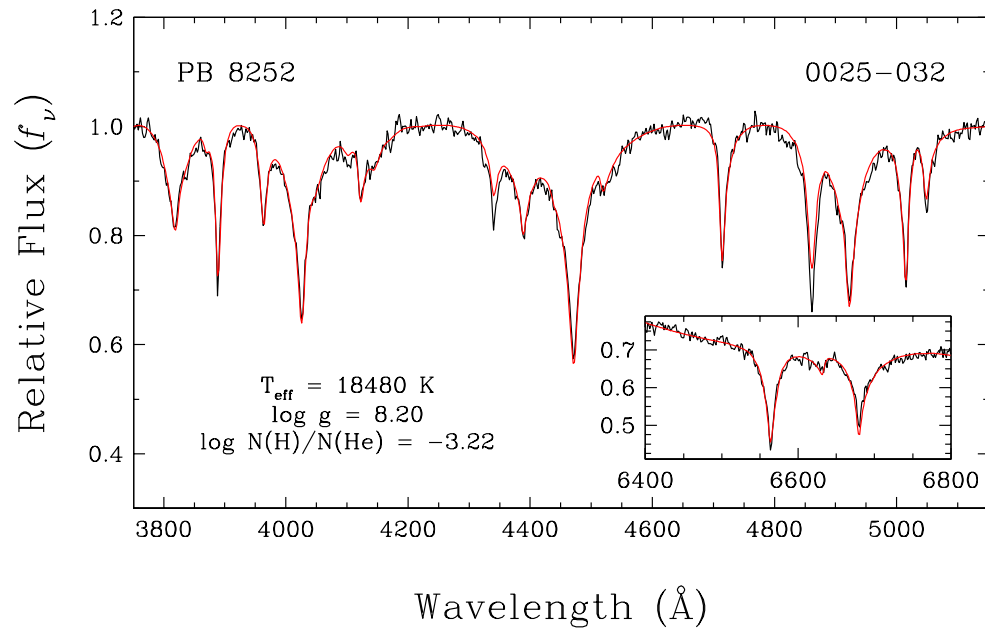


Fig. 4.— Example of a full spectroscopic fit where the H α line profile (inset) is used to measure, or constrain, the hydrogen abundance of the overall solution.

above, some objects have noisier data and these limits are simply not reached. The ratio of DBA stars to the total number of white dwarfs in our sample now reaches 63%, significantly higher than the value of 44% reported by Bergeron et al. (2011), thanks to our improved high S/N spectroscopic data at $H\alpha$, which revealed the presence of hydrogen in objects where $H\beta$ was spectroscopically invisible. This higher ratio now compares favorably well with the value of 75% reported by Koester & Kepler (2015) for the highest S/N DB spectra in the SDSS, although this ratio drops to a value of 32% in their overall sample. The results of Koester & Kepler for the DBA white dwarfs from the SDSS — i.e., with hydrogen features detected — are also reproduced in Figure 5. Although both sets of hydrogen abundance determinations overlap very nicely, the upper limits for the DB stars in our sample are about 1 dex smaller due to the much higher S/N of our observations compared to the SDSS spectra, as discussed above, thus putting more severe constraints on the amount of hydrogen present in the DB stars with no detectable $H\alpha$ feature.

The mass distribution as a function of effective temperature is shown in Figure 6 for the same white dwarfs as in Figure 5. These results are comparable to those displayed in Figure 21 of Bergeron et al. (2011), although all cool white dwarfs that appeared massive in their analysis now *all show hydrogen features*, while DB stars in our sample without detectable $H\alpha$ have normal masses. As discussed by Bergeron et al., the high masses inferred for these cool DBA stars can probably be attributed to some inaccurate treatment of van der Waals broadening in our models (Beauchamp et al. 1996). We can also see a definite trend for the bulk of white dwarfs in our sample to show higher masses ($\sim 0.7 M_{\odot}$) at low effective temperatures than at the hot end of the sample ($\lesssim 0.6 M_{\odot}$).

2.2. Hydrogen in cool, He-rich DA stars

2.2.1. Spectroscopic and Photometric Observations

Because we are interested in studying the hydrogen abundance pattern in all helium-atmosphere white dwarfs below $T_{\text{eff}} \sim 30,000$ K, we also need to extend our search to the cool end of the white dwarf sequence by including cool, helium-atmosphere DA and DZA stars such as L745-46A and Ross 640 discussed in the Introduction, which are usually found in the ~ 8000 – $12,000$ K temperature range. In general, the only hydrogen line visible in their spectra is $H\alpha$, which appears very broad and shallow as a result of van der Waals broadening. These He-rich DA white dwarfs can be easily distinguished from the much cooler ($T_{\text{eff}} \lesssim 6000$ K), hydrogen-atmosphere DA stars in which the $H\alpha$ absorption feature is much sharper (see, e.g., Figure 23 of Bergeron et al. 1997). The latter are also much redder photometrically.

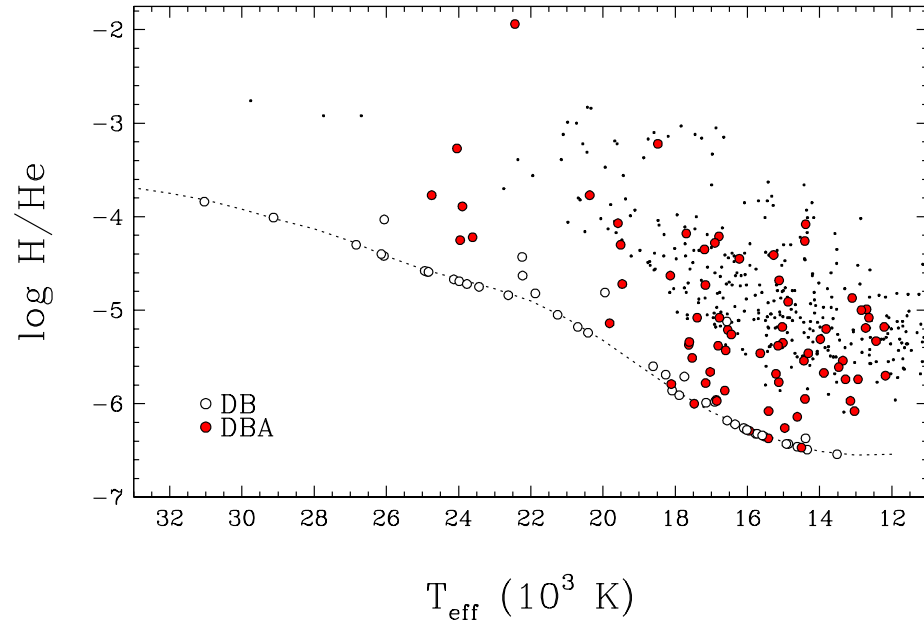


Fig. 5.— Hydrogen-to-helium abundance ratio as a function of effective temperature for all DB (white symbols) and DBA (red symbols) white dwarfs in our sample. Limits on the hydrogen abundance set by our spectroscopic observations at $H\alpha$ (200 mÅ equivalent width) are shown by the dotted line; the hydrogen abundances for DB stars thus represent only upper limits. Also shown as small dots are the results from Koester & Kepler (2015) for DBA white dwarfs (hydrogen detected) in the SDSS.

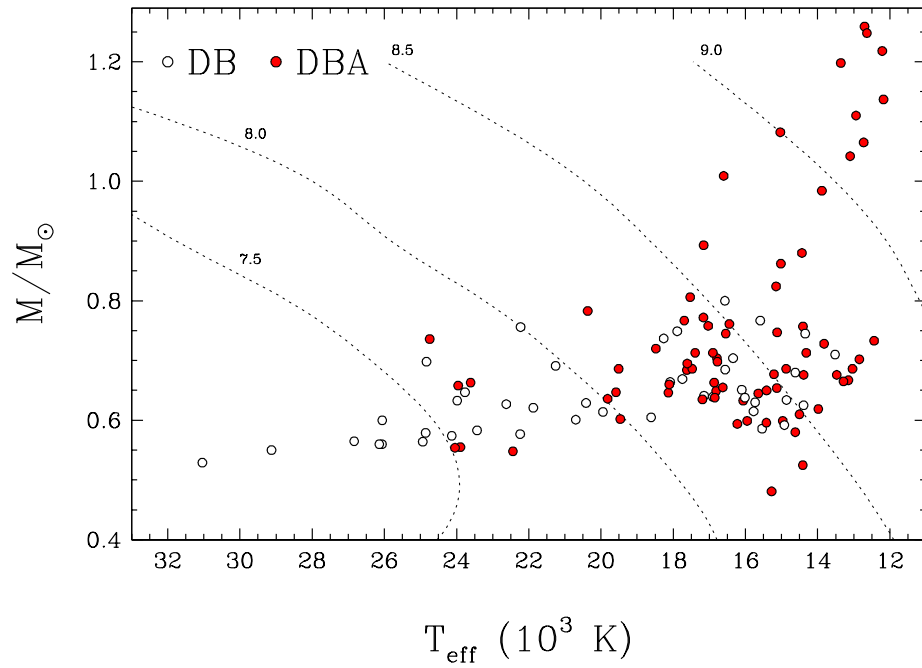


Fig. 6.— Distribution of mass as a function of effective temperature for the 42 DB (white symbols) and 73 DBA (red symbols) white dwarfs in our sample. Also shown as dotted lines are the theoretical isochrones from our evolutionary models, labeled as $\log \tau$ where τ is the white dwarf cooling age in years.

With this idea in mind, we searched the Data Release 7 from the SDSS catalog of Kleinman et al. (2013) with $(g-r) < 0.5$, $(u-g) < 0.8$, and a magnitude cut-off of $g < 19.5$, and retained 28 He-rich DA white dwarf candidates, previously identified by P. Dufour (private communication). This sample is not complete in any sense, but it is considered representative of the hydrogen abundance pattern in cool, helium-rich atmospheres. These cool, He-rich DA stars can be analyzed using a hybrid photometric and spectroscopic technique, described in the next section, which requires *ugriz* photometry as well as optical spectra in the region around $H\alpha$. The *ugriz* photometry for our 28 SDSS white dwarfs was taken from Kleinman et al. (2013) while the corresponding spectra were retrieved from the SDSS database; these cover the 4000–9200 Å wavelength range, with an average signal-to-noise ratio of $S/N \sim 15$.

2.2.2. Model Atmosphere Analysis

An examination of the theoretical spectra displayed in Figure 3 reveals that the number of hydrogen and helium absorption lines that can be detected in the optical spectra of cool ($T_{\text{eff}} \lesssim 12,000$ K), helium-dominated atmospheres becomes increasingly small. As a result, the spectroscopic technique alone fails to yield reliable measurements of the atmospheric parameters for such white dwarfs. In order to overcome this problem, we developed a hybrid approach that relies on both photometry and spectroscopy near the $H\alpha$ region (see also Giammichele et al. 2012). The first step is based on the photometric technique developed by Bergeron et al. (1997, 2001), where the observed magnitudes are converted into average fluxes and compared to the predictions of model atmosphere calculations. Briefly, every magnitude m_λ is transformed into an average flux f_λ^m using the relation

$$m_\lambda = -2.5 \log f_\lambda^m + c_m \quad (1)$$

where

$$f_\lambda^m = \frac{\int_0^\infty f_\lambda S_m(\lambda) \lambda d\lambda}{\int_0^\infty S_m(\lambda) \lambda d\lambda}, \quad (2)$$

f_λ is the monochromatic flux received at Earth from the star, c_m is a zero point calibration constant, and $S_m(\lambda)$ is the transmission function of the corresponding bandpass. The zero points and transmission functions are taken from Holberg & Bergeron (2006), where an expression similar to that above is also provided for the SDSS *ugriz* photometric system

(AB₉₅). These average observed fluxes can then be compared with the model predictions using the relation

$$f_{\lambda}^m = 4\pi (R/D)^2 H_{\lambda}^m \quad (3)$$

where R/D is the ratio of the radius of the star to its distance from Earth, and H_{λ}^m is the average model flux obtained by substituting f_{λ} in Equation 2 for the monochromatic Eddington fluxes H_{λ} , which depend on the atmospheric parameters T_{eff} , $\log g$, and H/He.

The fitting procedure relies on the Levenberg-Marquardt nonlinear least-square method where the χ^2 value is taken as the sum over all bandpasses of the difference between both sides of Equation 3, properly weighted by the corresponding observational uncertainties. Only T_{eff} and the solid angle $\pi (R/D)^2$ are considered free parameters at a fixed value of the hydrogen abundance. In principle, trigonometric parallax measurements can be used to constrain the $\log g$ value, but since no such data is available for our sample of cool, He-rich DA white dwarfs from the SDSS, we simply assume $\log g = 8$ throughout. When a satisfactory fit to the energy distribution is reached at some initial value of the hydrogen abundance, the resulting values of T_{eff} and $\log g$ are then used to measure the hydrogen-to-helium abundance ratio (H/He) by fitting the H α spectroscopic data using the same fitting procedure as that described above for the DBA white dwarfs. The entire procedure is then repeated iteratively until a consistent set of T_{eff} , $\log g$, and H/He values is reached. Because the limits on the hydrogen abundance depend on the S/N of the observations at H α , and that the average S/N of our cool white dwarf sample from the SDSS is ~ 5.4 times lower than the average of our hotter DB sample, we adopt a detection limit of 1100 mÅ for the equivalent width of H α .

2.2.3. Selected Results

Our fits to the 28 cool, He-rich DA white dwarfs in the SDSS sample are displayed in Figure 7. The main panels show the photometric fits to the observed *ugriz* energy distributions, while the insets show the corresponding spectroscopic fits in the region covering H α and He I $\lambda 5876$. Since it is also possible that some of these objects could be unresolved DA+DC white dwarf binaries, we also made sure that our solutions are consistent with the observed spectra in the blue portion of the spectrum (H β and blueward), within the signal-to-noise of the observations. The atmospheric parameters for all objects, assuming a value of $\log g = 8$, are provided in Table 2, together with the same information as in Table 1, with the exception that the absolute magnitude is given here for the *g* filter (M_g). We also added

a note for possible DA+DC systems.

The hydrogen abundances as a function of effective temperature for all cool, He-rich DA white dwarfs in our sample are displayed in Figure 8, together with our spectroscopic results for the DB and DBA stars; also shown are the limits on the hydrogen abundance for both subsamples. For completeness, we reproduce in this figure the results of Dufour et al. (2007a) for the DZA white dwarfs from the SDSS, for which the hydrogen abundances have been determined spectroscopically, as well as the three bright DZA stars from Giammichele et al. (2012). The location of our cool, He-rich DA stars and DZA white dwarfs in this plot indicates that these two populations are very alike. They cover essentially the same range of hydrogen abundances, with a similar dispersion, and most importantly, they display the same behavior with respect to effective temperature. Note that cool, He-rich DA/DZA white dwarfs most certainly exist below the detection threshold at $H\alpha$ displayed in Figure 8, although objects with very large hydrogen abundances have not been found in our analysis. Since hydrogen has been detected — or inferred — in 27% of the DZ stars analyzed by Dufour et al. (2007a), our results suggest, as a conservative estimate, that the cool, He-rich DA white dwarfs represent around 25% of the total DC population below $\sim 12,000$ K, at least in the range of temperature where $H\alpha$ can be detected in helium-rich atmospheres ($T_{\text{eff}} \gtrsim 6000$ K).

The results displayed in Figure 8 represent the best picture we have so far of the hydrogen abundance pattern in helium-atmosphere white dwarfs below $T_{\text{eff}} \sim 30,000$ K, both in terms of the quality of the photometric and spectroscopic data currently available to us, but also in terms of model atmospheres and fitting techniques. Any viable model of the spectral evolution of white dwarfs involving the convective dilution — or mixing — of the thin hydrogen layer with the deeper helium envelope, or accretion from the interstellar medium or other external bodies, must be able to account self-consistently for the observed hydrogen abundance pattern depicted in Figure 8.

3. MODEL ENVELOPE STRUCTURES

In the absence of competing mechanisms, gravitational settling would gradually make the hydrogen present in DBA white dwarfs and cool, He-rich DA/DZA stars float up to the surface, resulting in the creation of a hydrogen-dominated atmosphere in a time frame much smaller than the typical white dwarf cooling time. In the temperature range considered here ($T_{\text{eff}} \lesssim 30,000$ K), however, convective energy transport within the thick helium envelope is the main mechanism competing with element diffusion, and hydrogen is thus expected to be thoroughly mixed within the helium convection zone, resulting in a helium-dominated

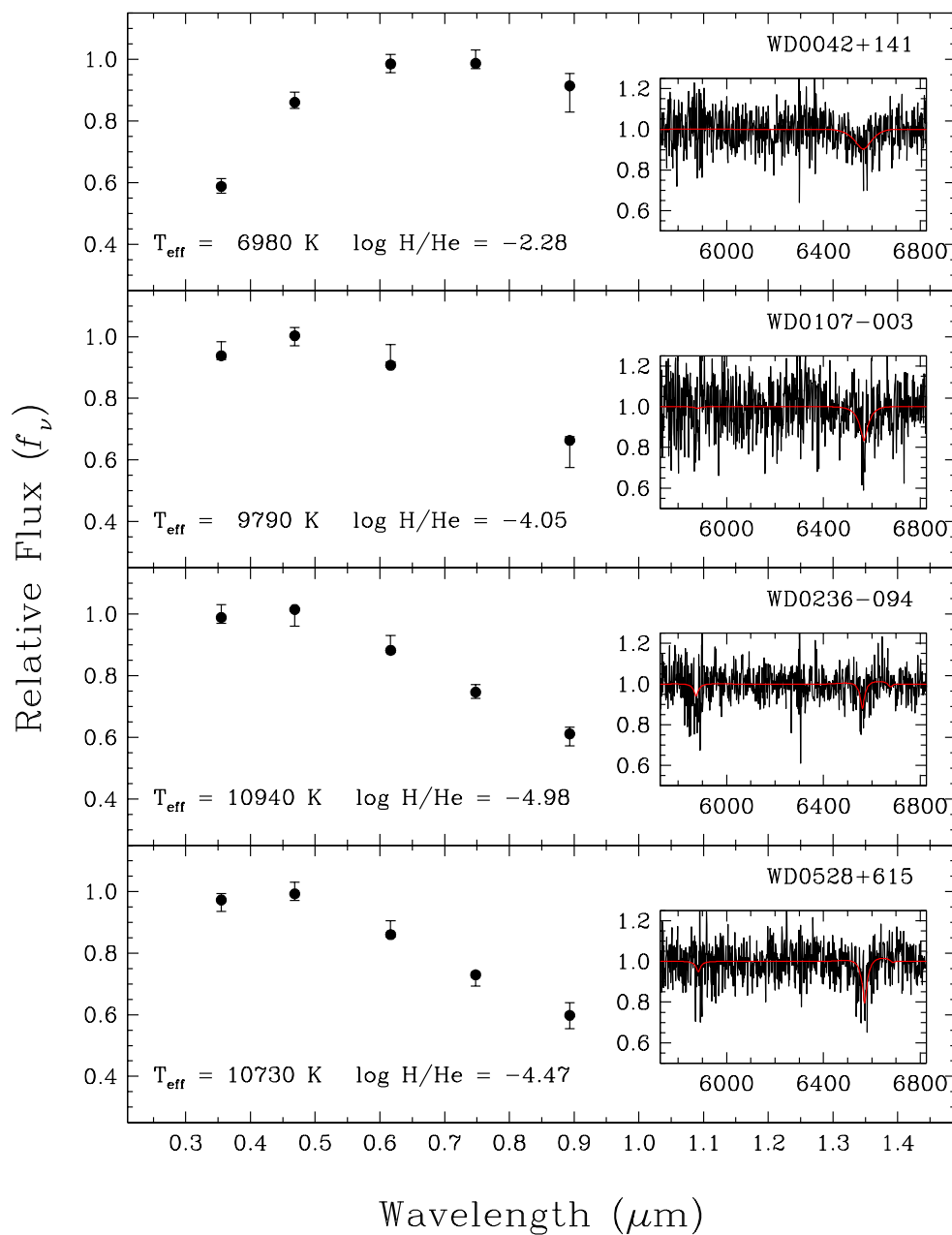


Fig. 7.— Fits obtained from the hybrid fitting method for cool, He-rich DA stars with homogeneous models at $\log g = 8$. The *ugriz* photometric observations are represented by error bars, while the model fluxes are shown by filled circles. The inset shows our fit to the spectrum near the H α region, normalized to a continuum set to unity, which is used to measure the hydrogen abundance.

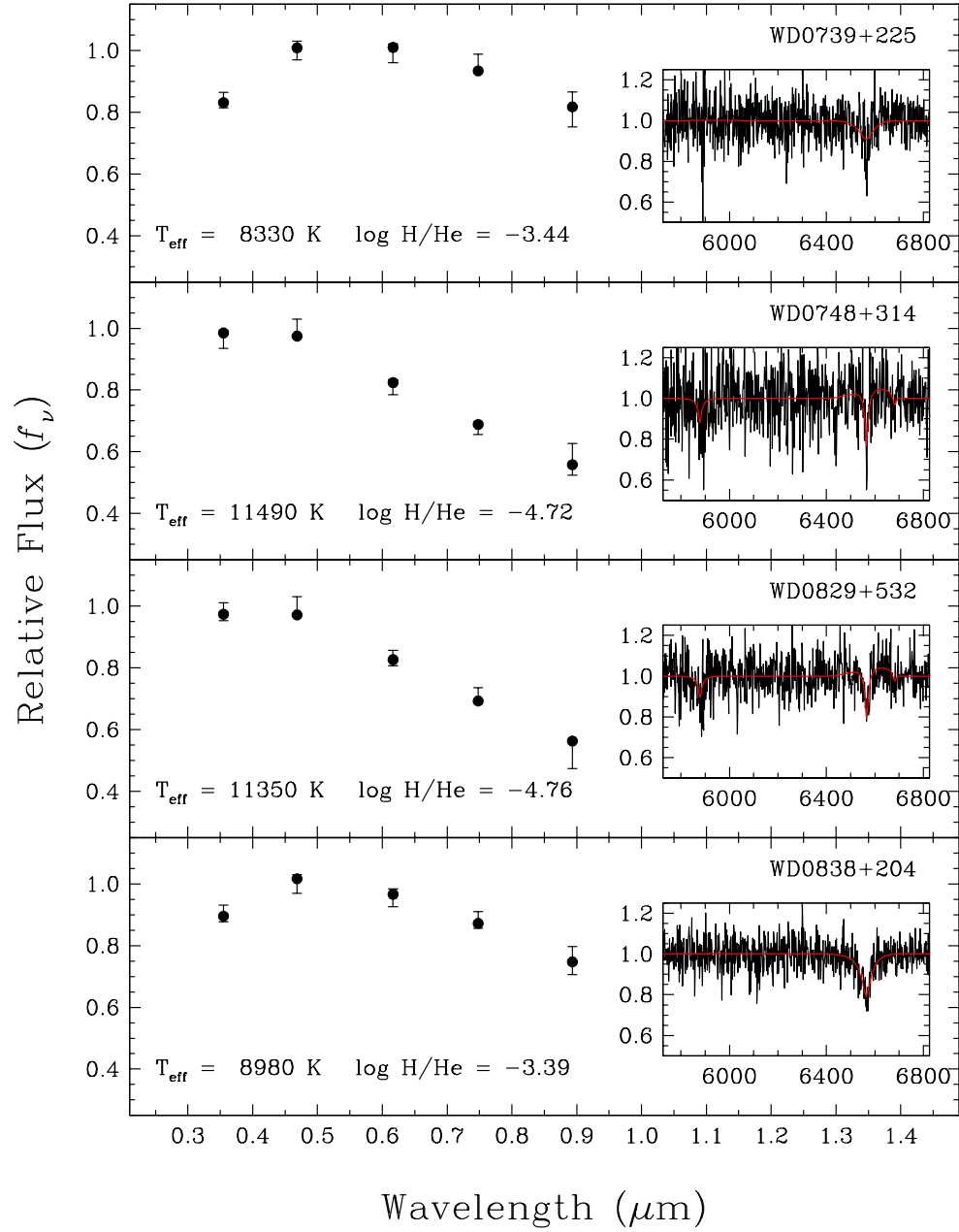


Fig. 7.— (Continued)

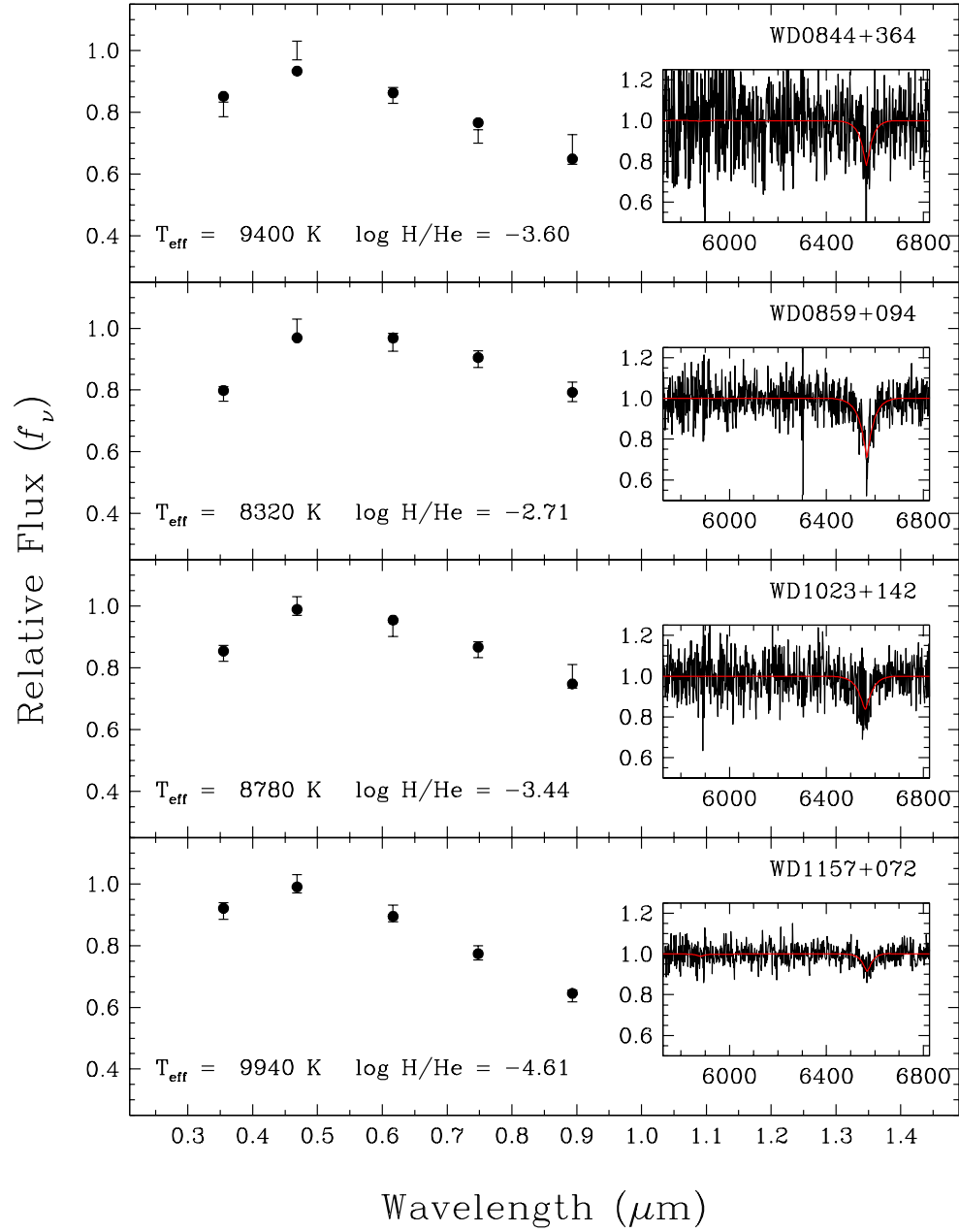


Fig. 7.— (Continued)

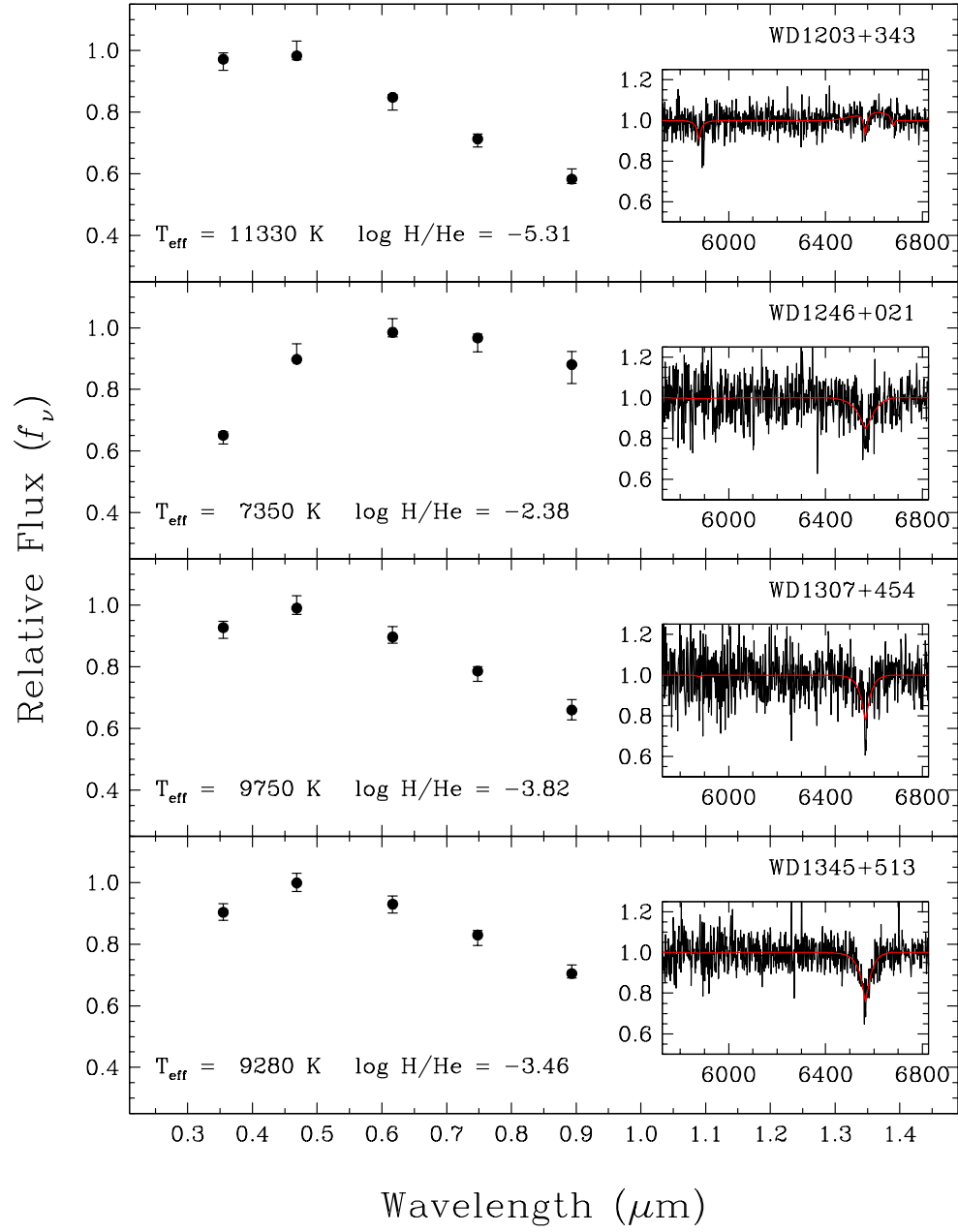


Fig. 7.— (Continued)

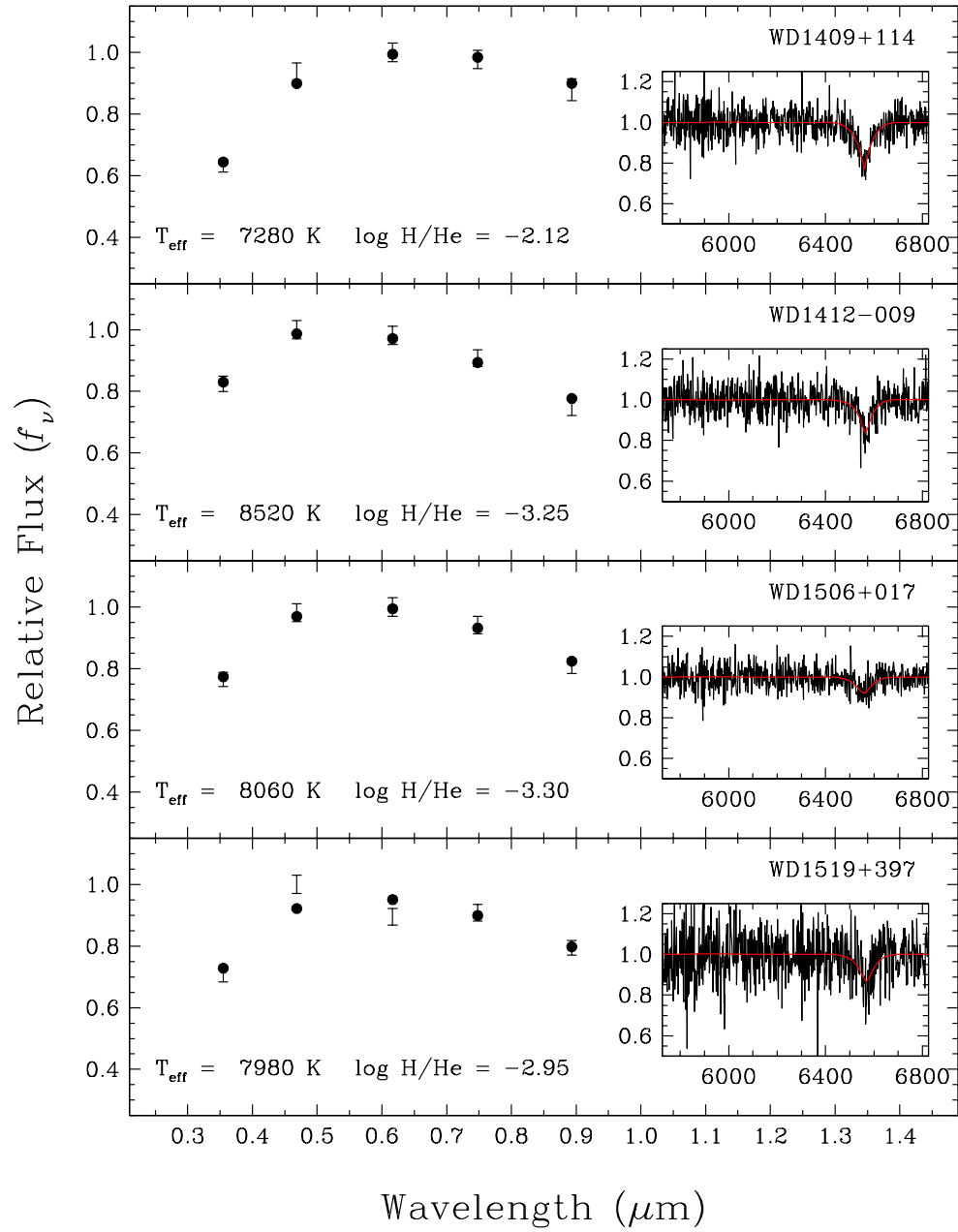


Fig. 7.— (Continued)

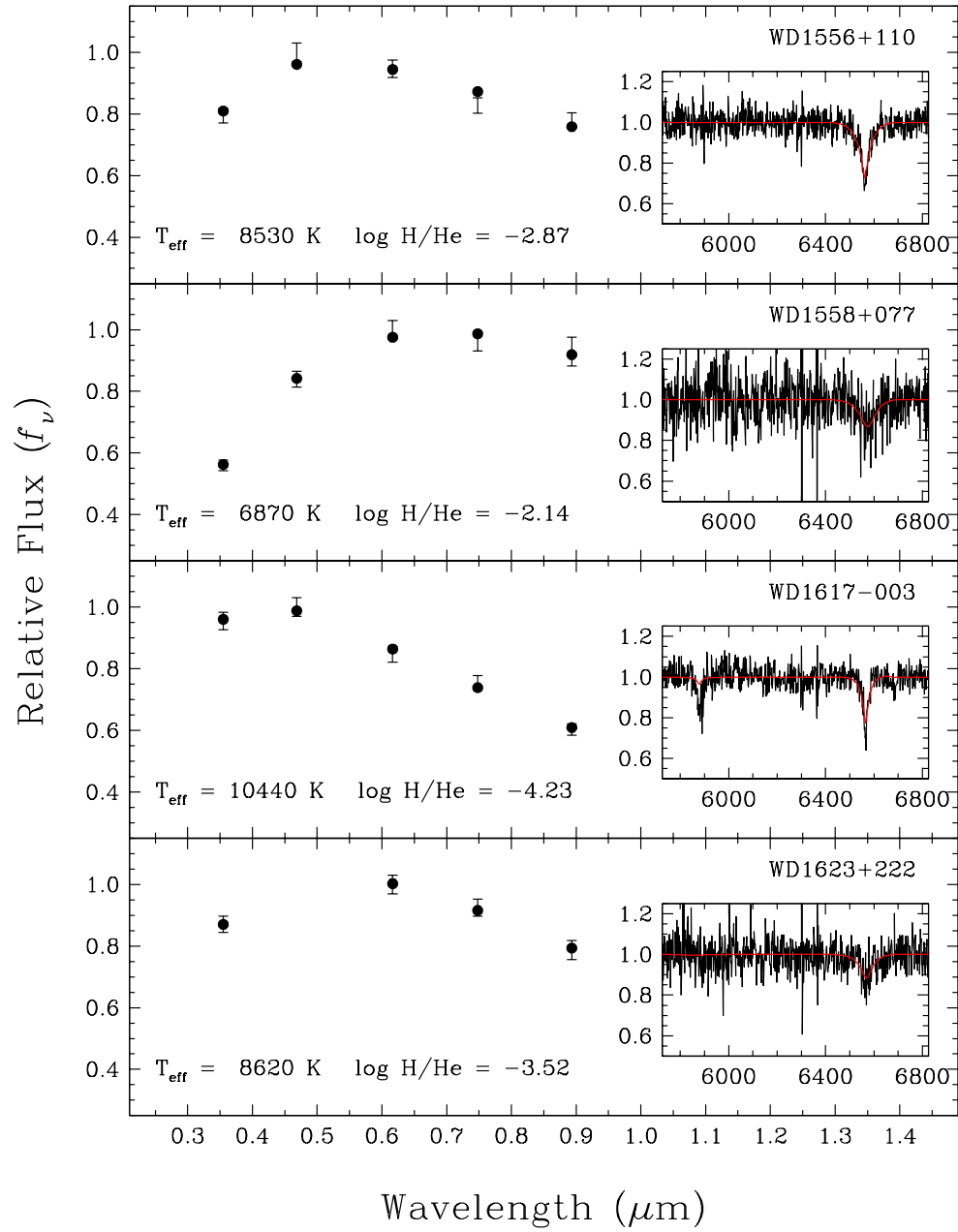


Fig. 7.— (Continued)

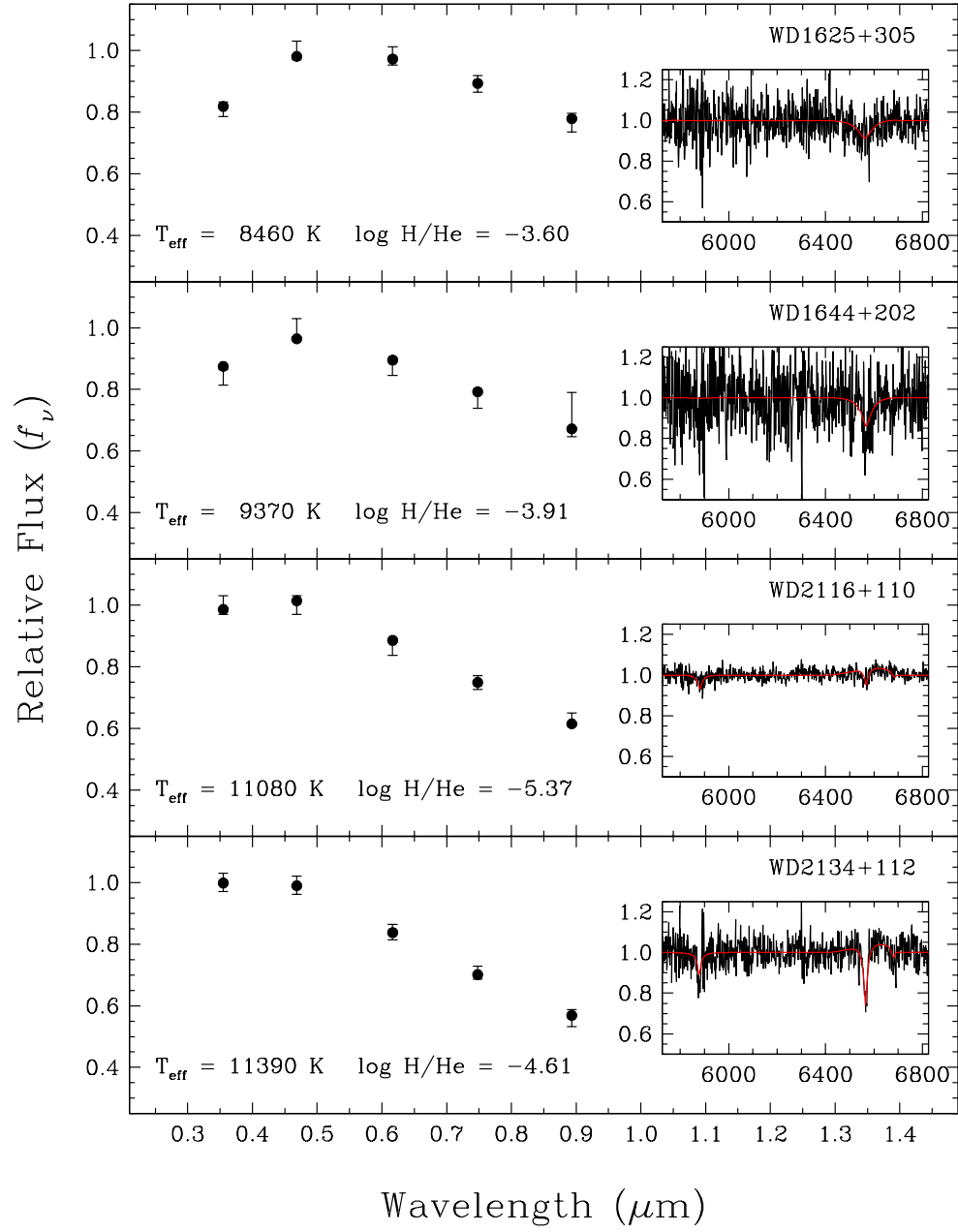


Fig. 7.— (Continued)

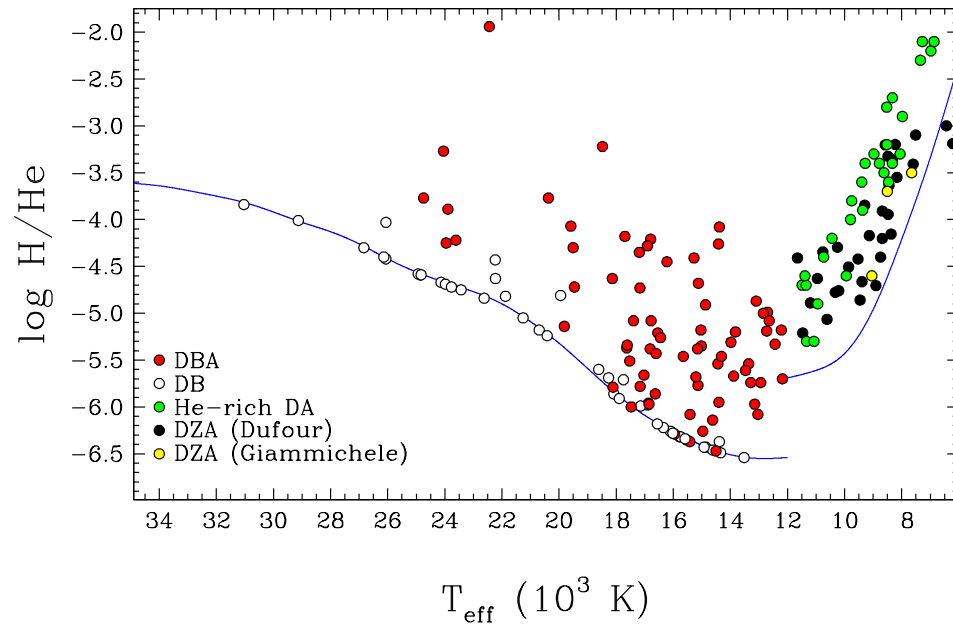


Fig. 8.— Hydrogen-to-helium abundance ratio as a function of effective temperature for all DB, DBA, and cool, He-rich DA white dwarfs in our SDSS sample; the DZA stars from Dufour et al. (2007a) and Giammichele et al. (2012) are also displayed. The hydrogen detection limits at $H\alpha$ are indicated by blue lines for the subsamples above and below $T_{\text{eff}} = 12,000 \text{ K}$.

atmosphere with a homogeneous H/He abundance profile. As discussed in the Introduction, the progenitors of some of the DB white dwarfs are probably DA stars with sufficiently thin radiative hydrogen layers, of the order of $M_{\text{H}} \sim 10^{-15} M_{\odot}$, which are transformed into helium-atmosphere white dwarfs as a result of the *convective dilution* of this thin hydrogen layer with the deeper and more massive convective helium envelope. Cool ($T_{\text{eff}} \lesssim 12,000$ K), helium-atmosphere white dwarfs that show only traces of hydrogen (and sometimes metals), on the other hand, could be interpreted as DBA stars that have simply cooled off, or alternatively, they could also be interpreted as the result of convectively mixed DA stars, when the bottom of the hydrogen convection zone in a DA white dwarf eventually reaches the underlying and more massive convective helium envelope, resulting in the *convective mixing* of the hydrogen and helium layers, a process believed to occur when the hydrogen layer mass is in the range $M_{\text{H}} \sim 10^{-14} - 10^{-6} M_{\odot}$.

The structure of both types of DA progenitors described above is thus a thin hydrogen layer — convective or not — sitting on top of a massive helium envelope. To describe these structures, as well as the homogeneously mixed hydrogen and helium structures, we make use of the latest version of the Montréal white dwarf model-building code in its envelope mode (see Brassard & Fontaine 1994 for a first description). This code uses the same input physics as the full evolutionary models described at length in Fontaine et al. (2001), but with updates discussed briefly in Giammichele et al. (2016). Models with both homogeneously mixed and chemically stratified compositions have been computed for a large set of effective temperatures, stellar masses, and assumed convective efficiencies. These are described in turn.

3.1. Homogeneously Mixed Composition Models

Our static, homogeneously mixed models are characterized by $q(\text{env}) \equiv M_{\text{env}}/M_{\star} = 10^{-2}$ — which are representative of helium-rich white dwarfs — with a homogeneous hydrogen and helium abundance profile from the surface to the bottom of the stellar envelope. Note that the presence of hydrogen uniformly distributed below the mixed H/He convection zone may not be very realistic, but, importantly, it does not affect in any way the location of the bottom of this convection zone in our structures. We use these models below to compute the mass of hydrogen contained in the convection zone only. Our homogeneous grid covers a range of effective temperature between $T_{\text{eff}} = 60,000$ K and 30,000 K by steps of 500 K, and between $T_{\text{eff}} = 30,000$ K and 4000 K by steps of 50 K. The hydrogen mass fraction in the envelope ranges from $\log X = -8.5$ to -2.5 by steps of 0.5 dex, and from $\log X = -2.50$ to 0.35 with a varying mesh between 0.20 or 0.25 dex. We also explore the so-called $\text{ML2}/\alpha = 0.6$ and

$\alpha = 2$ parameterizations of the mixing-length theory to treat convective energy transport. These two values bracket the convective efficiencies mostly used in the context of white dwarf atmospheres and envelopes (see, e.g., Tassoul et al. 1990; Tremblay et al. 2015).

Envelope structures for various hydrogen-to-helium abundance ratios (H/He), stellar masses, and convective efficiencies, are displayed in Figures 9 and 10 for $ML2/\alpha = 0.6$ and $\alpha = 2$ models, respectively. The extent of the convection zones (color coded with the fraction of the total flux carried out by convection) as well as the location of the photosphere are indicated in each panel. The smallest and largest hydrogen abundances illustrated here correspond to almost pure helium and pure hydrogen compositions, respectively, in terms of their structures. In the most helium-rich models with $ML2/\alpha = 0.6$, a small convection zone is present at high temperatures, due to the partial ionization of He II, but with only $\sim 1\%$ of the flux transported by convection; the depth of this convection zone is significantly larger with $\alpha = 2$, with a much larger fraction of the total flux being transported by convection. Below $T_{\text{eff}} \sim 28,000$ K, a second, more superficial, convection zone appears, due this time to the partial ionization of He I. Eventually, both convection zones merge below $\sim 25,000$ K. As the hydrogen content is increased, the temperature at which these two convection zones merge decreases, and another convection zone develops due to the partial ionization of hydrogen (mixed with the superficial helium convection zone), which appears as a bump at the top of the convection zone near 16,000 K in the models with $\log H/He \gtrsim +0.26$ shown in Figures 9 and 10. In addition, we note that the increase in hydrogen content gradually delays the development of the deep, mixed H/He convection zone. At the largest hydrogen abundances illustrated here, the convection zone due to the partial ionization of He II at high temperatures is also totally suppressed. Finally, in the range of effective temperatures and hydrogen abundances where DBA white dwarfs are found in our sample ($T_{\text{eff}} \sim 12,000 - 30,000$ K, $\log H/He < -4$), the structure of the helium convection zone remains unaffected by the presence of hydrogen. In this particular temperature range, hydrogen starts to affect the structure of the convection zone only above $\log H/He \sim -3.4$.

For the cooler envelope models ($T_{\text{eff}} \lesssim 10,000$ K) displayed in Figures 9 and 10 — more representative of the cool, He-rich DA stars analyzed above — the situation is somewhat different. First, we note that the top of the convection zone, which coincides with the location of the photosphere, becomes increasingly deeper in cooler models as a result of the decrease in total opacity. Since neutral helium is particularly transparent with respect to hydrogen at low temperatures ($T_{\text{eff}} \lesssim 6000$ K), the location of the photosphere and the top of the convection zone are orders of magnitude deeper (when expressed in fractional mass) in the cool, hydrogen-poor models than in the hydrogen-rich models. The effect on the location of the bottom of the mixed H/He convection zone is also significant.

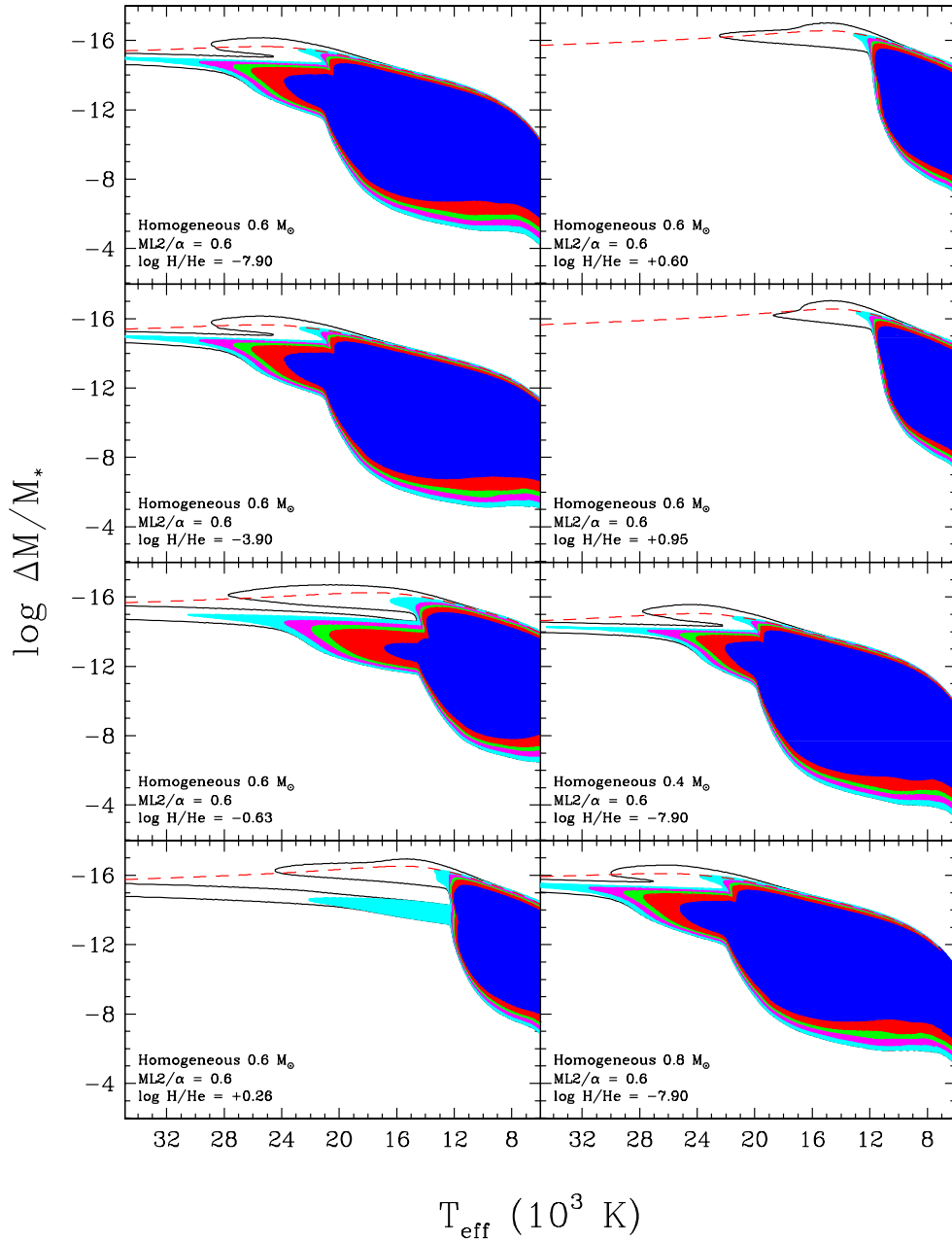


Fig. 9.— Examples of envelope structures for white dwarf models with homogeneously mixed compositions as a function of effective temperature. The depth is expressed as the fractional mass above the point of interest with respect to the total mass of the star. The models illustrated here are (from upper left to bottom right) for $0.6 M_{\odot}$ with increasing hydrogen abundances, with the exception of the last two panels that show the results at 0.4 and $0.8 M_{\odot}$ for an almost pure helium composition, and they all assume a $ML2/\alpha = 0.6$ parameterization of the convective efficiency. The red dashed line corresponds to the location of the photosphere, while the contours with various colors represent the convection zones with 0.1, 1, 50, 75, 85, and 95% of the total flux being transported by convection.

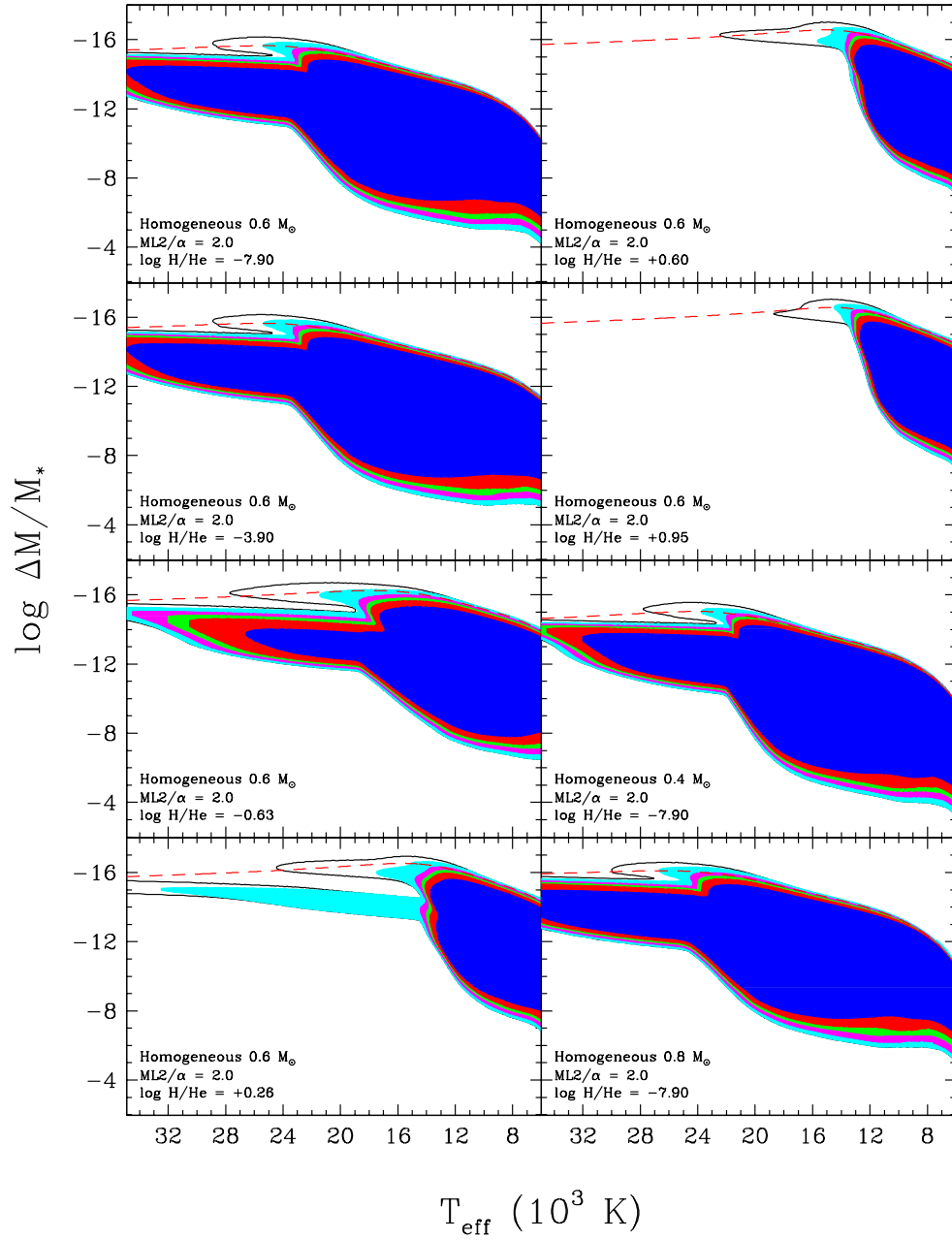


Fig. 10.— Same as Figure 9 but for models assuming a $ML2/\alpha = 2$ parameterization of the convective efficiency.

As discussed above, the behavior of the $ML2/\alpha = 2$ models displayed in Figure 10 are qualitatively similar to the $ML2/\alpha = 0.6$ models, with the notable exception that at a given effective temperature, the mixed H/He convection zone extends significantly deeper in the star. This implies that for a given hydrogen-to-helium abundance ratio observed at the photosphere, a larger hydrogen mass will be inferred using models with more efficient convection. Below roughly 10,000 K, however, convection becomes adiabatic and both sets of envelope structures are identical at the bottom of the convection zone. We also note that the assumed convective efficiency has a negligible effect at the surface. Finally, an examination of our almost pure helium models at 0.4 and 0.8 M_{\odot} reveals that the He II convection zone starts to plunge into the star at higher temperatures in more massive white dwarfs — $T_{\text{eff}} \sim 30,000$ K at 0.8 M_{\odot} compared to $\sim 25,000$ K at 0.4 M_{\odot} — but the convection zone in the more massive models does not extend as deep below $\sim 20,000$ K. Since these differences remain small, we find it reasonable to assume only 0.6 M_{\odot} models in our discussion of the various evolutionary scenarios described below.

3.2. Stratified Composition Models

Our static, stratified composition models are characterized again by thick stellar envelopes of $q(\text{env}) = 10^{-2}$, but composed this time of a pure hydrogen envelope in diffusive equilibrium on top of a deeper helium mantle. This stratified model grid covers the same range of effective temperature as before, and the hydrogen layer mass varies between $\log q(\text{H}) = \log M_{\text{H}}/M_{\star} = -17.4$ and -4.0 by steps of 0.5 dex. Examples of these stratified models are displayed in Figures 11 and 12 for various values of $q(\text{H})$, stellar masses, and convective efficiencies. Note that in these models, the hydrogen layer is forced to remain in diffusive equilibrium on top of the helium layer, and is thus never allowed to mix with the underlying helium envelope, which of course may not be physically realistic in some cases.

In the thinnest hydrogen layer sequence displayed here, $\log q(\text{H}) = -16.43$, the structure of the helium convection zone above $T_{\text{eff}} \sim 20,000$ K is nearly identical to the almost pure helium sequences shown in Figures 9 and 10. In cooler models, however, even the presence of a small amount of hydrogen at the surface of the star affects the location of the bottom of the helium convection zone, although such thin hydrogen layers would have certainly been convectively diluted by the helium convection zone at higher effective temperatures. As the thickness of the hydrogen layer is increased, the extent of the helium convection zone is significantly reduced at high temperatures ($T_{\text{eff}} \gtrsim 15,000$ K), to the point that it is conceivable that the hydrogen layer in these models always remains in diffusive equilibrium on top of the helium envelope — when $\log q(\text{H}) = -13.93$ for instance — at least until the

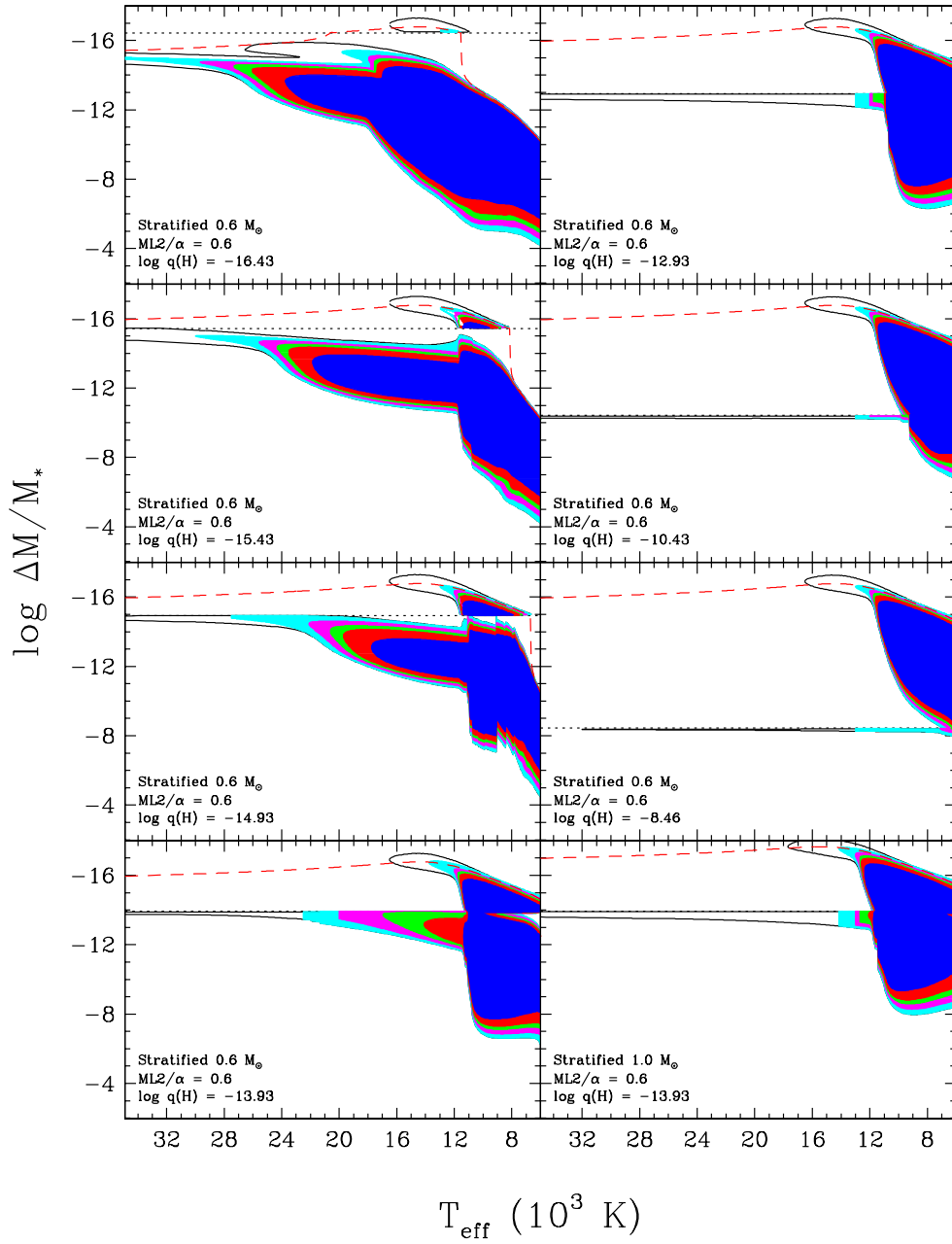


Fig. 11.— Same as Figure 9 but for stratified models. The models illustrated here are for $0.6 M_\odot$ with increasing thickness of the hydrogen layer (from upper left to bottom right) expressed as $\log q(\text{H}) = \log M_{\text{H}}/M_*$, with the exception of the bottom right panel that shows the results at $1.0 M_\odot$ and $\log q(\text{H}) = -13.93$ — i.e., the same value of $\log q(\text{H})$ as the panel to the left. The value of $\log q(\text{H})$ is indicated by a black dotted line in each panel. The results shown here assume a $\text{ML2}/\alpha = 0.6$ parameterization of the convective efficiency.

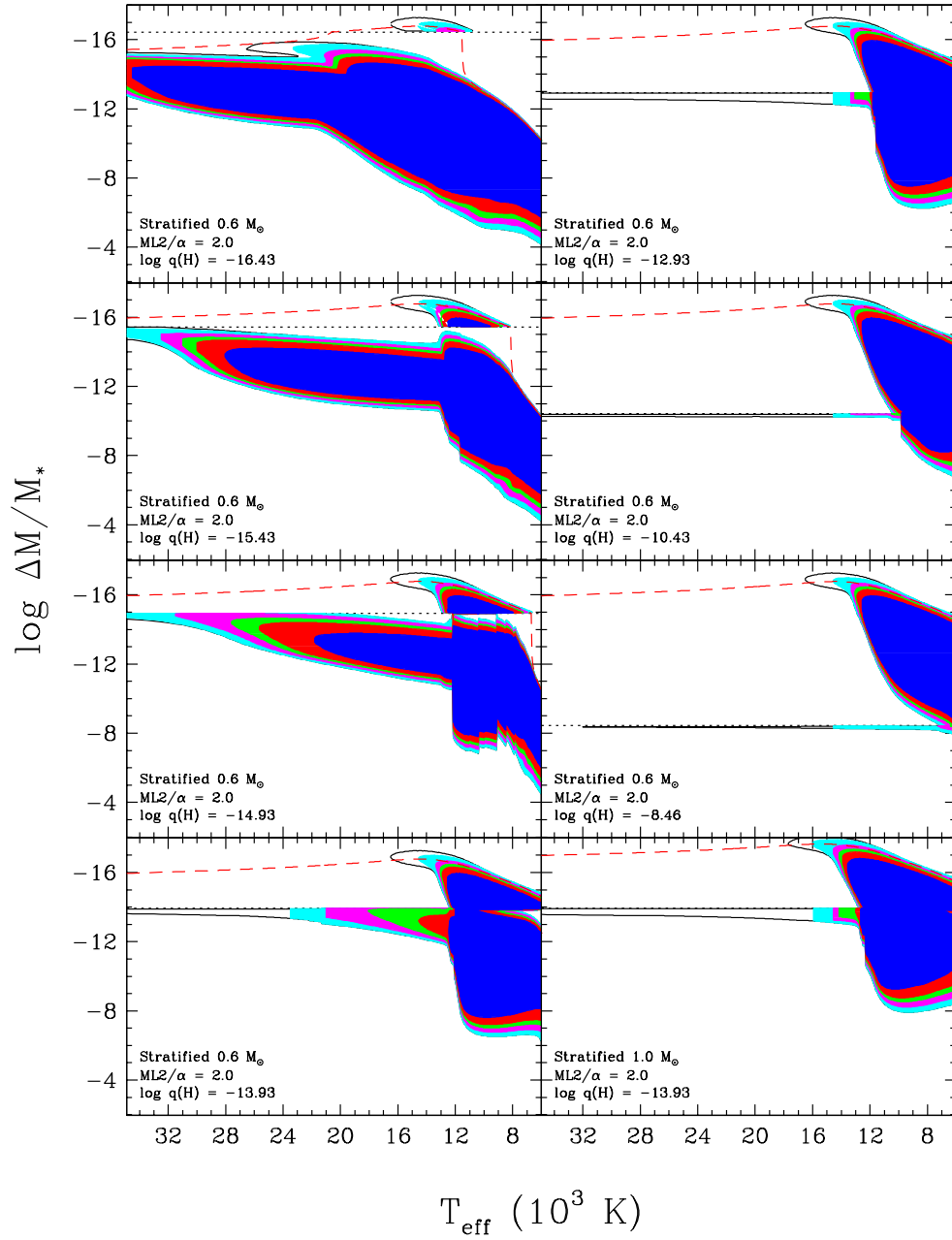


Fig. 12.— Same as Figure 11 but for models assuming a $ML2/\alpha = 2$ parameterization of the convective efficiency.

star cools down to $T_{\text{eff}} \sim 12,000$ K or so, where *convective mixing* might occur.

Indeed, below $T_{\text{eff}} \sim 16,000$ K, a small hydrogen convection zone starts to develop at the surface of these models. At lower effective temperatures, the bottom of the hydrogen convection zone becomes deeper, eventually reaching the underlying helium convection zone. At this point, it is believed that the hydrogen layer will be thoroughly mixed with the deeper and more massive helium convection zone, resulting in homogeneous H/He convective envelope structures, such as those illustrated in Figures 9 and 10. Furthermore, the temperature at which this mixing process occurs, and the resulting hydrogen-to-helium abundance ratio at the photosphere, will be a strongly dependent function of the thickness of the hydrogen layer of the DA progenitor — the thicker the hydrogen envelope, the lower the mixing temperature. Note that according to the models shown here, a DA star is never expected to mix if $\log q(\text{H}) \gtrsim -6$, which corresponds to the maximum depth of the hydrogen convective zone.

As for the homogeneous models, both the hydrogen and the helium convection zones extend much deeper at a given effective temperature in the models assuming the $\text{ML2}/\alpha = 2$ convective efficiency, shown in Figure 12. The most important consequence in the present context is that the convective mixing process will occur at higher effective temperatures in more efficient models. Finally, the effect of mass is illustrated in the bottom right panel of Figures 11 and 12 where we show the results at $1.0 M_{\odot}$ and $\log q(\text{H}) = -13.93$, which can be directly compared with the left panel at $0.6 M_{\odot}$ with the same value of $\log q(\text{H})$. For a fixed value of $\log q(\text{H})$, all convection zones are shifted upward in the more massive models; remember that $\log q(\text{H}) \equiv \log M_{\text{H}}/M_{\star}$ is scaled with respect to the mass of the star, so a given value of $\log q(\text{H})$ implies a more massive hydrogen layer in a more massive star. Consequently, the extent of the helium convection zone at high temperatures is much smaller, but more importantly in the present context, the effective temperature at which the hydrogen convection zone connects with the helium convective envelope is about ~ 500 K higher.

3.3. Total Hydrogen Mass

We now attempt to estimate the total mass of hydrogen present in a given helium-atmosphere white dwarf, after the superficial hydrogen layer has been thoroughly diluted — or convectively mixed — with the underlying helium envelope. Our working assumption is that *all* available hydrogen is found in a region covering the superficial convection zone extended below by a diffusion tail that must be created as the result of ordinary diffusion. As discussed in Section 3.1, our homogeneously mixed models are perfectly suitable to estimate

the mass of hydrogen contained in the convection zone. We recall in this context that the presence of hydrogen below the mixed H/He convection zone — and in particular the way it is distributed in these regions — does not affect in any way the location of the bottom of this convection zone in our structures.

Next, the ratio R of the mass of hydrogen contained in the diffusive tail over that contained in the convection zone can be estimated analytically following the approach of Vennes et al. (1988). Under the assumptions that 1) diffusive equilibrium has been reached, and 2) hydrogen is a trace species ($H \ll He$) in the convection zone, one can show that,

$$R = \frac{A_1}{A_1 Z_2 - A_2(Z_1 + 1)}, \quad (4)$$

where A_1 (Z_1) is the atomic weight (average charge) of the dominant element (helium here), and A_2 (Z_2) is the atomic weight (average charge) of hydrogen at the bottom of the convection zone. Under conditions of most interest here, hydrogen is completely ionized at the bottom of the convection zone ($Z_2 = 1$) while helium is nearly so ($Z_1 \simeq 2$). Taking $A_1 = 4$ and $A_2 = 1$, one finds $R \simeq 4$, i.e., there is four times more hydrogen “hidden” in the diffusion tail than present in the convection zone.

This value of R is necessarily an upper limit because of the following circumstances. First, if helium is not completely ionized, the diffusion tail is steeper and contains less hydrogen. For instance, assuming that $Z_1 = 1$ (He II), one finds $R = 2$. Second, the neglect of thermal diffusion in our derivation leads also to an overestimate of R as the diffusion tail would again be steeper otherwise. Third, the assumption of complete diffusive equilibrium may not be fully justified in the deeper regions of the diffusion tail as the diffusion timescale there may not be negligible anymore in front of the cooling timescale. And fourth, residual nuclear burning around $\log q \sim -4$ also limits the extension of the diffusion tail and its hydrogen content. In practice, we assume somewhat arbitrarily in the remainder of our analysis that $R = 2$. Hence, the total amount of hydrogen, M_H , is equal to that measured in the convection zone with our uniformly mixed models multiplied by $(1 + R)$.

Under these assumptions, it is now possible to calculate the total mass of hydrogen contained in our grid of homogeneous models at various effective temperatures as a function of the observed photospheric hydrogen abundance H/He. The results are summarized in Figure 13 where we show, for the two convective efficiencies explored in our analysis, the total hydrogen mass contained in the model as a function of H/He at various effective temperatures ranging from $T_{\text{eff}} = 6000$ K to 40,000 K. An illustrative example for a total hydrogen mass of $M_H = 10^{-13} M_\odot$ is also indicated by a red dashed line. For this particular mass value (but other values as well), we can see that at certain effective temperatures ($T_{\text{eff}} = 18,000$ K

for instance), there are multiple values of H/He possible⁴, generally separated by orders of magnitude, for the same total hydrogen mass. This degeneracy reflects the possibility of mixing the same total amount of hydrogen in a deep, or in a shallow, helium convection zone (see also MacDonald & Vennes 1991).

A careful analysis of the results shown in Figure 13 also provides valuable information on the evolution of white dwarfs with homogeneously mixed H/He compositions. For instance, there is no homogeneously mixed envelope structure above $T_{\text{eff}} \sim 20,000$ K with a hydrogen mass of $\log M_{\text{H}}/M_{\odot} = -13$ for $\text{ML2}/\alpha = 0.6$ models (or above $T_{\text{eff}} \sim 25,000$ K with $\alpha = 2$). Envelope structures with such large hydrogen masses can only be stratified (see Figure 11), corresponding to DA star configurations. These considerations will thus define an area in the $T_{\text{eff}} - \text{H/He}$ parameter space inaccessible via normal white dwarf evolution with a constant hydrogen mass, as discussed further below.

4. EVOLUTIONARY SCENARIOS

4.1. Results from MacDonald & Vennes (1991)

Before discussing our own results, it is worth here summarizing some of the calculations from MacDonald & Vennes (1991) most relevant to our study. MacDonald & Vennes investigated stratified hydrogen/helium envelope models that are in full diffusive equilibrium for effective temperatures between 10,000 and 80,000 K, and including convective mixing using both Schwarzschild and Ledoux criteria with different convective efficiencies. Their results can be best summarized by examining their Figure 1 (Schwarzschild convection with $\alpha = 1$) where contours of constant total hydrogen mass are shown for $\log M_{\text{H}}/M_{\odot} = -16$ to -10 (by steps of 1.0 dex) in a diagram of He/H ratios (measured at a Rosseland optical depth of 2/3) as a function of effective temperature. To avoid further confusion, it is important to mention that MacDonald & Vennes refer to helium-to-hydrogen ratios (He/H) measured in *mass*, while we use throughout our analysis the inverse ratio (H/He) measured in *number*. Note also that since these are models in full equilibrium, all the hydrogen present in the envelope has already reached the surface in the hottest models ($T_{\text{eff}} = 80,000$ K). By examining this figure, one can see that at a given effective temperature, there can be multiple envelope structures (up to five in some cases) that have the same total mass of hydrogen. This is further illustrated in their Figure 6 where the He/H ratio is shown as a function of

⁴Note that MacDonald & Vennes (1991) find more solutions than we find here for some T_{eff} values because their grid includes models where helium is considered a trace element in diffusive equilibrium within the superficial hydrogen-rich layer (see their Figure 6).

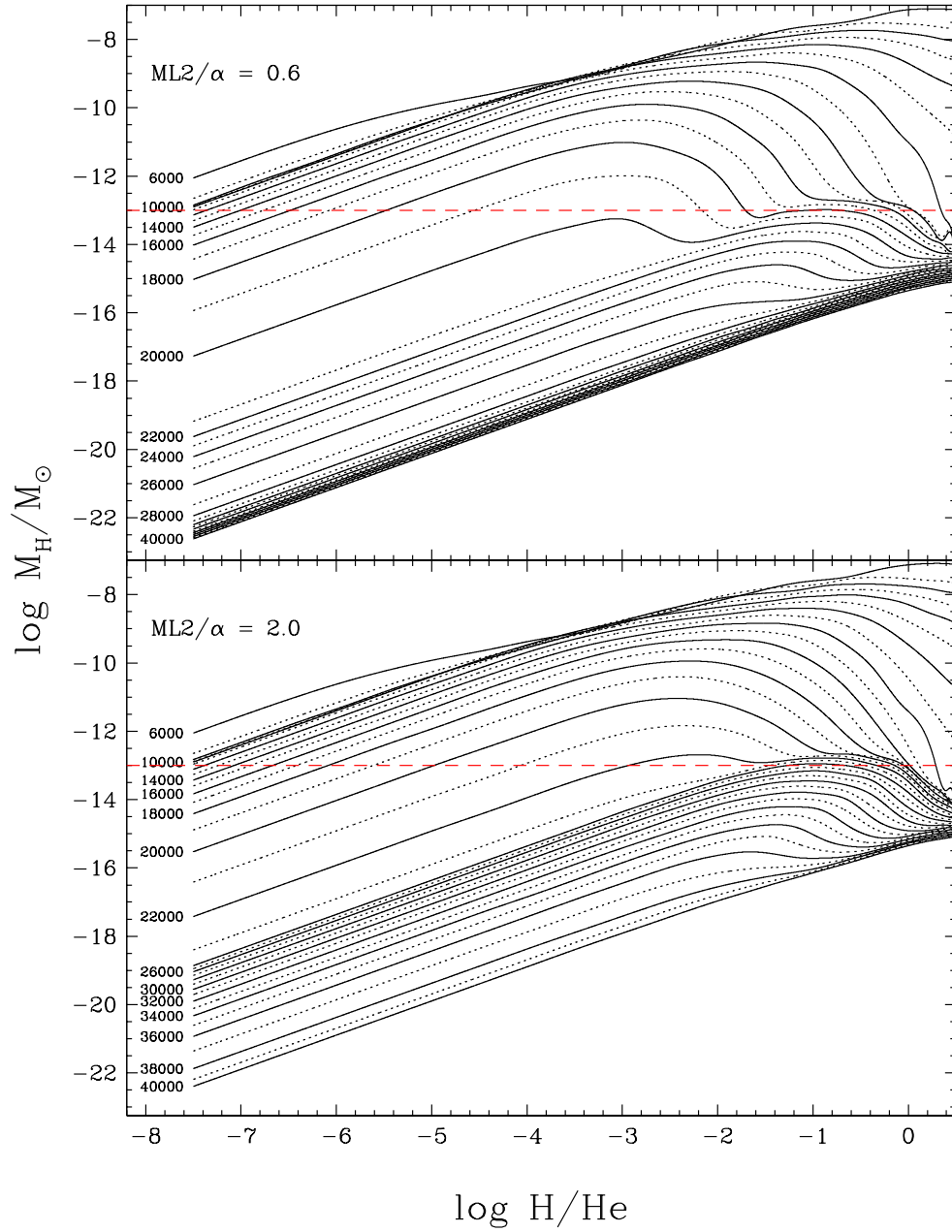


Fig. 13.— Total hydrogen mass contained in homogeneously mixed H/He envelope models at $0.6 M_{\odot}$ for various effective temperatures (labeled on each curve) as a function of the observed photospheric hydrogen abundance (H/He). The results are shown for two different convective efficiencies. An illustrative example for a total hydrogen mass of $\log M_{\text{H}}/M_{\odot} = -13$ is indicated by a red dashed line in each panel.

mass depth for five envelope models with $\log M_{\text{H}}/M_{\odot} = -13$ at $T_{\text{eff}} = 15,000$ K. As discussed above, such multiple solutions reflect the possibility of mixing hydrogen and helium in convection zones of various thicknesses and depths (shown by the flat He/H profiles in their Figure 6). In the same figure, model A (a typical DA structure with almost all the hydrogen floating at the surface) and model E (a typical DB structure with hydrogen being diluted in the deep helium convective envelope) correspond approximately to our own stratified and homogeneous envelope models, respectively. But there are also intermediate solutions (see also our Figure 13), which as discussed by MacDonald & Vennes, are either unstable (dotted lines in their Figure 1) or unlikely to occur in nature.

As discussed by the authors, the contours in their Figure 1 are not to be interpreted as evolutionary tracks, but the evolution of white dwarfs with fixed hydrogen mass can still be determined by studying the appropriate contour in the following way. For instance, MacDonald & Vennes (see their Section 3) discuss a particular example at $\log M_{\text{H}}/M_{\odot} = -13$. As the star cools from $T_{\text{eff}} = 80,000$ K down to $\sim 35,000$ K, the photospheric helium abundance — always a trace element — remains nearly constant, and then starts to decrease (following the lower branch in their Figure 1) since radiative acceleration no longer supports helium below 35,000 K. The He/H ratio reaches a minimum value near $T_{\text{eff}} = 14,000$ K, and then starts to increase steadily again due to the onset of the hydrogen convection zone, until a minimum in effective temperature is reached at $T_{\text{eff}} = 11,700$ K, which corresponds to the point where both helium and hydrogen convection zones connect. At this point, the He/H ratio discontinuously jumps to the upper branch of the contour. In our own terminology, this corresponds to the *convective mixing scenario* (see Figures 11 and 12).

Another example worth considering is the case with $\log M_{\text{H}}/M_{\odot} = -14$. Again, as the star cools, the photospheric helium abundance decreases steadily, eventually reaches a minimum value, and starts to rise slowly. However, for this particular total hydrogen mass value, the coolest model on the lower branch is at $T_{\text{eff}} = 17,900$ K, that is, cooler stratified hydrogen/helium envelope models in diffusive equilibrium where almost all the hydrogen floats on top of the star do not exist within their theoretical framework. So again here, the He/H ratio discontinuously jumps to the upper branch of the contour, reaching the DB star configurations. This corresponds to what we referred to as the *convective dilution scenario*. Note that MacDonald & Vennes refer to both convective mixing and convection dilution scenarios as *convective dredge-up*. In particular, their Table 1 provides effective temperatures at which the so-called convective dredge-up occurs (T_{ed}) for different total hydrogen masses and assumed convection models, but it is important to realize that these T_{ed} values include both convective dilution (above $T_{\text{eff}} \sim 13,000$ K) and convective mixing (below $T_{\text{eff}} \sim 13,000$ K) processes.

More importantly, we want to emphasize here that the effective temperatures at which the convection dilution process occurs in the study of MacDonald & Vennes are based on static equilibrium models. In other words, the convective dilution process itself is not modeled in any way. Following the example above with $\log M_{\text{H}}/M_{\odot} = -14$, no particular event occurs below $T_{\text{eff}} \sim 17,900$ K. This is just the temperature below which no envelope models can be found within the framework assumed by the authors. For instance, for the same value of M_{H} , our stratified envelope models extend to much lower temperatures (see bottom left panel of Figure 11) because we simply forced hydrogen to remain in equilibrium on top of the helium convection zone. Hence the real question is whether the underlying helium convection zone becomes efficient enough to dilute the superficial hydrogen layer, and if so, at which temperature. This is a *dynamical process*, which, to our knowledge, has never been modeled properly. With these considerations in mind, we now present the results of our own simulations.

4.2. Convective Dilution Scenario

We attempt in this section to interpret the hydrogen abundance pattern observed in DB/DBA white dwarfs and cool, He-rich DA/DZA stars, as depicted in Figure 8. We first begin by exploring the scenario where a thin, superficial hydrogen layer of a given mass has been convectively diluted within the helium envelope, resulting in a homogeneously mixed H/He convection zone, with some of this hydrogen lying below the convection zone, as discussed in Section 3.3. More specifically, we *assume* the hydrogen layer has been convectively diluted, and we do not pay attention to the dilution process, for the moment. The results of our simulations for homogeneously mixed models at $0.6 M_{\odot}$ are presented in Figure 14 for both the $\text{ML2}/\alpha = 0.6$ and $\alpha = 2$ versions of the mixing-length theory, together with the observed hydrogen abundance pattern reproduced from Figure 8. Each curve in this plot represents the location of white dwarf stars with a constant value of $\log M_{\text{H}}/M_{\odot}$, labeled in the figure. These results are similar to those presented in Figures 1 and 2 of MacDonald & Vennes (1991), although our calculations are restricted to $\text{H}/\text{He} < 1$ (i.e. the upper portions of their figures). For the models with $\log M_{\text{H}}/M_{\odot} \lesssim -14$, the sudden change of slope near 20,000 K for the $\text{ML2}/\alpha = 0.6$ models ($\sim 23,000$ K for the $\alpha = 2$ models) corresponds to the temperature where the bottom of the helium convection zone sinks deep into the star (see the top left panel of Figures 9 and 10, where hydrogen is considered a trace element).

The hottest DBA stars in our sample near $T_{\text{eff}} \sim 24,000$ K have inferred total hydrogen masses around $\log M_{\text{H}}/M_{\odot} \sim -16.5$ with $\text{ML2}/\alpha = 0.6$ models, and around -15 with $\alpha = 2$

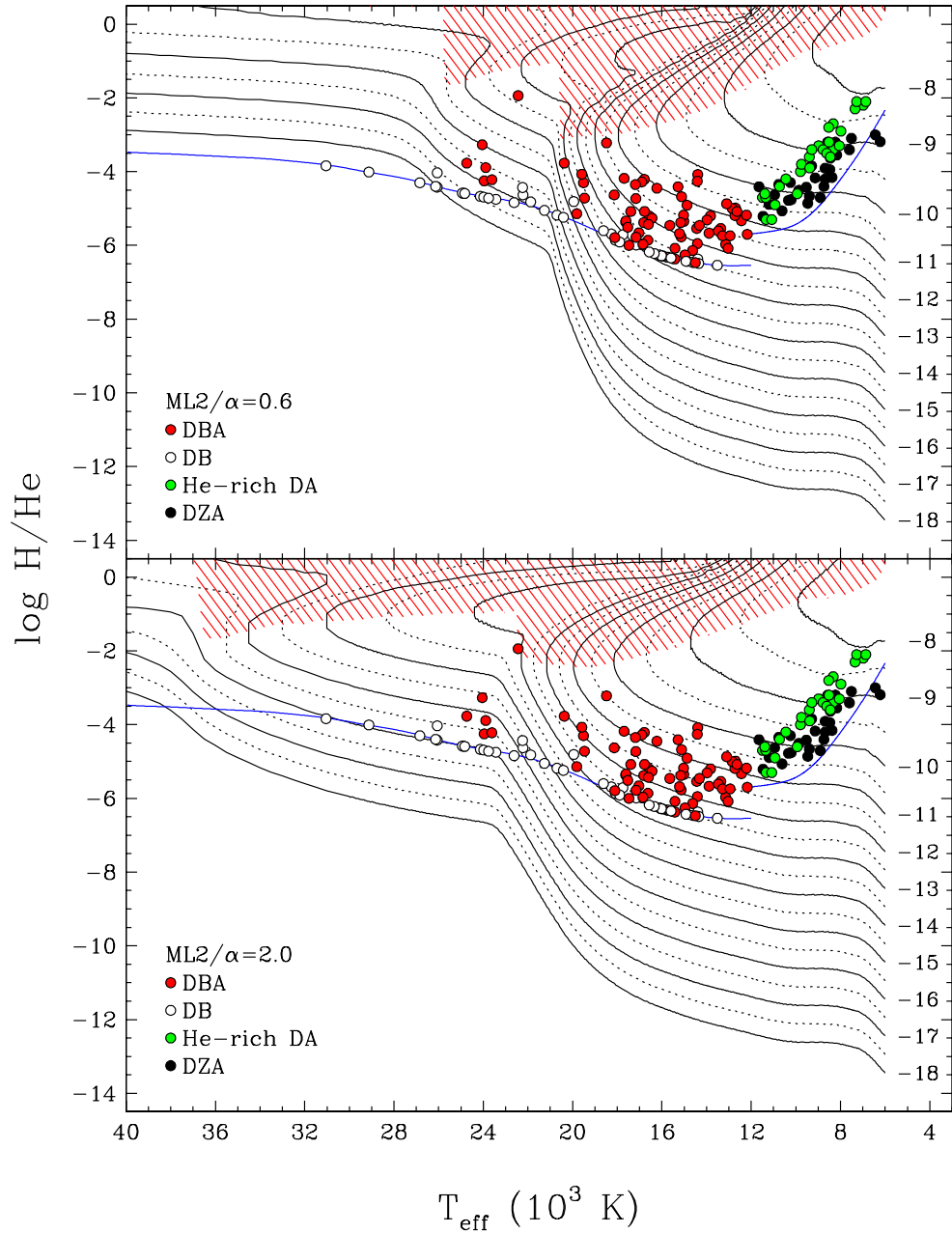


Fig. 14.— Results of our simulations for homogeneously mixed models at $0.6 M_{\odot}$ for both the $ML2/\alpha = 0.6$ (upper panel) and $\alpha = 2$ (lower panel) versions of the mixing-length theory. Each curve is labeled with the corresponding value of $\log M_{\text{H}}/M_{\odot}$. Results from Figure 8 are also reproduced; limits on the hydrogen abundance set by our spectroscopic observations are shown by the solid blue lines. The red hatched regions represent the forbidden region through which white dwarfs cannot evolve continuously with a constant total hydrogen mass (see text).

models. Larger hydrogen masses are required with $\alpha = 2$ models to produce the same photospheric hydrogen abundance since the convection zone is much deeper in these models (see Figures 9 and 10). Notice that these hot DBA white dwarfs will rapidly evolve as DB stars at lower effective temperatures — below our H α detection threshold — when the hydrogen content becomes increasingly more diluted within the growing helium convection zone, a conclusion also reached by Koester & Kepler (2015, see their Section 5.1). The bulk of the DBA stars in our sample, however, is found at lower temperatures ($T_{\text{eff}} \lesssim 20,000$ K). Bergeron et al. (2011) showed that this corresponds to the temperature range where the DB/DA ratio reaches a value of 25%, based on the luminosity function obtained from the subset of white dwarfs identified in the Palomar-Green survey, while this fraction drops to only half this value above $T_{\text{eff}} \sim 20,000$ K. As mentioned above, this corresponds also to the temperature at which the bottom of the helium convection zone sinks rapidly into the stellar envelope, strongly suggesting that the convective dilution model is the most likely scenario responsible for the transformation of some DA white dwarfs into DBA stars.

The results of Figure 14 indicate that the bulk of the DBA stars in our sample can be explained in terms of homogeneous models with total hydrogen masses between $\log M_{\text{H}}/M_{\odot} = -13$ and -10 according to our ML2/ $\alpha = 2$ models. Note how the DBA abundance determinations are well contained within these two boundaries. In particular, a DBA star in this temperature range ($T_{\text{eff}} \lesssim 20,000$ K) is expected to show H α almost all the way down to $\sim 12,000$ K when the helium lines vanish. This is not necessarily the case with the ML2/ $\alpha = 0.6$ models, which require thinner hydrogen layers of the order of $\log M_{\text{H}}/M_{\odot} \sim -15$ to account for the DBA stars around 20,000 K; hydrogen features in these stars would rapidly become undetectable as they cool off by only ~ 2000 K or so.

The cool, He-rich DA/DZA white dwarfs in Figure 14 require much larger hydrogen masses, ranging from $\log M_{\text{H}}/M_{\odot} = -11$ to -8 , regardless of the assumed convective efficiency. Clearly, the progenitors of these objects are not DBA white dwarfs, which have much lower hydrogen content; DBA stars are likely to evolve instead into DC stars below $T_{\text{eff}} \sim 12,000$ K since their expected hydrogen abundances will be below our H α detection threshold in this temperature range. Note, however, that the distinction between these two populations cannot be easily made at the boundary near 12,000 K, and some of the He-rich DA/DZA white dwarfs with the lowest hydrogen abundances can probably be interpreted as cooled off DBA stars. We can also see that under the assumption of a constant total hydrogen mass, a given He-rich DA/DZA star will evolve at an almost constant photospheric hydrogen abundance, and will eventually (and rather quickly) turn into a DC star, that is, below our H α detection threshold. Because of the large differences in total hydrogen mass between the DBA white dwarfs and the cool, He-rich DA/DZA stars, we must conclude that the latter have a different origin, most likely resulting from the mixing of the convective

hydrogen layer with the deeper helium convection zone, a scenario we explore further in Section 4.4.

We now turn our attention to the convective dilution process more specifically. In order for a DBA star to cool off with a constant total mass of hydrogen already homogeneously mixed within the convective layer, it must be able to evolve *continuously* from the left to the right in Figure 14 along a single sequence with a given value of $\log M_{\text{H}}/M_{\odot}$. In other words, the sequence cannot turn back towards higher temperatures at any point (see also MacDonald & Vennes 1991). These considerations thus allow us to define a region in the $T_{\text{eff}} - \text{H/He}$ parameter space — represented by the red hatched regions in Figure 14 — through which white dwarfs cannot evolve continuously with a constant hydrogen mass. For instance, we already presented an example in Figure 13 where we showed that homogeneously mixed stellar envelopes with a total hydrogen mass of $\log M_{\text{H}}/M_{\odot} = -13$ could not exist above $T_{\text{eff}} \sim 20,000$ K with $\text{ML2}/\alpha = 0.6$ (or above $T_{\text{eff}} \sim 25,000$ K with $\alpha = 2$), in agreement with the results of Figure 14. White dwarfs containing such large amounts of hydrogen can only exist as chemically stratified white dwarfs above these temperatures, with hydrogen floating in diffusive equilibrium on top of the helium envelope, corresponding to a DA star configuration. Similar conclusions can be reached from an examination of the results displayed in Figures 1 and 2 of MacDonald & Vennes (1991).

The results presented in Figure 14 indicate that some white dwarfs can indeed evolve with a constant hydrogen mass diluted within the convection zone, but only if the total hydrogen mass is very small, i.e. $\log M_{\text{H}}/M_{\odot} \lesssim -15.5$ for $\text{ML2}/\alpha = 0.6$ models, and $\log M_{\text{H}}/M_{\odot} \lesssim -16$ for $\alpha = 2$ models. Incidentally, the hottest DBA stars in our sample near $T_{\text{eff}} \sim 24,000$ K can be explained by this scenario, but only if the convective efficiency is low. All the cooler DBA stars in our sample can only be explained by some kind of *dynamical transformation*, such as the convective dilution scenario, where the superficial hydrogen layer of a chemically stratified DA white dwarf is convectively diluted by the underlying helium convective envelope. In other words, this convective dilution process will allow a given DA star to cross the red-hatched region in Figure 14, directly into the region where DBA stars are found. The question is, under which physical circumstances?

As discussed in Section 4.1, MacDonald & Vennes (1991) concluded that DA stars could be transformed into DB white dwarfs near $T_{\text{eff}} \sim 18,000$ K if the hydrogen layer mass was of the order of $\log M_{\text{H}}/M_{\odot} \sim -14$. We emphasize that this so-called convective dredge-up temperature (T_{ed}) given in their Table 1 corresponds simply to the coolest stratified DA model in their grid for this particular hydrogen layer mass (i.e., the coolest point on the lower branch in their Figure 1). If we now take these results at face value, this implies — according to our results displayed in Figures 11 and 12 — that the convective dilution of

a hydrogen layer with $\log M_{\text{H}}/M_{\odot} \sim -14$ will occur near $T_{\text{eff}} \sim 20,000$ K if at least $\sim 50\%$ of the total energy flux (the magenta contours) is transported by convection⁵. If we adopt arbitrarily this fraction of the total flux for the convective dilution process to occur, we find that the DA-to-DB transition will take place at $T_{\text{eff}} \sim 32,000$ K for $\alpha = 2$ models with $\log M_{\text{H}}/M_{\odot} \sim -15$, a temperature that is entirely consistent with the results of MacDonald & Vennes (see the S2 results in their Table 1). More importantly, however, for hydrogen layers between $\log M_{\text{H}}/M_{\odot} = -13$ and -10 , where the bulk of the DBA stars in our sample are found, the underlying helium convection zone is almost completely inhibited, and the thin convection zone still present in our models is most certainly too inefficient (less than 1% of the total flux) to dilute the superficial hydrogen layer.

We must therefore conclude that most — but not all — helium-atmosphere white dwarfs below $T_{\text{eff}} \sim 30,000$ K that contain traces of hydrogen cannot be explained in terms of a convective dilution scenario. The total amount of hydrogen present in these white dwarfs implies that their DA progenitors had hydrogen layers that were far too thick to allow the convective dilution process to occur. A similar conclusion has also been reached by MacDonald & Vennes (1991). The most common solution proposed to solve this problem is to assume that a significant fraction of DB stars are indeed the result of a convective dilution scenario, with DA progenitors having very thin hydrogen layers ($\log M_{\text{H}}/M_{\odot} \lesssim -15$). After the DA-to-DB transition, accretion of hydrogen from the interstellar medium or other external bodies (comets, disrupted asteroids, etc.) increases the hydrogen content in the stellar envelope, up to the level observed in DBA stars (see, e.g., MacDonald & Vennes 1991). We explore this scenario more quantitatively in the next section.

4.3. Accretion of Hydrogen from External Sources

Our results from the previous section strongly suggest that a simple convective dilution model with a constant hydrogen mass is an unlikely evolutionary scenario for the origin of DBA and cool, He-rich DA/DZA white dwarfs. We explore here the possibility of accretion from external sources, either from the interstellar medium, or from other bodies such as comets, disrupted asteroids, or small planets. To model this process, the various episodes of accretion occurring during the white dwarf evolution are averaged with a constant accretion rate. We first compute the total accreted mass of hydrogen for various rates ranging from $\log M_{\text{H}}/M_{\odot} = -27.5$ to -17.0 per year by steps of 0.5 dex using the cooling times of a typical

⁵Note that the hydrogen layer masses in Figures 11 and 12 are given in terms of $\log q(\text{H}) \equiv \log M_{\text{H}}/M_{\star} = \log M_{\text{H}}/M_{\odot} - 0.22$ for a $0.6 M_{\odot}$ white dwarf.

DB star at $0.6 M_{\odot}$ (see Section 2.1.3). For a given effective temperature, these hydrogen masses are then converted into hydrogen-to-helium abundance ratios using our $T_{\text{eff}} - \text{H}/\text{He}$ parameter space map (Figure 13). We assume here for simplicity that the material has been accreted on top of a pure helium atmosphere; results obtained with a small initial hydrogen mass of $\log M_{\text{H}}/M_{\odot} \sim -15$ are almost identical to those presented here since such a small amount of hydrogen yields photospheric abundances of only $\text{H}/\text{He} \sim 10^{-10} - 10^{-8}$ in the temperature range where most of the DBA stars are found (see Figure 14).

Results of these simulations are displayed in Figure 15 for both prescriptions of the mixing-length theory considered in this study. Our results indicate that the amount of hydrogen observed in the bulk of DBA white dwarfs in our sample can be accounted for with average accretion rates ranging from 10^{-22} to $10^{-19} M_{\odot} \text{ yr}^{-1}$, and from 10^{-20} to $10^{-17} M_{\odot} \text{ yr}^{-1}$ for the cool, He-rich DA/DZA stars. These rates are totally compatible with those estimated in previous studies (MacDonald & Vennes 1991; Dufour et al. 2007a; Voss et al. 2007; Bergeron et al. 2011; Koester & Kepler 2015). The fundamental problem with this accretion scenario, however, is that for such a range of accretion rates, our simulations at higher effective temperatures predict hydrogen abundances in the $T_{\text{eff}} - \text{He}/\text{H}$ plane where homogeneously mixed models cannot evolve in a continuous fashion. In other words, for the accretion model to be valid, the evolutionary tracks would have to cross the “forbidden” red hatched regions in Figure 15, as was the case for the convective dilution scenario.

As a simple example, a pure DB star will take roughly $\sim 10^7$ years to cool down to $T_{\text{eff}} = 30,000$ K (see Figure 6), and even for an accretion rate as low as $10^{-20} M_{\odot} \text{ yr}^{-1}$, will have accumulated $\sim 10^{-13} M_{\odot}$ of hydrogen during this period. By referring to the results shown in Figure 13, one can see that this configuration is impossible as a homogeneously mixed white dwarf, with either version of the mixing-length theory. Such an object can only exist as a DA star, with all the hydrogen floating in diffusive equilibrium on top of the helium envelope, which according to Figures 9 and 10 (right panels), will not mix until it reaches $T_{\text{eff}} \sim 11,000$ K. We are thus forced to conclude that the hydrogen abundances measured in DBA white dwarfs, and cool He-rich DA/DZA stars as well, cannot be accounted for by any kind of accretion mechanism onto a pure helium DB star. Our conclusion remains the same even if we allow for an initial hydrogen mass of $\log M_{\text{H}}/M_{\odot} \sim -15$ instead of a DB white dwarf with a pure helium atmosphere.

Note that it is always possible to invoke the accretion of large bodies such as comets, disrupted asteroids, or small planets as the source of hydrogen in DBA stars if the accretion process begins only *after* the white dwarf has evolved through the forbidden red hatched region in Figure 15 — either as a pure helium-atmosphere DB star or as a DA star with a very thin hydrogen layer — but this would require extraordinary circumstances for such a

process to occur precisely below 20,000 K for a significant fraction of DB stars.

4.4. Convective Mixing Scenario

At lower effective temperatures ($T_{\text{eff}} \lesssim 13,000$ K), DA white dwarfs with thin enough hydrogen layers may get a second opportunity to turn into helium-dominated atmospheres as a result of *convective mixing*, which occurs when the bottom of the superficial hydrogen convective envelope sinks into the star, and eventually connects with the underlying and more massive helium convection zone (see Figures 11 and 12). At this point, it is generally assumed that both hydrogen and helium convection zones merge, with the total hydrogen content homogeneously mixed within this H/He convective layer. As discussed in the Introduction, convective mixing is the most likely explanation to account for the significant increase in the ratio of non-DA to DA stars below $T_{\text{eff}} \sim 10,000$ K. After convective mixing occurs, the star will continue its evolution with a homogeneously mixed envelope with constant total hydrogen mass, a scenario already described in Section 4.2. Our stratified model structures, displayed in Figures 11 and 12, indicate that this mixing process can occur if the mass of the hydrogen layer is in the range $\log M_{\text{H}} \sim 10^{-15}$ to $10^{-6} M_{\star}$, where the upper limit is set by the maximum depth reached by the bottom of the hydrogen convection zone near $T_{\text{eff}} \sim 5000$ K (see also Figure 40 of Bergeron et al. 1997). However, for hydrogen layers thinner than $M_{\text{H}} \sim 10^{-14} M_{\star}$, the convective dilution process discussed in Section 4.2 is most likely to occur at much higher temperatures ($T_{\text{eff}} \gtrsim 20,000$ K), hence a more realistic lower limit for the occurrence of convective mixing is set here at $M_{\text{H}} = 10^{-14} M_{\star}$. To model the convective mixing scenario, we thus calculated the effective temperature at which the hydrogen and helium convection zones connect in a $0.6 M_{\odot}$ stratified envelope model, for a given value of the total hydrogen mass M_{H} . From that point on, we assume complete mixing, and follow the evolution at lower effective temperatures using the homogeneous sequences with the corresponding value of M_{H} , as described in Section 4.2.

Results of our convective mixing simulations are displayed in Figure 16 for both prescriptions of the mixing-length theory considered in this study. The blue solid line in this figure indicates the effective temperature at which mixing occurs, and the predicted H/He abundance ratio upon mixing. After mixing, the white dwarf evolves at a constant value of M_{H} in the region represented by the cyan area in Figure 16. The particular behavior of the mixing temperature as a function of H/He can be explained qualitatively in the following way. Since the bottom of the hydrogen convection zone gets deeper as the white dwarf cools off (see right panels of Figures 11 and 12), the effective temperature at which convective mixing occurs will depend strongly on the thickness of the hydrogen layer — the thicker the

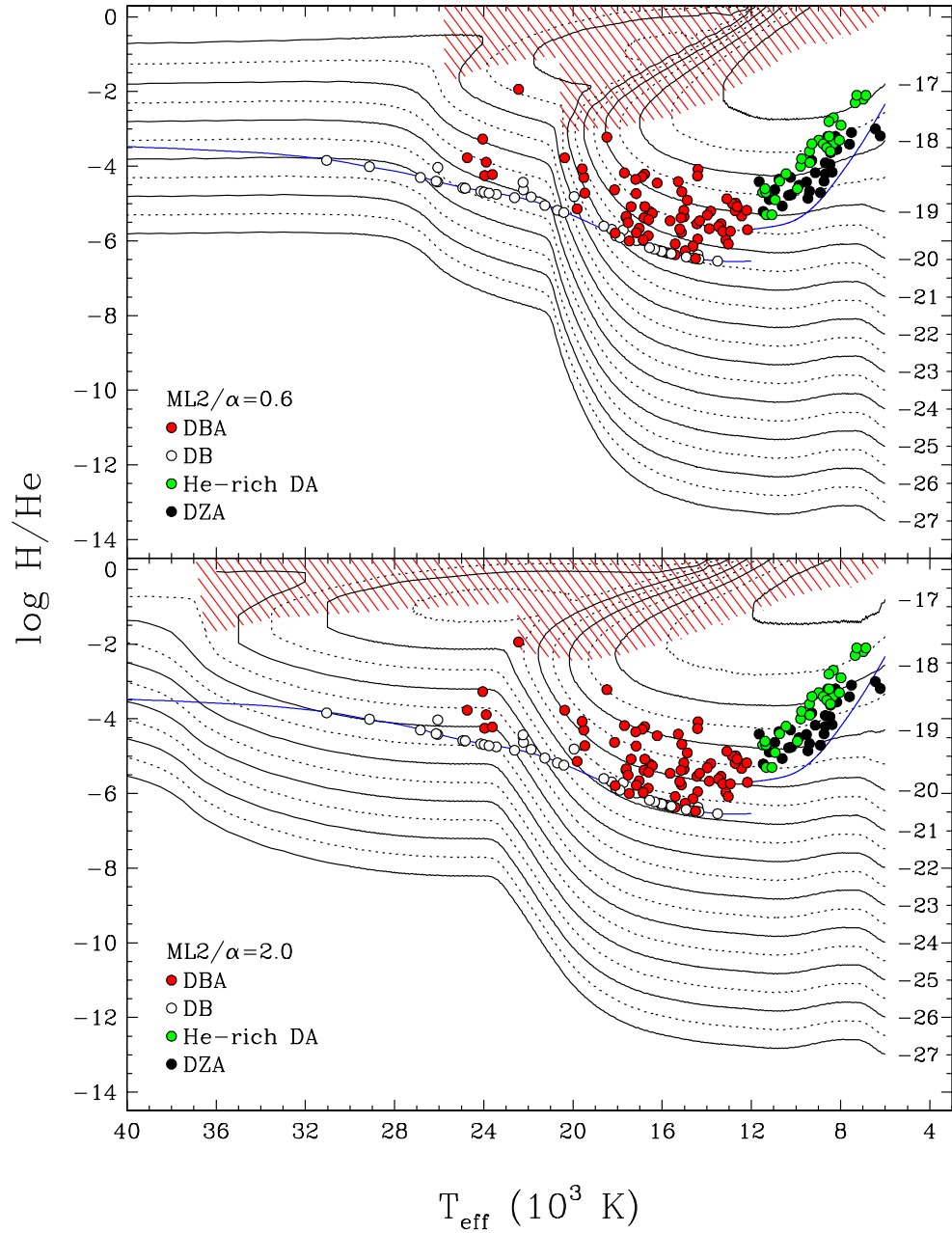


Fig. 15.— Results of our accretion simulations for models at $0.6 M_{\odot}$ subject to constant accretion rates of hydrogen. Each curve is labeled with the corresponding total mass of hydrogen accreted in M_{\odot} per year on a logarithmic scale. Calculations are shown for both the $ML2/\alpha = 0.6$ (upper panel) and $\alpha = 2$ (lower panel) versions of the mixing-length theory. Results from Figure 8 are also reproduced. The red hatched regions represent the forbidden region through which white dwarfs cannot evolve continuously (see text).

hydrogen envelope, the lower the mixing temperature. Furthermore, since the depth of the mixed H/He convection zone remains almost constant in this temperature range (see Figures 9 and 10), the predicted H/He abundance ratio upon mixing increases with decreasing mixing temperature, as shown by our simulations in Figure 16. This mixing temperature can also be made significantly hotter in our calculations if we allow for even a modest convective overshooting. For instance, we show in Figure 17 the extent of the convection zones in a typical sequence of stratified models from our grid, by allowing both hydrogen and helium convection zones to overshoot over a distance of one pressure scale height, a completely reasonable assumption (see, for instance, Tremblay et al. 2015). In the example displayed in Figure 17, this simple prescription increases the mixing temperature by ~ 500 K. The results of convective overshooting applied to all our models are indicated by the dashed blue line in Figure 16.

Also reproduced in Figure 16 are the hydrogen abundances measured in cool, He-rich DA/DZA stars, which are the objects of interest in the present context. As discussed in Section 4.2, under the assumption of a constant total hydrogen mass, He-rich DA/DZA stars will evolve at an almost constant photospheric hydrogen abundance, and will eventually turn into DC (or DZ) stars, that is, below our $H\alpha$ detection threshold (see Figure 8). Due to these observational limitations, the observed sequence in Figure 16 defines in fact only the blue edge of a region in T_{eff} and H/He where these objects could be found; higher signal-to-noise observations should allow the detection of hydrogen in helium-rich atmospheres at even lower temperatures.

Interestingly enough, the overall trend of the H/He abundance ratio predicted by the convective mixing scenario, as a function of the mixing temperature, represents an excellent match to the blue edge defined by the measured hydrogen abundances in cool, He-rich DA and DZA stars, particularly if we allow for a more convective efficiency ($ML2/\alpha = 2$) and a modest convective overshooting (cyan region defined by the dashed blue line in the bottom panel of Figure 16). More specifically, the convective mixing scenario predicts higher hydrogen abundances in cooler white dwarfs, as observed here. Also, note the absence of white dwarfs at $T_{\text{eff}} \sim 10,000$ K in our sample with large hydrogen abundances, as predicted by the models. The overall agreement between the location of the cool, He-rich DA/DZA stars and the region predicted by our simulations (shown in cyan) clearly demonstrates that the convective mixing scenario is the most plausible interpretation for the presence of traces of hydrogen in cool, helium-atmosphere white dwarfs.

In the same context, we also show in Figure 16 the five helium-atmosphere white dwarfs with exceptionally high hydrogen abundances discussed in Gentile Fusillo et al. (2017) and references therein; these are, from hottest to coolest, SDSS J124231.07+522626.6, GD 16,

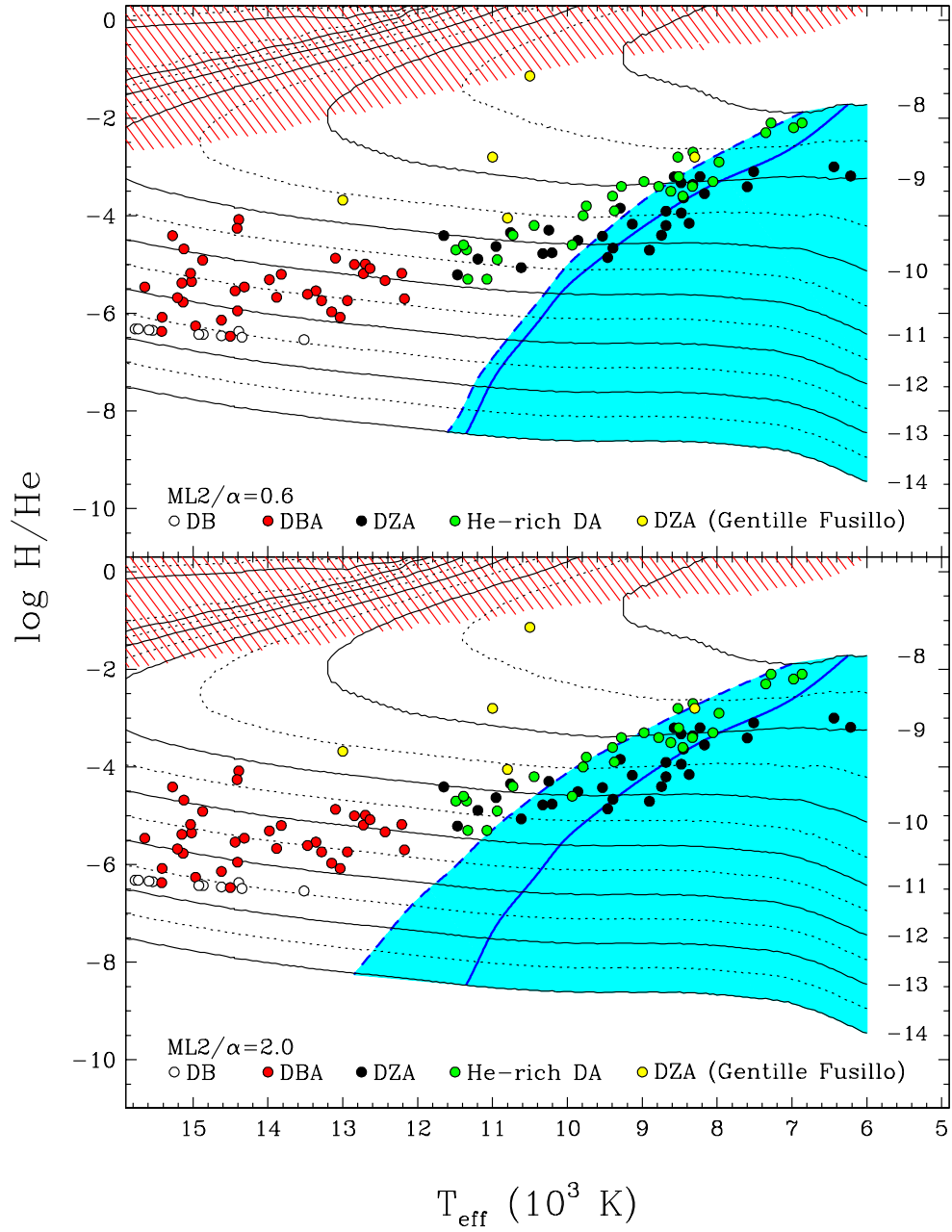


Fig. 16.— Results of our convective mixing simulations for models at $0.6 M_{\odot}$, assuming that after mixing occurs, the total hydrogen mass is distributed in the way described in Section 3.3. Each curve is labeled with the corresponding value of $\log M_{\text{H}}/M_{\odot}$. The solid blue line shows the predicted hydrogen-to-helium abundance ratio as a function of the temperature at which mixing occurs, while the dashed blue line allows for convective overshooting over one pressure scale height; the filled cyan area represents the region where white dwarfs will evolve after mixing has occurred. Calculations are shown for both the $ML2/\alpha = 0.6$ (upper panel) and $\alpha = 2$ (lower panel) versions of the mixing-length theory. Results from Figure 8 are also reproduced, together with the objects discussed in Gentile Fusillo et al. (2017, see text).

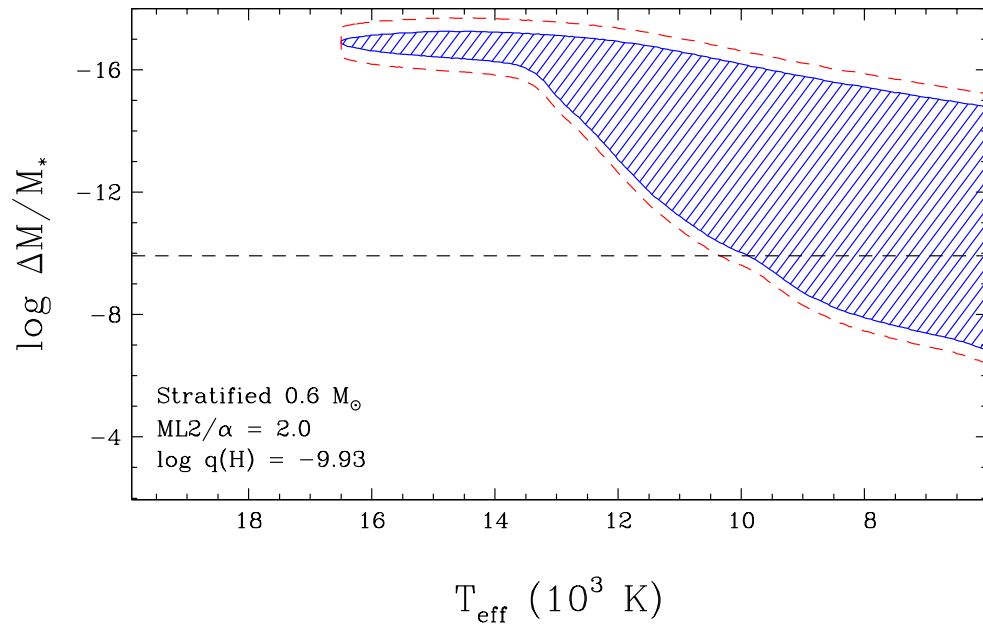


Fig. 17.— Example of envelope structures, as a function of effective temperature, for chemically stratified white dwarf models, with parameters given in the figure. The convection zones are shown by the hatched region, while the red dashed line shows the extent of the hydrogen and helium convection zones allowing for convective overshooting over a distance of one pressure scale height.

PG 1225–079, GD 362, and GD 17. While the amount of hydrogen in these objects has been considered exceptional, thus requiring large external sources of hydrogen — from the accretion of water-bearing planetesimals for instance — our results indicate that even though this is probably true for SDSS J124231.07+522626.6, GD 16, and GD 362, *convective mixing alone* can provide sufficient amounts of hydrogen without invoking additional sources in the case of PG 1225–079 and GD 17.

We end this section by summarizing in Table 3 the effective temperatures at which the transition from a hydrogen-atmosphere to a helium-atmosphere white dwarf occurs as a function of the thickness of the hydrogen layer ($\log M_{\text{H}}/M_{\odot}$), for both the convective dilution and convective mixing scenarios, and for both prescriptions of the mixing-length theories assumed in our study. We also provide the predicted hydrogen-to-helium abundance ratios when the transition occurs. As discussed in Section 4.2, we simply assume here that the convection dilution process occurs when $\sim 50\%$ of the total energy flux is transported by convection, and for the convective mixing process, we allow both hydrogen and helium convection zones to overshoot over a distance of one pressure scale height, as discussed above. When comparing our results with those presented in Table 1 of MacDonald & Vennes (1991), we find that our transition temperatures compare remarkably well with their convective dredge-up temperatures, both qualitatively and quantitatively, especially given the many different assumptions made in both studies. And once again here, we want to emphasize that neither of these two analyses have properly modeled the convective dilution process, which is a time-dependent *dynamical process*.

5. DISCUSSION

5.1. The origin of hydrogen in DBA stars

The existence of a DB-gap — or DB-deficiency — in the 30,000 to 45,000 K temperature range clearly demonstrates that the DA-to-DB transition must necessarily occur in nature below 30,000 K or so. The only viable physical mechanism for this transition to occur in this temperature regime is the convective dilution of a thin radiative hydrogen layer at the surface of a DA star with the deeper and more massive convective helium zone. Bergeron et al. (2011) showed, however, that the significant increase in the number of DB stars in this temperature range occurs only below $T_{\text{eff}} \sim 20,000$ K, rather than the canonical 30,000 K, where the hottest DB white dwarfs have been identified in the PG survey. This makes perfect sense when looking at our Figures 11 and 12, since the helium convection zone becomes efficient only at much lower temperatures in stratified H/He atmospheres. Since most, but not all, DB white dwarfs below $\sim 20,000$ K in our sample now show traces of hydrogen, with respect

to our previous analysis (Bergeron et al. 2011), it is reasonable to conclude that hydrogen must have a primordial origin.

Actually, 63% of all DB white dwarfs in our enlarged sample are DBA stars, but this fraction increases to 75% if we consider only the objects below 20,000 K. We note that pure DB stars — at least in the optical — still exist in this temperature range, with limits as low as $H/He \lesssim 10^{-6}$. Because of the higher S/N of our sample, these limits are much more stringent than those reported by Koester & Kepler (2015) based on SDSS spectra. We can identify at least two, or perhaps three, channels that could account for the existence of these hydrogen-deficient DB stars. The first one corresponds to the hot DB white dwarfs in the gap. These, apparently, did not have enough hydrogen left in their envelope to build a hydrogen atmosphere and to become DA stars over time, and they will most likely evolve as helium-rich atmospheres throughout their lifetime. The hottest DB stars in our sample above $T_{\text{eff}} \sim 25,000$ K probably belong to this category. A second channel corresponds to DA stars with very thin hydrogen layers — of the order of $M_{\text{H}} \sim 10^{-15} M_{\odot}$ — that would turn into DBA stars at $T_{\text{eff}} \sim 24,000$ K according to our results displayed in Figure 14. But as shown in the same figure, such objects would rapidly turn into pure DB stars as the small amount of hydrogen present in these stars is further diluted in the growing helium convection zone at lower effective temperatures. Finally, there is probably a third, but numerically less important channel producing hydrogen-deficient DB stars at low temperatures, the so-called Hot DQ stars (Dufour et al. 2007b). As discussed in Bergeron et al. (2011, see also Dufour et al. 2008), because the coolest Hot DQ star currently known has a temperature near 18,000 K, these must somehow turn into DB white dwarfs at lower effective temperatures, through a process currently unknown. But the number of known Hot DQ stars is so small, that this particular channel is certainly negligible from an ensemble point of view.

The convective dilution scenario alone can probably account for the amount of hydrogen in the few hottest DBA stars in our sample near $T_{\text{eff}} \sim 24,000$ K. It is worth mentioning in this context that the hot ($T_{\text{eff}} \sim 30,000$ K) DBA star SDSS 1509–0108, which Manseau et al. (2016, see their Figure 14) interpreted as a chemically stratified white dwarf with $\log M_{\text{H}}/M_{\odot} \sim -16.7$, represents an obvious progenitor of these hottest DBA stars in our sample. For the bulk of the DBA white dwarfs, however, the total amount of hydrogen inferred from the photospheric hydrogen abundance is simply too large. DA progenitors with such large hydrogen masses — of the order of $M_{\text{H}} \sim 10^{-13} M_{\odot}$ — would have stratified atmospheres with hydrogen layers so thick that they would not stand a chance to turn into helium-atmosphere DB stars in the appropriate temperature range. We thus conclude that the total mass of hydrogen estimated in DBA stars, assuming complete mixing within the stellar envelope, is too large, and incompatible with a scenario involving the transformation of a DA star progenitor into a DB white dwarf through the convective dilution of a thin

hydrogen atmosphere with the deeper and more massive helium convection zone. DA stars with such massive hydrogen layers would not mix until they reach temperatures that are significantly cooler than the entire DBA population.

Accretion of hydrogen from external sources has thus been invoked repeatedly to explain the total mass of hydrogen determined in DBA stars. One of the most recent studies by Veras et al. (2014) suggested, for instance, the gradual accretion of hydrogen from exo-Oort cloud comets. However, we found in our study that the required amount of accreted material, with even a moderate accretion rate, would build a superficial hydrogen layer thick enough by the time the white dwarf reaches a temperature of $T_{\text{eff}} \sim 30,000$ K, that this object — presumably a DA star — would never turn into a helium-atmosphere DB star. Another obvious problem with the accretion scenario is that even modest amounts of hydrogen accreted at the surface of hot helium-atmosphere white dwarfs in the $\sim 30,000$ K temperature range would easily show up spectroscopically since the extent of the helium convection zone at these temperatures is too small to allow any significant dilution of the accreted material into the deeper envelope (see Figures 9 and 10). We thus conclude that the hydrogen abundances measured in DBA stars cannot be accounted for by any kind of accretion mechanism onto a pure helium DB star progenitor.

Hence we are left with no satisfactory explanation for the presence of hydrogen in the bulk of DBA white dwarfs at the observed abundance level. One explanation proposed by Genest-Beaulieu & Bergeron (2017) is that perhaps hydrogen tends to float in the radiative zone on top of the photosphere rather than being completely mixed within the helium convection zone. They explored this possibility by calculating spectra with an abundance profile given by the diffusive equilibrium approximation in the radiative layers above the convection zone, as illustrated, for instance, in Figure 6 of MacDonald & Vennes (1991). Based on their preliminary calculations, Genest-Beaulieu & Bergeron suggested that the hydrogen-to-helium abundance ratios measured in DBA white dwarfs could be overestimated by perhaps 2 orders of magnitude due to the inhomogeneous H and He abundance profiles in the upper radiative atmosphere. The inhomogeneous profile was only used in their calculation of the synthetic spectrum, however, and the next step, currently underway, is to implement this inhomogeneous hydrogen abundance profile in the calculation of the atmospheric structure itself to get a self-consistent solution.

Yet another possibility, not envisaged explicitly in our analysis, is that primordial hydrogen, highly diluted in a post-born-again PG1159 progenitor, may not have had the time to diffuse upward completely during the cooling process, contrary to what is generally assumed. In that case, not all of the hydrogen would find itself distributed in the convection zone of a DBA star (including a diffusion tail), so that the *observable* hydrogen content could

be much less than the actual amount of that element in a given star. With passing time, more hydrogen would enrich the convection zone of a DBA star from below (as opposed to from above as in the case of accretion). Such a process could potentially explain why a DBA star at $T_{\text{eff}} \sim 18,000$ K, say, with a relatively large quantity of hydrogen in its outer convection zone, could still be the descendant of a $T_{\text{eff}} \sim 25,000$ K star rather characterized by a much smaller amount of hydrogen pollution in its convective atmosphere-envelope. To go further in that direction, however, requires demanding and detailed time-dependent calculations combining evolution, convective mixing, and diffusion. This is beyond the scope of the present paper but deserves consideration for the future.

5.2. The origin of hydrogen in cool, He-rich DA/DZA stars

We have shown that the presence of hydrogen in cool ($T_{\text{eff}} \lesssim 12,000$ K), helium-rich atmosphere white dwarfs discovered in the SDSS is a common phenomenon, although the exact fraction showing $\text{H}\alpha$ remains undetermined. The hydrogen abundances determined in these objects define a sequence in the $\text{H}/\text{He} - T_{\text{eff}}$ diagram — with cooler objects showing larger hydrogen abundances — which overlaps with the abundances measured in DZA white dwarfs, suggesting that the only difference between these two populations is the presence or not of a source of accreted material such as comets, disrupted asteroids, small planets, etc. The cool edge of the sequence is probably just a selection effect due to the increasing difficulty of detecting $\text{H}\alpha$ at low temperatures (see the detection threshold in Figure 8). The blue edge of the sequence is well defined, however, and objects to the left of this sequence could easily be detected; they are thus obviously rare, with a few exceptions discussed in Gentile Fusillo et al. (2017) and in Section 4.4 (see Figure 16). The blue edge of the sequence must therefore have an astrophysical origin.

Our envelope models with constant total hydrogen mass (see Figure 14) clearly show that DBA white dwarfs will not turn into cool, He-rich DA stars, but will instead become DC stars when the hydrogen abundances fall below the detection threshold at low temperatures ($T_{\text{eff}} \lesssim 12,000$ K). Instead our simulations indicate that convective mixing of the thin hydrogen layer with the deeper helium convection zone is the most likely explanation for the presence of hydrogen in cool, He-rich DA/DZA white dwarfs. After mixing, these stars will evolve at an almost constant hydrogen abundance (see Figure 16), eventually turning into DC or DZ stars when $\text{H}\alpha$ falls below the detection threshold. With these considerations in mind, if we assume that the non-DA to DA ratio below $\sim 10,000$ K is near unity (see, e.g., Fontaine & Wesemael 1987) and that $\sim 20\%$ of white dwarfs are DB/DBA stars in the appropriate temperature range (Bergeron et al. 2011), we can estimate that convective mixing eventually occurs for

40% of cool DA stars.

It is also interesting in this context to speculate about the origin of cool DQ stars. Since practically none of them show traces of hydrogen (with a few notable exceptions where a CH feature is present), perhaps the progenitors of these stars are the pure DB stars that show no traces of hydrogen either. Then the reason why some cool non-DA white dwarfs show carbon features while others do not could be related to the same reason why some DB stars appear to have very little, or no hydrogen at all. In the latter case, hydrogen has probably been completely depleted during the earlier born-again post-AGB evolutionary phases. Perhaps then, the overall stellar structure of the progenitor has been affected in such a way to facilitate the carbon dredge-up from the core at low effective temperatures. This could even explain the absence of DQZ stars if these earlier post-AGB phases have somehow managed to wipe out any material surrounding the white dwarf progenitor, preventing any further accretion of heavy elements during the course of its evolution.

We also note that the highest mixing temperature in Figure 16 is $T_{\text{eff}} \sim 13,000$ K, which occurs for $M_{\text{H}} = 10^{-14} M_{\odot}$ in $\text{ML2}/\alpha = 2$ models, that is *above* the blue edge of the ZZ Ceti instability strip (see for instance Figure 33 of Gianninas et al. 2011), while the red edge of the strip at $T_{\text{eff}} \sim 11,000$ K corresponds to a mixing temperature of models with $M_{\text{H}} \sim 10^{-11}$. Hence it is possible that DA stars mix above, or even within, the ZZ Ceti instability strip, implying that asteroseismological analyses of ZZ Ceti stars may not be sampling the entire range of hydrogen layer masses in DA stars.

Many of the ideas and speculations presented in this paper can be studied further by performing statistical analyses of large white dwarf samples such as the SDSS sample. Unfortunately, there are many selection effects in the SDSS, and it is therefore difficult to define a statistically meaningful sample to study the spectral evolution of white dwarf stars. To do things properly, one would require accurate distances for these white dwarfs, a situation that will greatly be improved with the trigonometric parallax measurements from the *Gaia* mission that will be released in the very near future.

We would like to thank the director and staff of Steward Observatory and Kitt Peak National Observatory for providing observing time for this project. We are also grateful to M.-M. Limoges, N. Giammichele, L. Séguin-Charbonneau, and E. M. Green for acquiring some of the spectra used in our analysis. This work was supported in part by the NSERC Canada and by the Fund FRQ-NT (Québec).

REFERENCES

- Beauchamp, A., Wesemael, F., & Bergeron, P. 1997, *ApJS*, 108, 559
- Beauchamp, A., Wesemael, F., Bergeron, P., Fontaine, G., Saffer, R. A., Liebert, J., & Brassard, P. 1999, *ApJ*, 516, 887
- Beauchamp, A., Wesemael, F., Bergeron, P., Liebert, J., & Saffer, R. A. 1996, in *Astronomical Society of the Pacific Conference Series*, Vol. 96, *Hydrogen Deficient Stars*, ed. C. S. Jeffery & U. Heber, 295
- Bergeron, P., Leggett, S. K., & Ruiz, M. T. 2001, *ApJS*, 133, 413
- Bergeron, P., Rolland, B., Limoges, M.-M., Giammichele, N., Séguin-Charbonneau, L., & Green, E. M. 2015, in *Astronomical Society of the Pacific Conference Series*, Vol. 493, *19th European Workshop on White Dwarfs*, ed. P. Dufour, P. Bergeron, & G. Fontaine, 33
- Bergeron, P., Ruiz, M. T., & Leggett, S. K. 1997, *ApJS*, 108, 339
- Bergeron, P., Wesemael, F., Dufour, P., Beauchamp, A., Hunter, C., Saffer, R. A., Gianninas, A., Ruiz, M. T., Limoges, M.-M., Dufour, P., Fontaine, G., & Liebert, J. 2011, *ApJ*, 737, 28
- Brassard, P. & Fontaine, G. 1994, in *IAU Colloq. 147: The Equation of State in Astrophysics*, ed. G. Chabrier & E. Schatzman, Vol. 147, 560
- Castanheira, B. G., Kepler, S. O., Handler, G., & Koester, D. 2006, *A&A*, 450, 331
- Dantona, F. & Mazzitelli, I. 1979, *A&A*, 74, 161
- Deridder, G. & van Renspergen, W. 1976, *A&AS*, 23, 147
- Dufour, P., Bergeron, P., Liebert, J., Harris, H. C., Knapp, G. R., Anderson, S. F., Hall, P. B., Strauss, M. A., Collinge, M. J., & Edwards, M. C. 2007a, *ApJ*, 663, 1291
- Dufour, P., Fontaine, G., Liebert, J., Schmidt, G. D., & Behara, N. 2008, *ApJ*, 683, 978
- Dufour, P., Liebert, J., Fontaine, G., & Behara, N. 2007b, *Nature*, 450, 522
- Fontaine, G., Brassard, P., & Bergeron, P. 2001, *PASP*, 113, 409
- Fontaine, G. & Wesemael, F. 1987, in *IAU Colloq. 95: Second Conference on Faint Blue Stars*, ed. A. G. D. Philip, D. S. Hayes, & J. W. Liebert, 319–326

- Friedrich, S., Koester, D., Christlieb, N., Reimers, D., & Wisotzki, L. 2000, *A&A*, 363, 1040
- Genest-Beaulieu, C. & Bergeron, P. 2017, in *Astronomical Society of the Pacific Conference Series*, Vol. 509, 20th European White Dwarf Workshop, ed. P.-E. Tremblay, B. Gaensicke, & T. Marsh, 201
- Gentile Fusillo, N. P., Gänsicke, B. T., Farihi, J., Koester, D., Schreiber, M. R., & Pala, A. F. 2017, *MNRAS*, 468, 971
- Giammichele, N., Bergeron, P., & Dufour, P. 2012, *ApJS*, 199, 29
- Giammichele, N., Fontaine, G., Brassard, P., & Charpinet, S. 2016, *ApJS*, 223, 10
- Gianninas, A., Bergeron, P., & Ruiz, M. T. 2011, *ApJ*, 743, 138
- Holberg, J. B. & Bergeron, P. 2006, *AJ*, 132, 1221
- Hummer, D. G. & Mihalas, D. 1988, *ApJ*, 331, 794
- Kleinman, S. J., Kepler, S. O., Koester, D., Pelisoli, I., Peçanha, V., Nitta, A., Costa, J. E. S., Krzesinski, J., Dufour, P., Lachapelle, F.-R., Bergeron, P., Yip, C.-W., Harris, H. C., Eisenstein, D. J., Althaus, L., & Córscico, A. 2013, *ApJS*, 204, 5
- Koester, D. 1976, *A&A*, 52, 415
- Koester, D. & Kepler, S. O. 2015, *A&A*, 583, A86
- Limoges, M.-M., Bergeron, P., & Lépine, S. 2015, *ApJS*, 219, 19
- MacDonald, J. & Vennes, S. 1991, *ApJ*, 371, 719
- Manseau, P. M., Bergeron, P., & Green, E. M. 2016, *ApJ*, 833, 127
- McCook, G. P. & Sion, E. M. 1999, *ApJS*, 121, 1
- Schatzman, E. 1945, *Annales d’Astrophysique*, 8, 143
- Subasavage, J. P., Jao, W.-C., Henry, T. J., Harris, H. C., Dahn, C. C., Bergeron, P., Dufour, P., Dunlap, B. H., Barlow, B. N., Ianna, P. A., Lépine, S., & Margheim, S. J. 2017, *AJ*, 154, 32
- Tassoul, M., Fontaine, G., & Winget, D. E. 1990, *ApJS*, 72, 335
- Tremblay, P.-E. & Bergeron, P. 2009, *ApJ*, 696, 1755

Tremblay, P.-E., Ludwig, H.-G., Freytag, B., Fontaine, G., Steffen, M., & Brassard, P. 2015, ApJ, 799, 142

Vauclair, G. & Reisse, C. 1977, A&A, 61, 415

Vennes, S., Pelletier, C., Fontaine, G., & Wesemael, F. 1988, ApJ, 331, 876

Veras, D., Shannon, A., & Gänsicke, B. T. 2014, MNRAS, 445, 4175

Voss, B., Koester, D., Napiwotzki, R., Christlieb, N., & Reimers, D. 2007, A&A, 470, 1079

Wesemael, F., Greenstein, J. L., Liebert, J., Lamontagne, R., Fontaine, G., Bergeron, P., & Glaspey, J. W. 1993, PASP, 105, 761

Table 1. Atmospheric Parameters of DB and DBA White Dwarfs

WD	Name	T_{eff} (K)	$\log g$	$\log \text{H/He}$	M/M_{\odot}	M_V	$\log L/L_{\odot}$	V	$D(\text{pc})$	$\log \tau$	Notes
0000–170	G266-32	13,880 (361)	8.63 (0.12)	–5.67 (0.52)	0.98 (0.07)	12.51	–2.67	14.69	27	8.86	
0002+729	GD 408	14,410 (351)	8.27 (0.09)	–5.95 (0.79)	0.76 (0.06)	11.79	–2.36	14.33	32	8.52	
0017+136	Feige 4	18,130 (438)	8.08 (0.05)	–4.63 (0.21)	0.65 (0.03)	10.98	–1.85	15.37	75	8.07	
0025–032	PB 8252	18,480 (437)	8.20 (0.04)	–3.22 (0.04)	0.72 (0.02)	11.12	–1.89	15.69	82	8.14	
0031–186	KUV 00312–1837	15,020 (396)	8.43 (0.11)	–5.35 (0.34)	0.86 (0.07)	11.96	–2.39	16.66	87	8.60	
0100–068	G270-124	19,820 (531)	8.06 (0.04)	–5.14 (1.06)	0.64 (0.03)	10.78	–1.68	13.95	43	7.91	
0112+104	EGGR 409	31,040 (1056)	7.83 (0.03)	< –3.84 (0.84)	0.53 (0.02)	9.89	–0.75	15.36	123	7.20	1
0119–004	G271-47A	16,060 (404)	8.07 (0.06)	–6.27 (1.70)	0.63 (0.04)	11.23	–2.05	16.00	89	8.24	
0125–236	G274-39	16,550 (436)	8.24 (0.07)	–5.21 (0.32)	0.74 (0.05)	11.43	–2.11	15.38	61	8.33	
0129+246	PG 0129+247	16,450 (461)	8.27 (0.09)	–5.26 (0.40)	0.76 (0.06)	11.49	–2.13	16.09	83	8.35	
0158–160	G272-B2A	24,130 (1369)	7.94 (0.03)	< –4.67 (1.39)	0.57 (0.02)	10.40	–1.26	14.38	62	7.38	
0203–181	HE 0203–180	12,180 (652)	8.90 (0.42)	–5.70 (2.43)	1.14 (0.24)	13.35	–3.12	16.00	33	9.16	
0211+646	Lan 150	20,700 (719)	8.00 (0.04)	< –5.18 (2.18)	0.60 (0.03)	10.62	–1.57	17.43	230	7.77	
0214+699	Lan 158	29,130 (1329)	7.88 (0.05)	< –4.01 (0.97)	0.55 (0.02)	10.07	–0.89	16.60	202	6.96	
0215–024	PB 6822	16,870 (402)	8.12 (0.09)	–5.96 (1.35)	0.66 (0.06)	11.19	–2.00	16.13	97	8.20	
0220+480	GD 27	16,570 (403)	8.33 (0.05)	< –5.12 (0.21)	0.80 (0.03)	11.57	–2.16	15.11	51	8.39	2
0224+683	Lan 142	18,270 (471)	8.23 (0.10)	< –5.69 (2.42)	0.74 (0.07)	11.18	–1.92	17.78	208	8.18	
0244+414	PM J02478+4138	17,170 (439)	8.28 (0.10)	–4.73 (0.27)	0.77 (0.06)	11.41	–2.07	17.40	157	8.31	
0249+346	KUV 02499+3442	13,360 (436)	9.02 (0.21)	–5.54 (1.16)	1.20 (0.11)	13.36	–3.05	16.40	40	9.15	
0249–052	KUV 02498–0515	17,630 (549)	8.15 (0.08)	–5.37 (0.43)	0.68 (0.05)	11.13	–1.94	16.60	123	8.16	
0258+683	Lan 143	14,390 (364)	8.14 (0.10)	–4.08 (0.05)	0.68 (0.07)	11.60	–2.29	16.80	109	8.44	
0300–013	GD 40	14,620 (399)	7.99 (0.12)	–6.14 (1.58)	0.58 (0.07)	11.34	–2.17	15.56	69	8.32	
0308–565	L175-34	22,840 (2016)	8.07 (0.05)	< –4.82 (3.04)	0.64 (0.03)	10.60	–1.43	14.07	49	7.63	2
0336+625	Lan 174	23,960 (2532)	8.09 (0.05)	–4.25 (1.40)	0.66 (0.03)	10.60	–1.36	17.15	203	7.57	
0349+015	KUV 03493+0131	24,860 (1936)	7.95 (0.05)	< –4.59 (1.79)	0.58 (0.03)	10.39	–1.22	17.20	230	7.32	
0414–045	HE 0414–043	13,470 (334)	8.14 (0.10)	–5.61 (0.32)	0.68 (0.07)	11.76	–2.40	15.70	61	8.53	
0418–539	BPM 17731	19,090 (464)	8.10 (0.03)	< –4.57 (0.20)	0.66 (0.02)	10.90	–1.77	15.32	76	8.00	2
0423–145	HE 0423–143	16,900 (401)	8.08 (0.07)	< –5.98 (1.23)	0.64 (0.04)	11.12	–1.97	16.21	104	8.17	
0429–168	HE 0429–165	15,540 (415)	7.99 (0.15)	< –6.35 (3.11)	0.59 (0.09)	11.20	–2.07	15.82	83	8.24	
0435+410	GD 61	16,790 (408)	8.18 (0.08)	–4.21 (0.07)	0.70 (0.05)	11.30	–2.04	14.86	51	8.26	
0437+138	LP 475-242	15,120 (361)	8.25 (0.07)	–4.68 (0.06)	0.75 (0.04)	11.65	–2.27	14.92	45	8.45	
0503+147	KUV 05034+1445	15,640 (382)	8.09 (0.06)	–5.46 (0.28)	0.65 (0.04)	11.33	–2.11	13.80	31	8.29	
0513+260	KUV 05134+2605	24,740 (1334)	8.21 (0.03)	–3.77 (0.34)	0.74 (0.02)	10.76	–1.38	16.70	154	7.67	1
0517+771	GD 435	13,150 (337)	8.13 (0.12)	–5.97 (0.76)	0.67 (0.08)	11.80	–2.44	16.01	69	8.55	
0615–591	L182-61	15,770 (373)	8.04 (0.04)	< –6.32 (1.08)	0.61 (0.03)	11.23	–2.07	13.92	34	8.25	

Table 1—Continued

WD	Name	T_{eff} (K)	$\log g$	$\log \text{H/He}$	M/M_{\odot}	M_V	$\log L/L_{\odot}$	V	$D(\text{pc})$	$\log \tau$	Notes
0716+404	GD 85	17,150 (408)	8.08 (0.06)	< -5.99 (1.28)	0.64 (0.04)	11.09	-1.95	14.94	58	8.16	
0825+367	CBS 73	16,100 (443)	8.10 (0.09)	< -6.26 (2.47)	0.65 (0.06)	11.27	-2.07	17.00	139	8.26	
0835+340	CSO 197	22,230 (1348)	8.25 (0.05)	< -4.63 (1.83)	0.76 (0.03)	10.89	-1.59	16.00	105	7.90	
0838+375	CBS 78	13,520 (553)	8.20 (0.49)	< -6.54 (5.89)	0.71 (0.31)	11.83	-2.43	17.71	149	8.56	
0840+262	TON 10	17,700 (420)	8.28 (0.04)	-4.18 (0.06)	0.77 (0.03)	11.33	-2.01	14.78	49	8.26	
0840+364	CBS 82	21,260 (863)	8.15 (0.05)	< -5.05 (2.60)	0.69 (0.03)	10.80	-1.61	17.03	176	7.86	
0845-188	L748-70	17,470 (418)	8.15 (0.06)	-6.00 (1.55)	0.69 (0.04)	11.16	-1.95	15.55	75	8.18	
0900+142	PG 0900+142	14,860 (351)	8.07 (0.09)	< -6.43 (1.30)	0.63 (0.06)	11.43	-2.19	16.48	102	8.35	
0902+293	CBS 3	18,610 (502)	8.02 (0.07)	< -5.60 (2.22)	0.60 (0.04)	10.82	-1.76	17.00	171	7.98	
0906+341	CBS 94	17,750 (480)	8.12 (0.13)	< -5.71 (2.35)	0.67 (0.09)	11.08	-1.91	17.00	152	8.14	
0921+091	PG 0921+092	19,470 (522)	8.01 (0.04)	-4.72 (0.43)	0.60 (0.03)	10.73	-1.68	16.19	123	7.90	
0948+013	PG 0948+013	16,810 (430)	8.09 (0.05)	-5.38 (0.29)	0.65 (0.03)	11.16	-1.99	15.59	76	8.19	
0954+342	CBS 114	26,060 (1797)	7.98 (0.06)	< -4.03 (0.49)	0.60 (0.03)	10.38	-1.15	17.20	231	7.25	1
1006+413	KUV 10064+4120	15,030 (465)	8.80 (0.19)	-5.18 (0.49)	1.08 (0.11)	12.66	-2.67	17.83	108	8.91	
1009+416	KUV 10098+4138	16,600 (456)	8.67 (0.07)	-5.43 (0.47)	1.01 (0.04)	12.17	-2.40	16.33	67	8.70	
1011+570	GD 303	17,610 (475)	8.16 (0.05)	-5.34 (0.28)	0.69 (0.03)	11.16	-1.95	14.57	48	8.18	
1026-056	PG 1026-057	18,080 (425)	8.11 (0.07)	< -5.86 (1.32)	0.66 (0.04)	11.03	-1.87	16.94	152	8.10	
1038+290	Ton 40	16,630 (390)	8.10 (0.07)	-5.86 (0.82)	0.66 (0.05)	11.20	-2.01	16.94	140	8.22	
1046-017	GD 124	14,620 (352)	8.15 (0.12)	< -6.46 (1.62)	0.68 (0.08)	11.57	-2.26	15.81	70	8.42	
1056+345	G119-47	12,440 (336)	8.23 (0.14)	-5.33 (0.23)	0.73 (0.10)	12.09	-2.60	15.58	49	8.69	
1107+265	GD 128	15,130 (357)	8.11 (0.06)	-5.77 (0.46)	0.65 (0.04)	11.43	-2.18	15.89	78	8.35	
1115+158	PG 1115+158	23,890 (1726)	7.91 (0.05)	-3.89 (0.46)	0.56 (0.03)	10.36	-1.26	16.12	142	7.37	1
1129+373	PG 1129+373	13,040 (358)	8.16 (0.16)	-6.08 (1.25)	0.69 (0.10)	11.87	-2.47	16.23	74	8.58	
1144-084	PG 1144-085	15,730 (377)	8.06 (0.06)	< -6.32 (1.37)	0.63 (0.04)	11.28	-2.09	15.95	86	8.27	
1148+408	KUV 11489+4052	17,530 (615)	8.34 (0.10)	-5.51 (0.88)	0.81 (0.06)	11.45	-2.06	17.33	150	8.33	
1149-133	PG 1149-133	20,370 (574)	8.30 (0.03)	-3.77 (0.13)	0.78 (0.02)	11.08	-1.78	16.29	109	8.08	
1200+249	PM J12033+2439	13,820 (363)	8.22 (0.13)	-5.20 (0.20)	0.73 (0.09)	11.82	-2.41	18.00	171	8.55	
1240+212	PM J12430+2057	14,390 (364)	8.06 (0.11)	< -6.37 (1.68)	0.62 (0.07)	11.48	-2.24	17.37	150	8.39	
1252-289	EC 12522-2855	21,880 (756)	8.03 (0.03)	< -4.82 (1.17)	0.62 (0.02)	10.59	-1.49	15.85	112	7.69	
1311+129	LP 497-114	22,440 (584)	7.90 (0.04)	-1.94 (0.11)	0.55 (0.02)	10.39	-1.37	16.26	149	7.51	
1326-037	PG 1326-037	19,950 (533)	8.03 (0.04)	< -4.81 (0.53)	0.61 (0.02)	10.71	-1.65	15.60	94	7.87	
1332+162	PB 3990	16,780 (419)	8.17 (0.06)	-5.08 (0.26)	0.70 (0.04)	11.28	-2.04	15.98	86	8.25	
1333+487	GD 325	15,420 (370)	8.01 (0.09)	-6.37 (1.66)	0.60 (0.05)	11.24	-2.09	14.02	35	8.27	
1336+123	LP 498-26	15,950 (405)	8.01 (0.07)	-6.29 (1.90)	0.60 (0.04)	11.17	-2.03	14.72	51	8.22	
1351+489	PG 1351+489	26,070 (1522)	7.91 (0.04)	< -4.42 (0.90)	0.56 (0.02)	10.28	-1.11	16.38	166	7.18	1

Table 1—Continued

WD	Name	T_{eff} (K)	$\log g$	$\log \text{H/He}$	M/M_{\odot}	M_V	$\log L/L_{\odot}$	V	$D(\text{pc})$	$\log \tau$	Notes
1352+004	PG 1352+004	13,980 (340)	8.05 (0.09)	-5.31 (0.17)	0.62 (0.06)	11.54	-2.29	15.72	68	8.42	
1403-010	G64-43	15,420 (372)	8.10 (0.06)	-6.08 (0.91)	0.65 (0.04)	11.37	-2.14	15.90	80	8.32	
1411+218	PG 1411+219	14,970 (369)	8.02 (0.07)	-6.26 (1.19)	0.60 (0.04)	11.32	-2.15	14.30	39	8.31	
1415+234	PG 1415+234	17,390 (478)	8.19 (0.06)	-5.08 (0.35)	0.71 (0.04)	11.23	-1.99	16.80	129	8.22	
1416+229	KUV 14161+2255	17,890 (444)	8.25 (0.12)	< -5.91 (2.21)	0.75 (0.08)	11.26	-1.97	16.60	117	8.22	
1419+351	GD 335	12,730 (620)	8.77 (0.40)	-5.19 (0.62)	1.06 (0.24)	12.98	-2.94	16.89	60	9.05	
1421-011	PG 1421-011	16,900 (411)	8.19 (0.07)	-4.28 (0.07)	0.71 (0.05)	11.30	-2.04	15.97	85	8.26	
1425+540	G200-39	14,410 (341)	7.89 (0.06)	-4.26 (0.03)	0.53 (0.04)	11.24	-2.14	15.04	57	8.29	
1444-096	PG 1444-096	17,030 (429)	8.26 (0.07)	-5.66 (0.91)	0.76 (0.04)	11.40	-2.07	14.98	52	8.30	
1445+152	PG 1445+153	20,420 (780)	8.05 (0.06)	< -5.24 (2.74)	0.63 (0.03)	10.71	-1.62	15.55	92	7.84	
1454-630	L151-81A	14,030 (334)	7.95 (0.07)	-4.83 (0.06)	0.56 (0.04)	11.39	-2.22	16.60	110	8.36	2
1456+103	PG 1456+103	24,050 (1206)	7.91 (0.06)	-3.27 (0.14)	0.55 (0.03)	10.35	-1.25	15.89	128	7.35	1
1459+821	G256-18	16,020 (397)	8.08 (0.06)	< -6.28 (1.59)	0.64 (0.04)	11.25	-2.06	14.78	50	8.25	
1540+680	PG 1540+681	22,240 (1304)	7.96 (0.04)	< -4.43 (0.89)	0.58 (0.02)	10.47	-1.42	16.19	139	7.58	
1542+182	GD 190	22,620 (978)	8.04 (0.02)	< -4.84 (1.41)	0.63 (0.01)	10.57	-1.44	14.72	67	7.62	
1542-275	LP 916-27	12,700 (384)	9.13 (0.14)	-4.99 (0.64)	1.26 (0.08)	13.70	-3.23	15.49	22	9.25	
1545+244	Ton 249	12,850 (331)	8.19 (0.12)	-5.00 (0.11)	0.70 (0.08)	11.94	-2.51	15.78	58	8.61	
1551+175	KUV 15519+1730	15,280 (380)	7.80 (0.12)	-4.41 (0.08)	0.48 (0.06)	10.97	-1.99	17.50	202	8.15	
1557+192	KUV 15571+1913	19,510 (546)	8.15 (0.05)	-4.30 (0.26)	0.69 (0.03)	10.93	-1.76	15.40	78	8.01	
1610+239	PG 1610+239	13,280 (332)	8.13 (0.11)	-5.74 (0.42)	0.67 (0.07)	11.77	-2.42	15.34	51	8.53	
1612-111	GD 198	23,430 (1782)	7.96 (0.04)	< -4.75 (2.10)	0.58 (0.02)	10.44	-1.33	15.53	104	7.46	
1644+198	PG 1644+199	15,210 (360)	8.14 (0.06)	-5.68 (0.39)	0.68 (0.04)	11.47	-2.19	15.20	55	8.37	
1645+325	GD 358	24,940 (1114)	7.92 (0.03)	< -4.58 (0.88)	0.56 (0.01)	10.34	-1.19	13.65	45	7.28	1
1654+160	PG 1654+160	26,140 (1211)	7.91 (0.03)	< -4.40 (0.64)	0.56 (0.02)	10.27	-1.10	16.55	180	7.17	1
1703+319	PG 1703+319	14,440 (360)	8.46 (0.10)	-5.54 (0.37)	0.88 (0.06)	12.10	-2.48	16.25	67	8.67	
1708-871	L7-44	23,980 (1686)	8.05 (0.03)	< -4.69 (1.93)	0.63 (0.02)	10.55	-1.34	14.38	58	7.51	
1709+230	GD 205	19,590 (504)	8.08 (0.03)	-4.07 (0.14)	0.65 (0.02)	10.83	-1.71	14.90	65	7.95	
1726-578	L204-118	14,320 (340)	8.20 (0.06)	-5.46 (0.19)	0.71 (0.04)	11.70	-2.33	15.27	51	8.49	
1822+410	GD 378	16,230 (383)	8.00 (0.06)	-4.45 (0.06)	0.59 (0.04)	11.11	-2.00	14.39	45	8.19	
1919-362		23,610 (988)	8.10 (0.02)	-4.22 (0.44)	0.66 (0.01)	10.62	-1.40	13.60	39	7.61	
1940+374	L1573-31	16,850 (406)	8.07 (0.09)	-5.97 (1.50)	0.64 (0.06)	11.13	-1.97	14.51	47	8.18	
2034-532	L279-25	17,160 (403)	8.47 (0.05)	-5.78 (0.59)	0.89 (0.03)	11.73	-2.19	14.46	35	8.48	
2058+342	GD 392A	12,210 (447)	9.05 (0.21)	-5.18 (1.09)	1.22 (0.11)	13.64	-3.23	15.68	25	9.24	
2129+000	G26-10	14,350 (349)	8.25 (0.12)	< -6.49 (1.65)	0.74 (0.08)	11.77	-2.36	15.27	50	8.52	
2130-047	GD 233	18,110 (426)	8.11 (0.07)	-5.79 (1.36)	0.66 (0.04)	11.02	-1.87	14.52	50	8.09	

Table 1—Continued

WD	Name	T_{eff} (K)	$\log g$	$\log \text{H/He}$	M/M_{\odot}	M_V	$\log L/L_{\odot}$	V	$D(\text{pc})$	$\log \tau$	Notes
2144−079	G26-31	16,340 (408)	8.18 (0.05)	< −6.22 (1.45)	0.70 (0.03)	11.36	−2.09	14.82	49	8.30	
2147+280	G188-27	12,940 (399)	8.86 (0.19)	−5.74 (0.96)	1.11 (0.10)	13.10	−2.97	14.68	20	9.08	
2222+683	G241-6	14,920 (383)	8.00 (0.19)	< −6.43 (2.84)	0.59 (0.12)	11.31	−2.15	15.65	73	8.31	
2229+139	PG 2229+139	14,870 (352)	8.15 (0.06)	−4.91 (0.08)	0.69 (0.04)	11.55	−2.24	15.99	77	8.41	
2234+064	PG 2234+064	23,770 (1770)	8.07 (0.03)	< −4.72 (2.10)	0.65 (0.02)	10.58	−1.37	16.03	122	7.56	
2236+541	KPD 2236+5410	15,590 (379)	8.28 (0.07)	< −6.34 (1.67)	0.77 (0.05)	11.63	−2.23	16.19	81	8.43	
2237−051	PHL 363	13,100 (460)	8.73 (0.24)	−4.87 (0.21)	1.04 (0.14)	12.83	−2.85	14.00	17	8.99	
2246+120	PG 2246+121	26,840 (1433)	7.92 (0.04)	< −4.30 (0.65)	0.56 (0.02)	10.25	−1.06	16.73	197	7.13	1
2250+746	GD 554	16,560 (390)	8.15 (0.03)	< −6.18 (0.68)	0.69 (0.02)	11.28	−2.05	16.69	120	8.26	
2253−062	GD 243	17,190 (436)	8.07 (0.09)	−4.35 (0.13)	0.64 (0.06)	11.07	−1.93	15.06	62	8.14	
2310+175	KUV 23103+1736	15,150 (370)	8.37 (0.07)	−5.38 (0.23)	0.82 (0.04)	11.84	−2.34	15.88	64	8.54	
2316−173	G273-13	12,640 (421)	9.11 (0.18)	−5.08 (0.87)	1.25 (0.10)	13.67	−3.22	14.08	12	9.24	
2328+510	GD 406	14,500 (362)	8.03 (0.16)	−6.47 (2.09)	0.61 (0.10)	11.43	−2.21	15.09	54	8.36	
2354+159	PG 2354+159	24,830 (1670)	8.15 (0.03)	< −4.59 (1.78)	0.70 (0.02)	10.67	−1.34	15.78	105	7.58	

Note. — (1) Variable white dwarf of the V777 Her class. (2) Hydrogen abundance based on $\text{H}\beta$.

Table 2. Atmospheric Parameters of Cool, He-rich DA White Dwarfs

WD	Name	T_{eff} (K)	$\log g$	$\log \text{H/He}$	M/M_{\odot}	M_g	$\log L/L_{\odot}$	g	$D(\text{pc})$	$\log \tau$	Notes
0042+141	SDSS J004513.88+142248.1	6980 (197)	8.00	-2.28 (0.13)	0.57	13.68	-3.48	19.20	126	9.19	
0107-003	SDSS J011012.48-000313.5	9790 (434)	8.00	-4.05 (0.23)	0.58	12.34	-2.88	19.38	255	8.82	
0236-094	SDSS J023856.77-092653.6	10,940 (463)	8.00	-4.98 (0.26)	0.58	12.00	-2.69	18.43	193	8.69	
0528+615	SDSS J074250.80+222444.7	10,730 (462)	8.00	-4.47 (0.20)	0.58	12.05	-2.72	19.27	277	8.71	
0739+225	SDSS J074250.80+222444.7	8330 (236)	8.00	-3.44 (0.30)	0.58	12.93	-3.17	19.13	173	9.01	
0748+314	SDSS J075113.24+313249.4	11,490 (550)	8.00	-4.72 (0.09)	0.58	11.85	-2.60	19.19	293	8.63	
0829+532	SDSS J083317.40+531335.5	11,350 (534)	8.00	-4.76 (0.16)	0.58	11.89	-2.62	18.82	243	8.65	
0838+204	SDSS J084113.94+203018.7	8980 (277)	8.00	-3.39 (0.17)	0.58	12.65	-3.04	18.66	159	8.92	
0844+364	SDSS J084757.57+362649.1	9400 (303)	8.00	-3.60 (0.24)	0.58	12.48	-2.96	19.46	248	8.86	
0859+094	SDSS J090150.74+091211.3	8320 (218)	8.00	-2.71 (0.20)	0.58	12.94	-3.17	18.60	135	9.01	
1023+142	SDSS J102626.01+135745.0	8780 (255)	8.00	-3.44 (0.22)	0.58	12.73	-3.07	18.92	172	8.94	
1157+072	SDSS J115948.51+070708.7	9940 (328)	8.00	-4.61 (0.18)	0.58	12.30	-2.86	17.55	112	8.80	
1203+343	SDSS J120555.16+341813.4	11,330 (445)	8.00	-5.31 (0.15)	0.58	11.89	-2.63	18.29	190	8.65	
1246+021	SDSS J124909.03+015559.3	7350 (176)	8.00	-2.38 (0.14)	0.57	13.45	-3.38	18.84	119	9.13	
1307+454	SDSS J130916.90+452342.6	9750 (325)	8.00	-3.82 (0.17)	0.58	12.36	-2.89	18.82	195	8.82	
1345+513	SDSS J134710.47+511640.8	9280 (263)	8.00	-3.46 (0.16)	0.58	12.53	-2.98	18.49	155	8.88	
1409+114	SDSS J141209.94+112902.6	7280 (162)	8.00	-2.12 (0.15)	0.57	13.49	-3.40	18.65	107	9.14	
1412-009	SDSS J141516.10-010912.1	8520 (225)	8.00	-3.25 (0.17)	0.58	12.85	-3.13	18.26	120	8.98	1
1506+017	SDSS J150856.93+013557.0	8060 (186)	8.00	-3.30 (0.15)	0.58	13.07	-3.22	17.98	96	9.04	
1519+397	SDSS J152145.91+393128.1	7980 (182)	8.00	-2.95 (0.17)	0.58	13.11	-3.24	18.54	122	9.05	
1556+110	SDSS J155903.81+105614.8	8530 (213)	8.00	-2.87 (0.15)	0.58	12.84	-3.12	18.52	136	8.98	1
1558+077	SDSS J160053.84+074803.4	6870 (155)	8.00	-2.14 (0.14)	0.57	13.76	-3.50	19.39	133	9.22	1
1617-003	SDSS J161948.91+003445.3	10,440 (359)	8.00	-4.23 (0.18)	0.58	12.14	-2.77	17.88	140	8.75	
1623+222	SDSS J162535.21+221516.4	8620 (242)	8.00	-3.52 (0.18)	0.58	12.80	-3.11	18.75	154	8.97	2
1625+305	SDSS J162721.62+304320.2	8460 (224)	8.00	-3.60 (0.23)	0.58	12.87	-3.14	18.74	149	8.99	
1644+202	SDSS J164645.22+200701.5	9370 (311)	8.00	-3.91 (0.20)	0.58	12.49	-2.96	19.37	237	8.87	
2116+110	SDSS J211852.10+111756.5	11,080 (412)	8.00	-5.37 (0.19)	0.58	11.96	-2.67	16.66	87	8.68	
2134+112	SDSS J213621.56+113726.8	11,390 (521)	8.00	-4.61 (0.16)	0.58	11.88	-2.62	18.29	191	8.64	

Note. — (1) Possible unresolved DA+DC degenerate binary. (2) g band omitted during atmospheric parameter determination.

Table 3. Hydrogen- to Helium-Atmosphere Transition Temperatures

$\log M_{\text{H}}/M_{\odot}$	$\text{ML2}/\alpha = 0.6$		$\text{ML2}/\alpha = 2.0$	
	T_{eff} (K)	$\log \text{H}/\text{He}$	T_{eff} (K)	$\log \text{H}/\text{He}$
–15.0	22,100	–2.8	31,500	–0.3
–14.5	21,000	–2.6	27,950	–2.7
–14.0	19,350	–5.1	22,250	–3.8
–13.5	16,850	–6.6	18,000	–6.6
–13.0	11,250	–7.5	12,350	–7.3
–12.5	11,050	–7.0	12,100	–6.9
–12.0	10,850	–6.7	11,800	–6.4
–11.5	10,550	–6.1	11,450	–6.0
–11.0	10,300	–5.6	11,150	–5.5
–10.5	10,050	–5.1	10,800	–5.0
–10.0	9700	–4.6	10,400	–4.6
–9.5	9250	–4.0	9900	–4.0
–9.0	8650	–3.3	9100	–3.4
–8.5	7850	–2.6	8150	–2.6
–8.0	6850	–1.9	7000	–1.9

6. Online Material

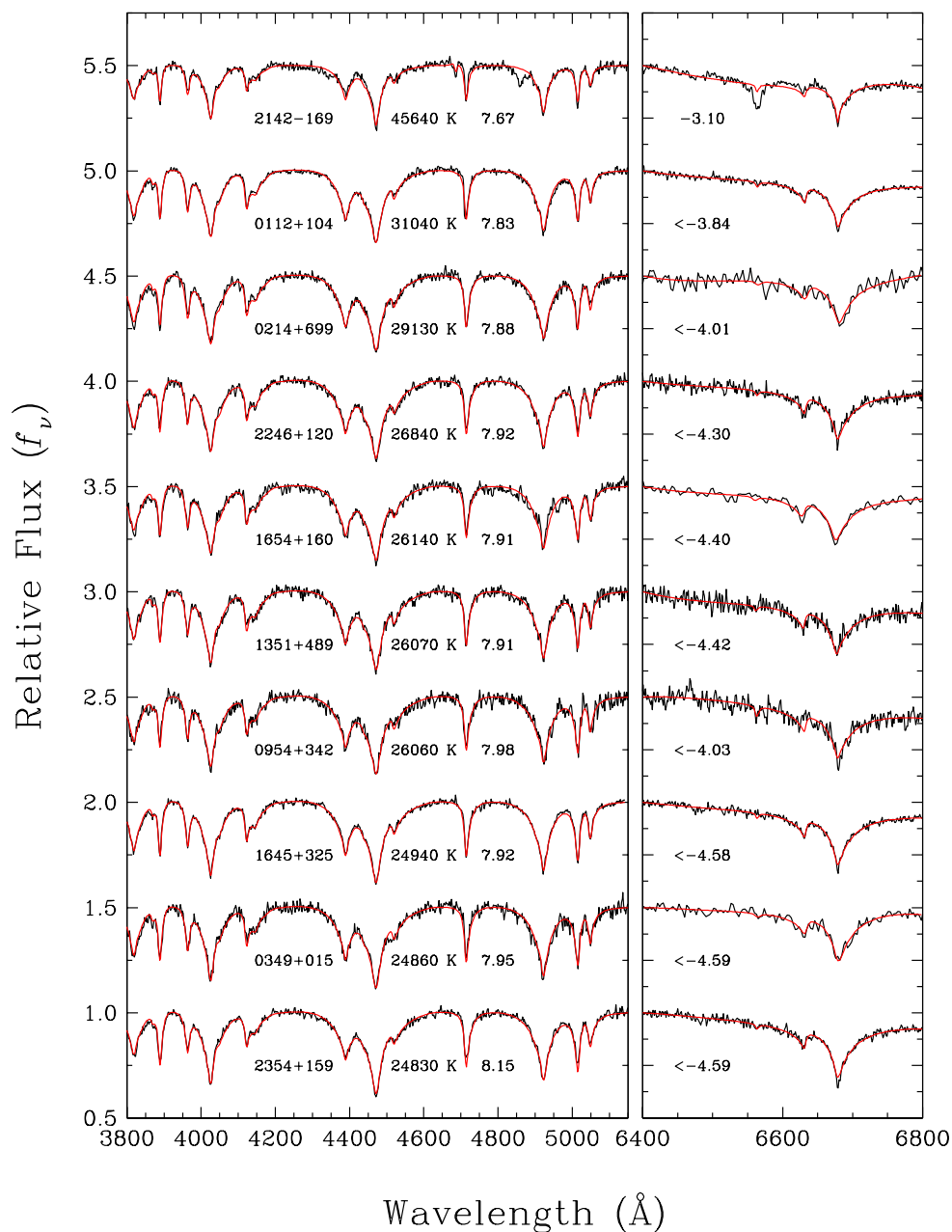


Fig. 18.— Spectroscopic fits for all DB and DBA stars in our sample, in order of decreasing effective temperature. The atmospheric parameters (T_{eff} , $\log g$, $\log \text{H/He}$) of each object are given in the figure. The region near $\text{H}\alpha$ (right panel) is used to measure, or to constrain, the hydrogen abundance. In the case of DB stars, these spectra only provide *upper limits* on the hydrogen-to-helium abundance ratio.

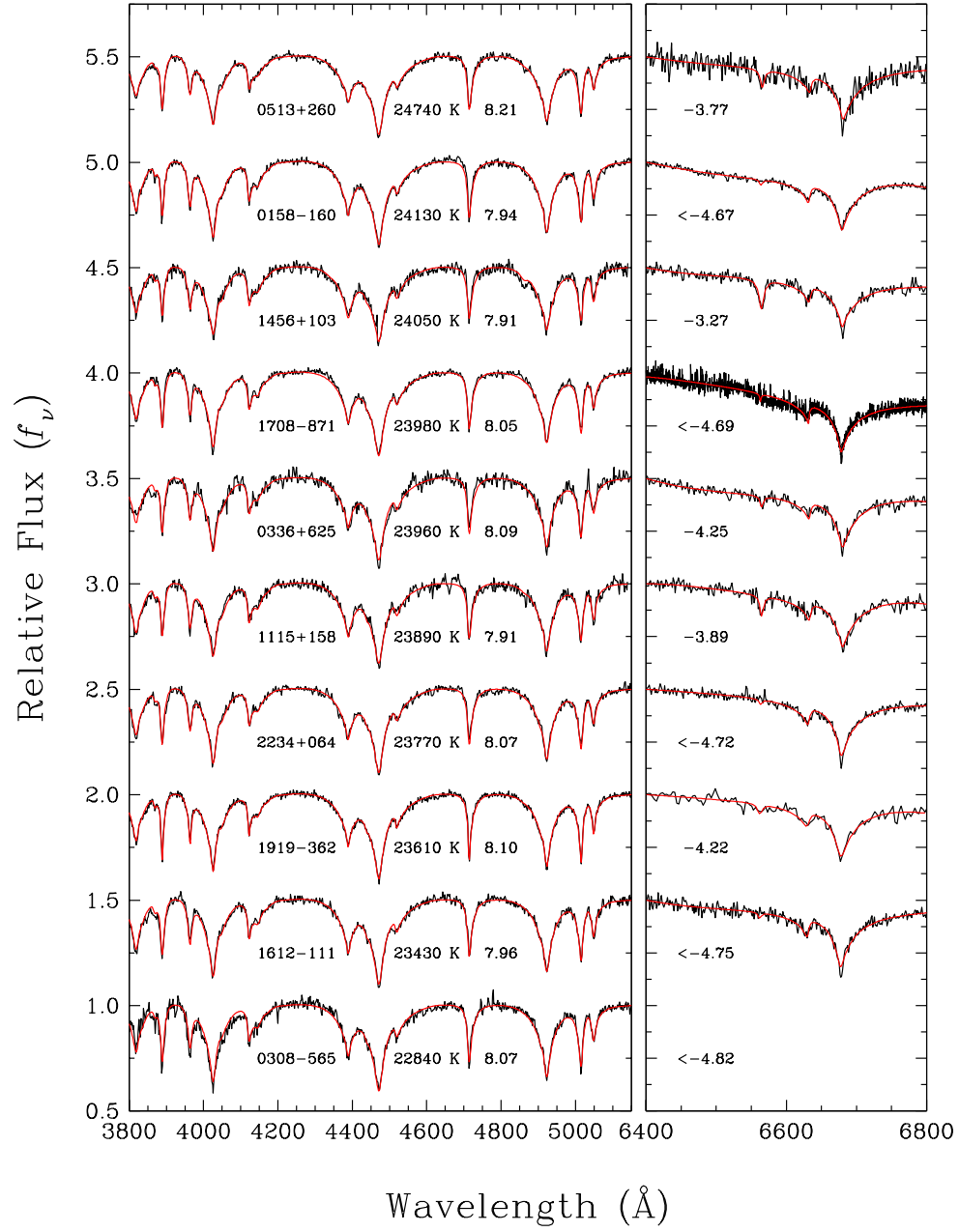


Fig. 18.— (Continued)

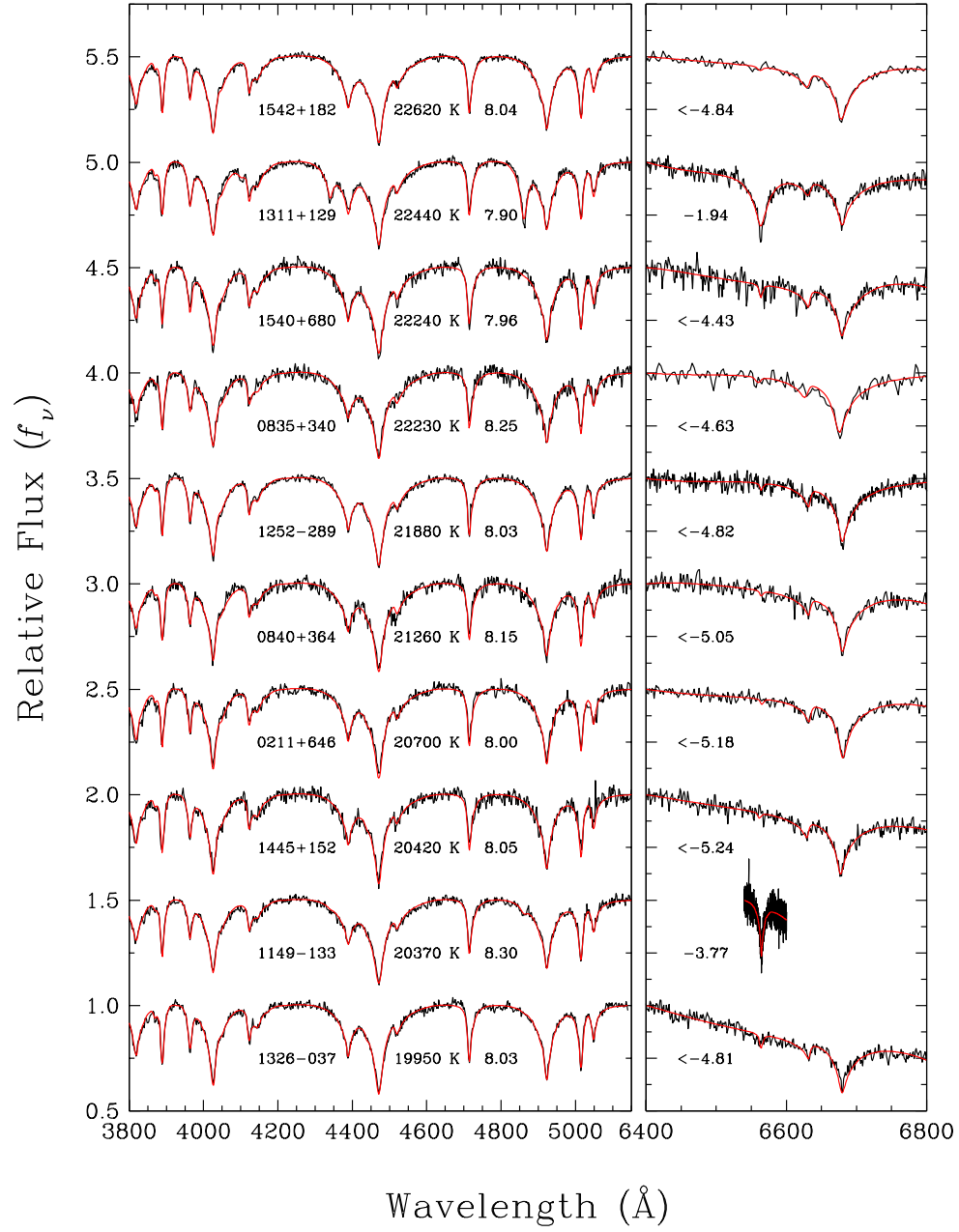


Fig. 18.— (Continued)

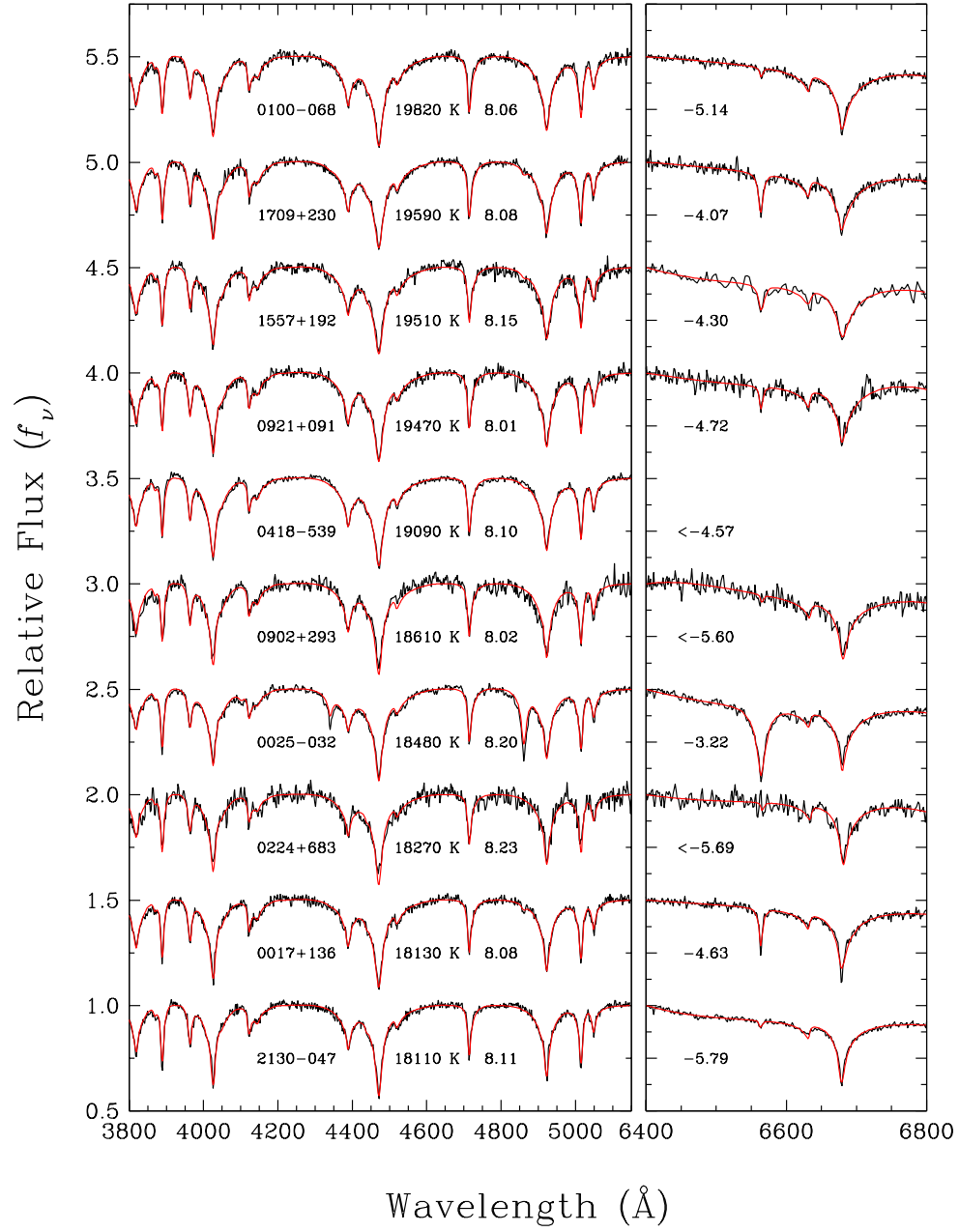


Fig. 18.— (Continued)

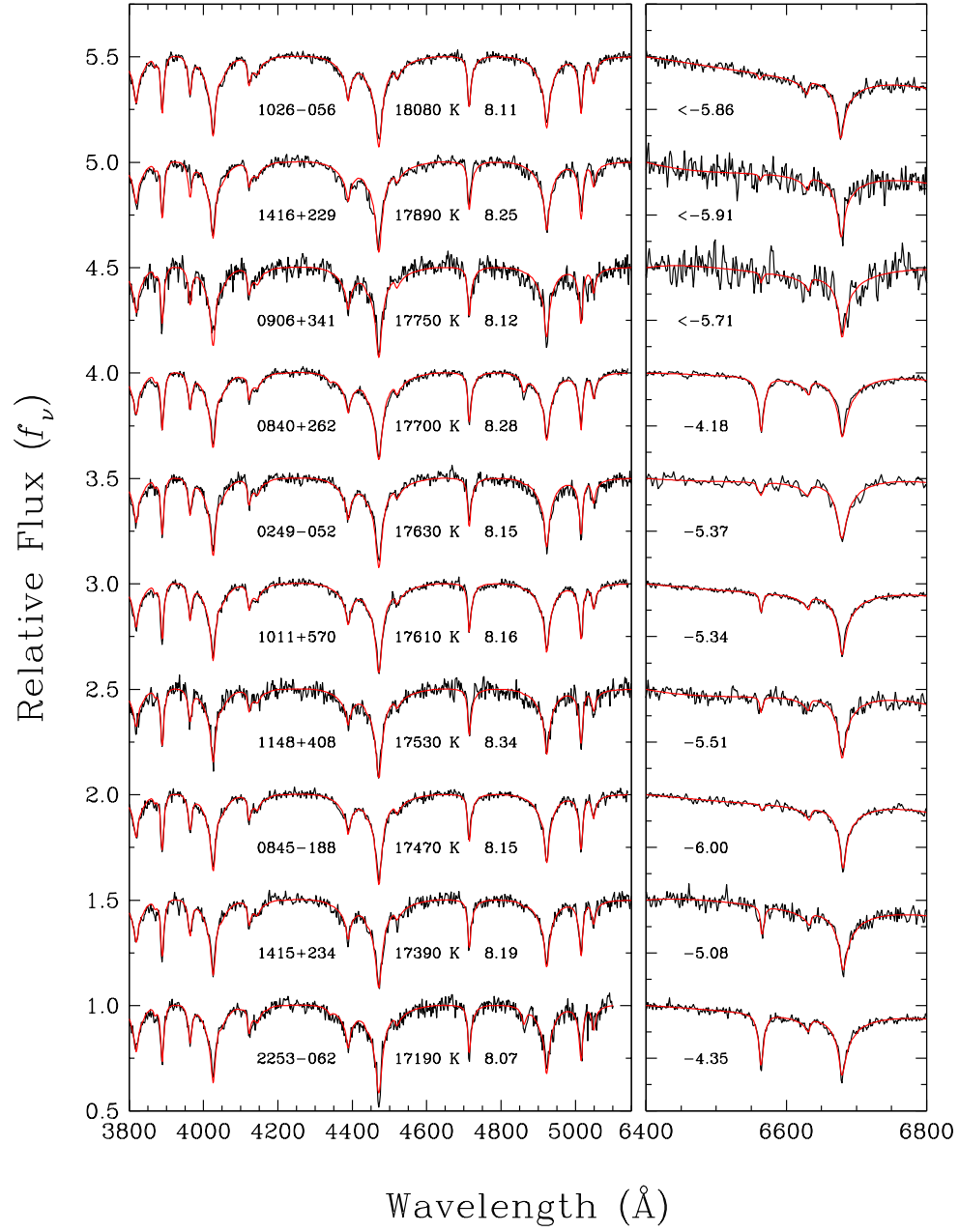


Fig. 18.— (Continued)

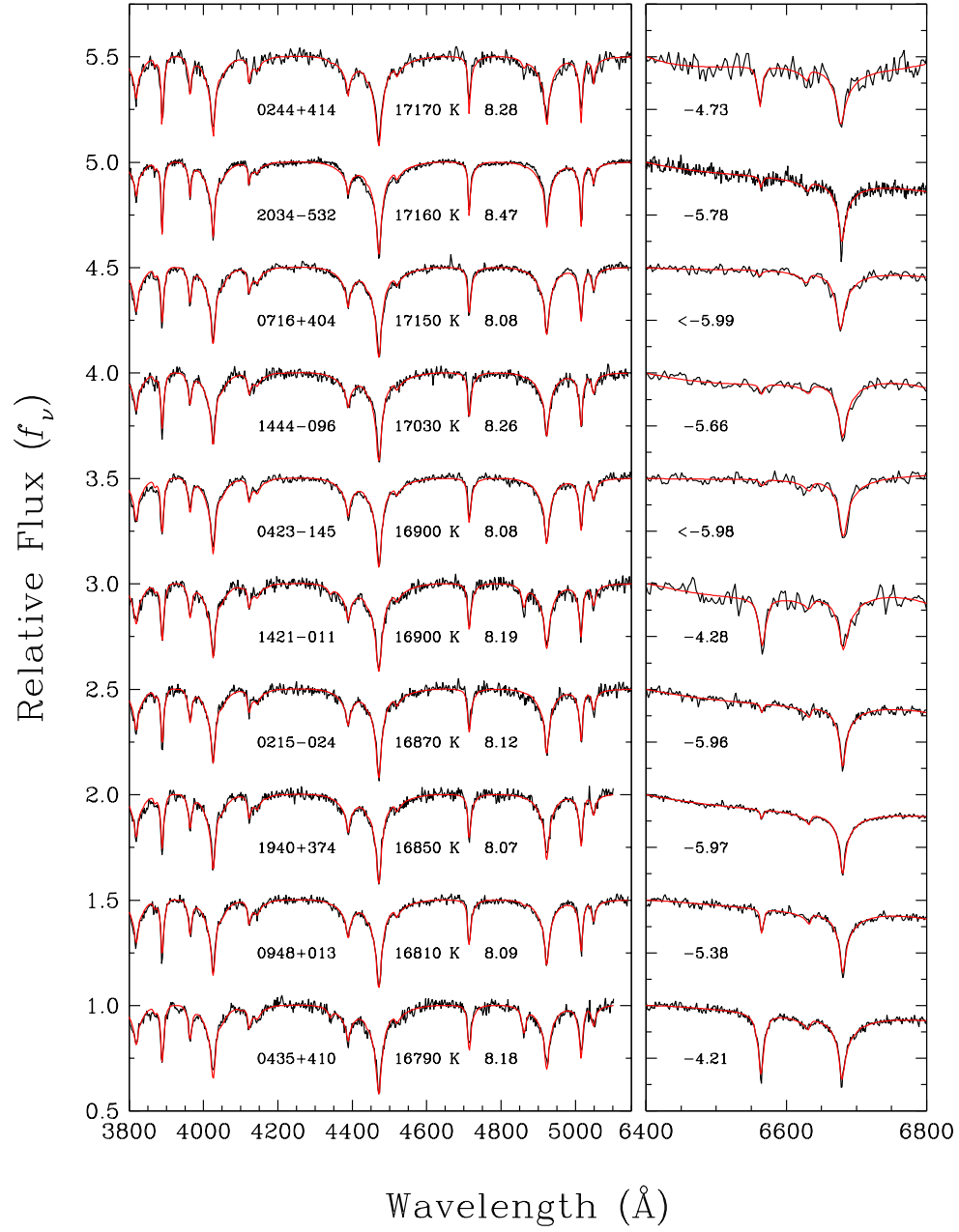


Fig. 18.— (Continued)

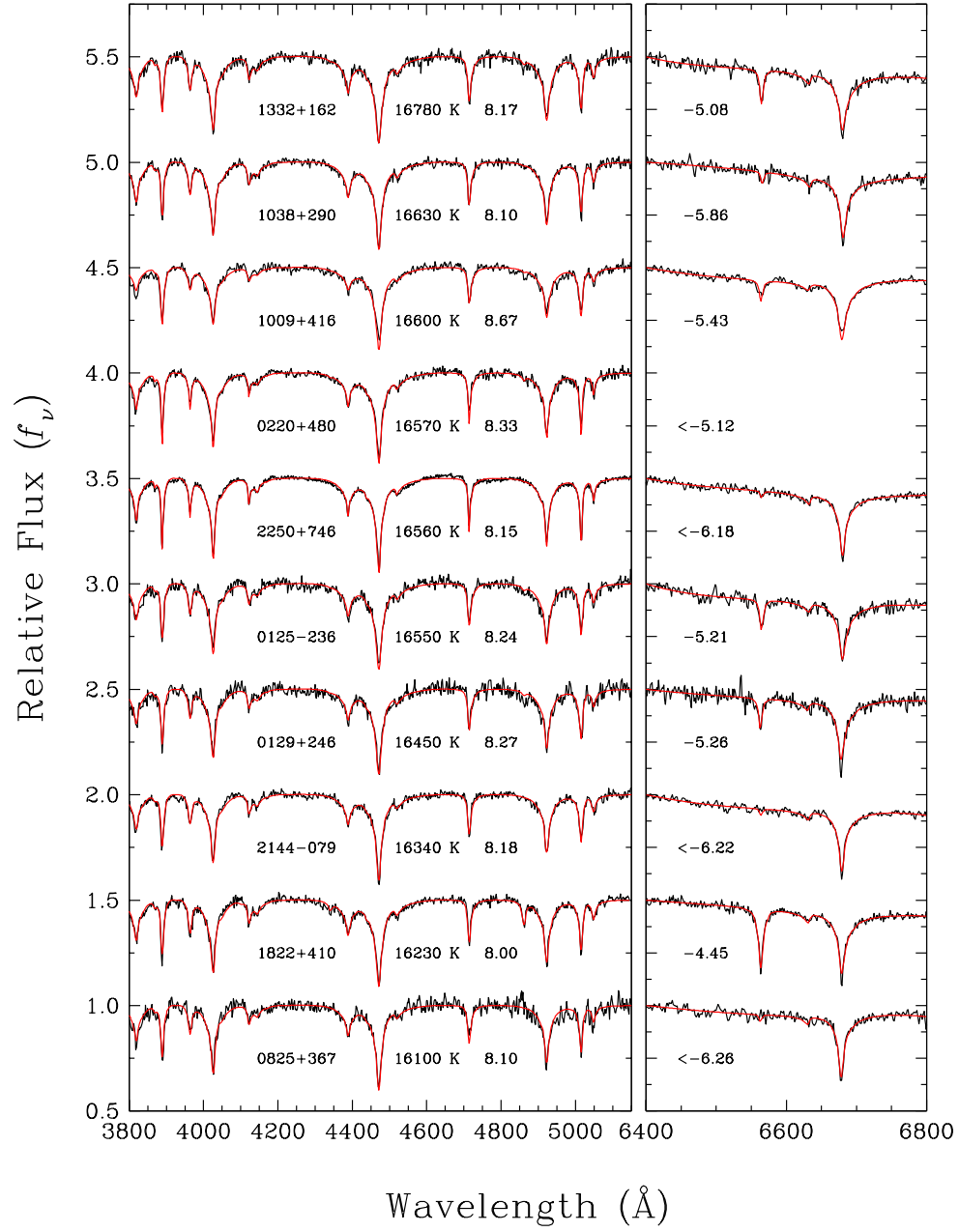


Fig. 18.— (Continued)

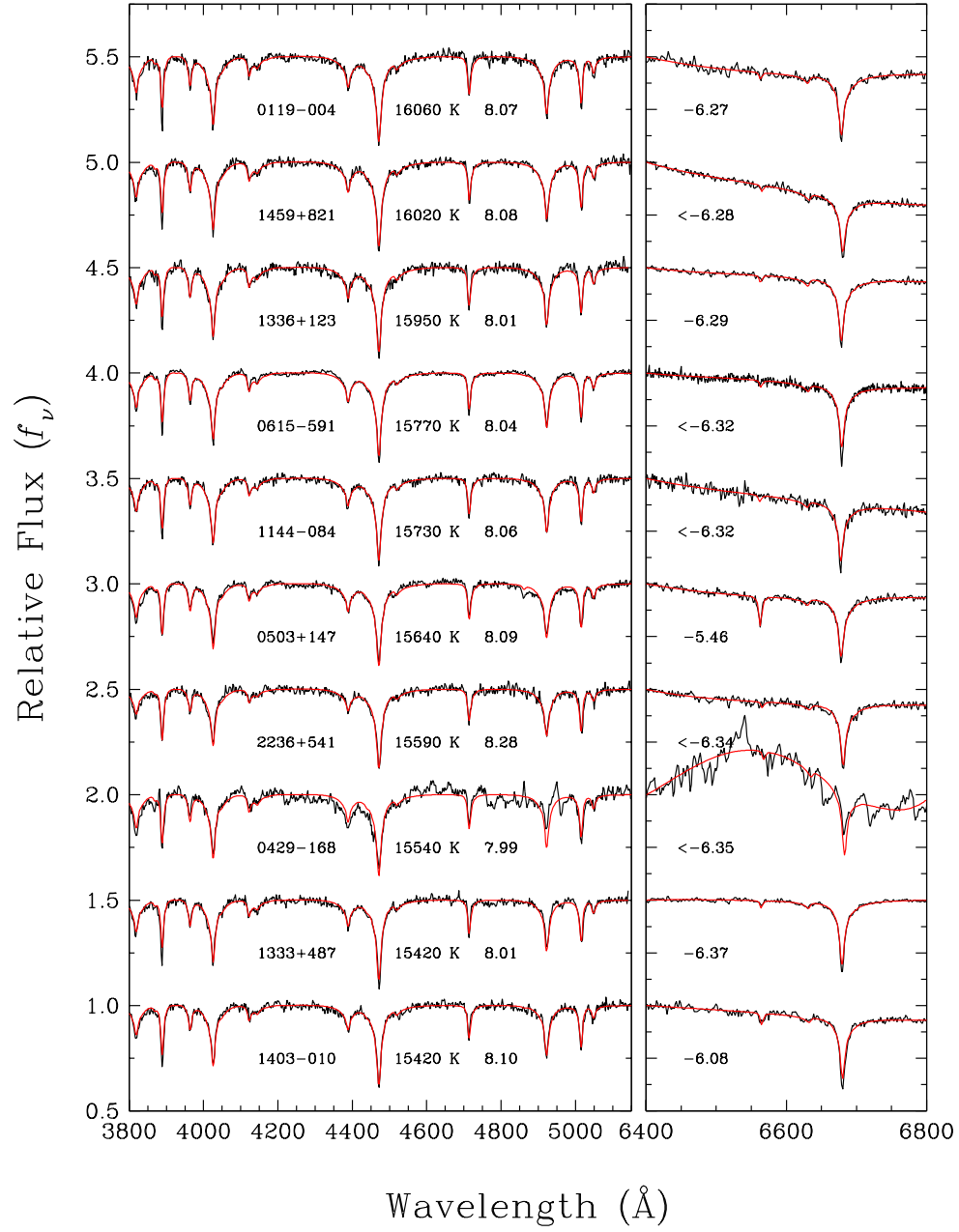


Fig. 18.— (Continued)

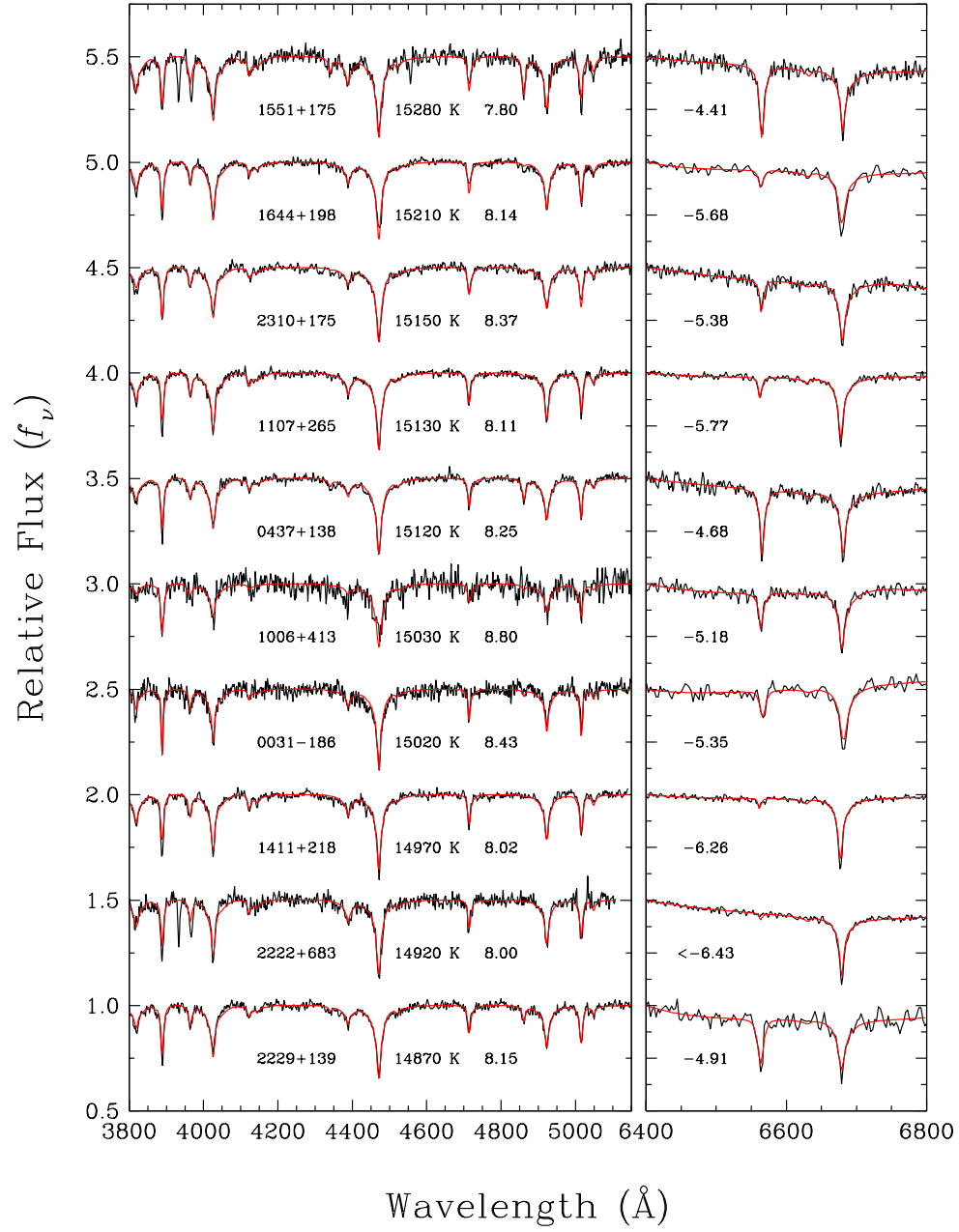


Fig. 18.— (Continued)

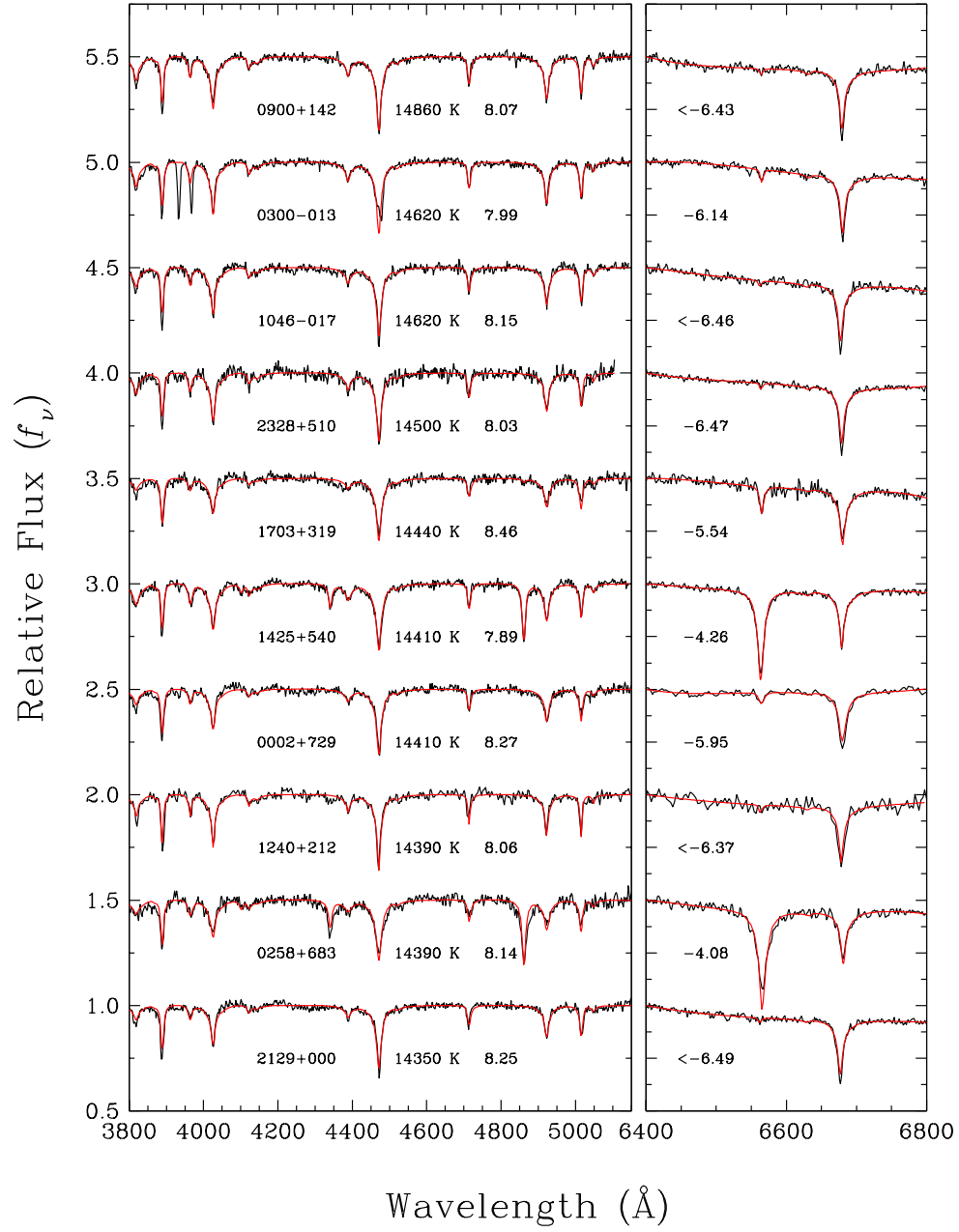


Fig. 18.— (Continued)

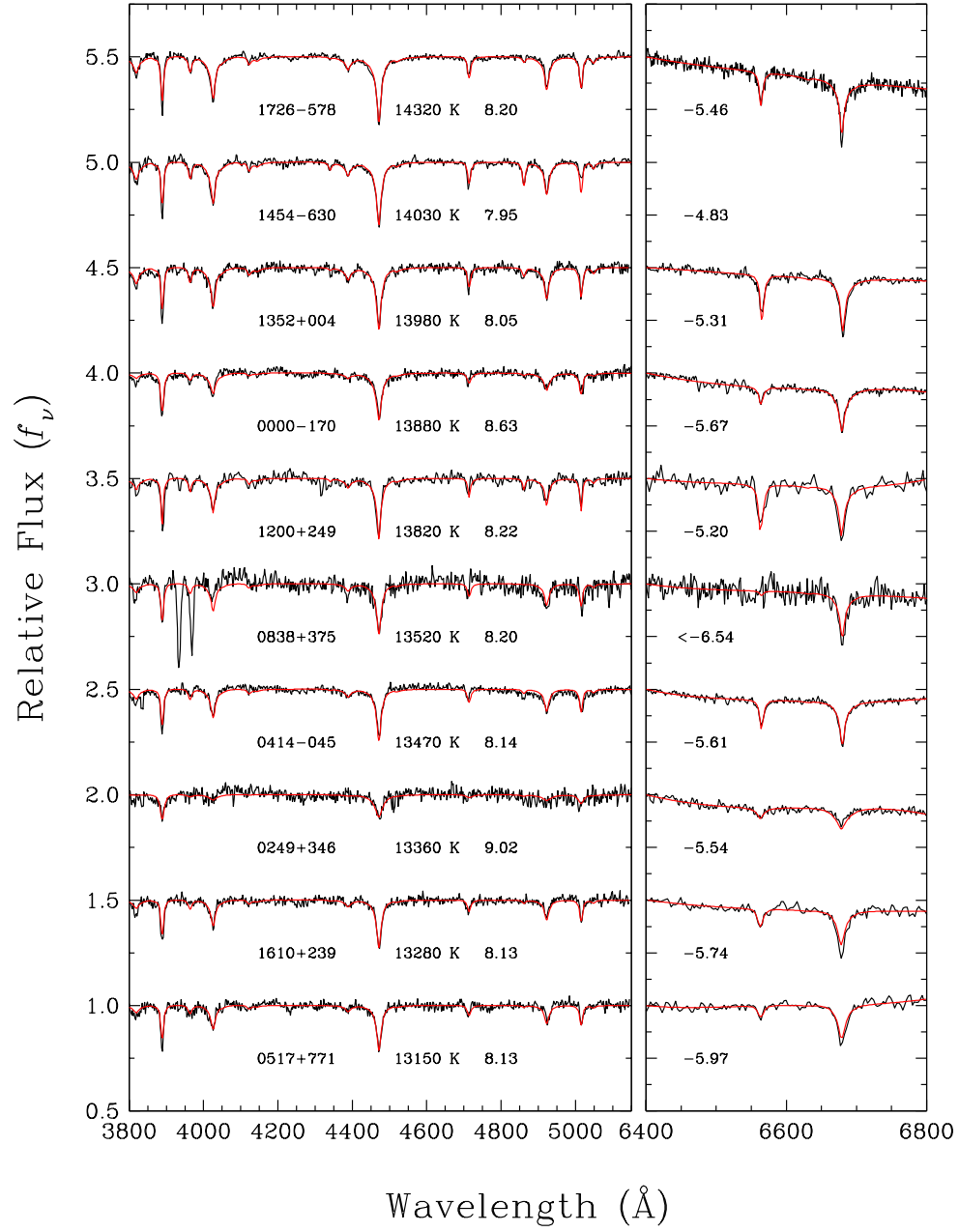


Fig. 18.— (Continued)

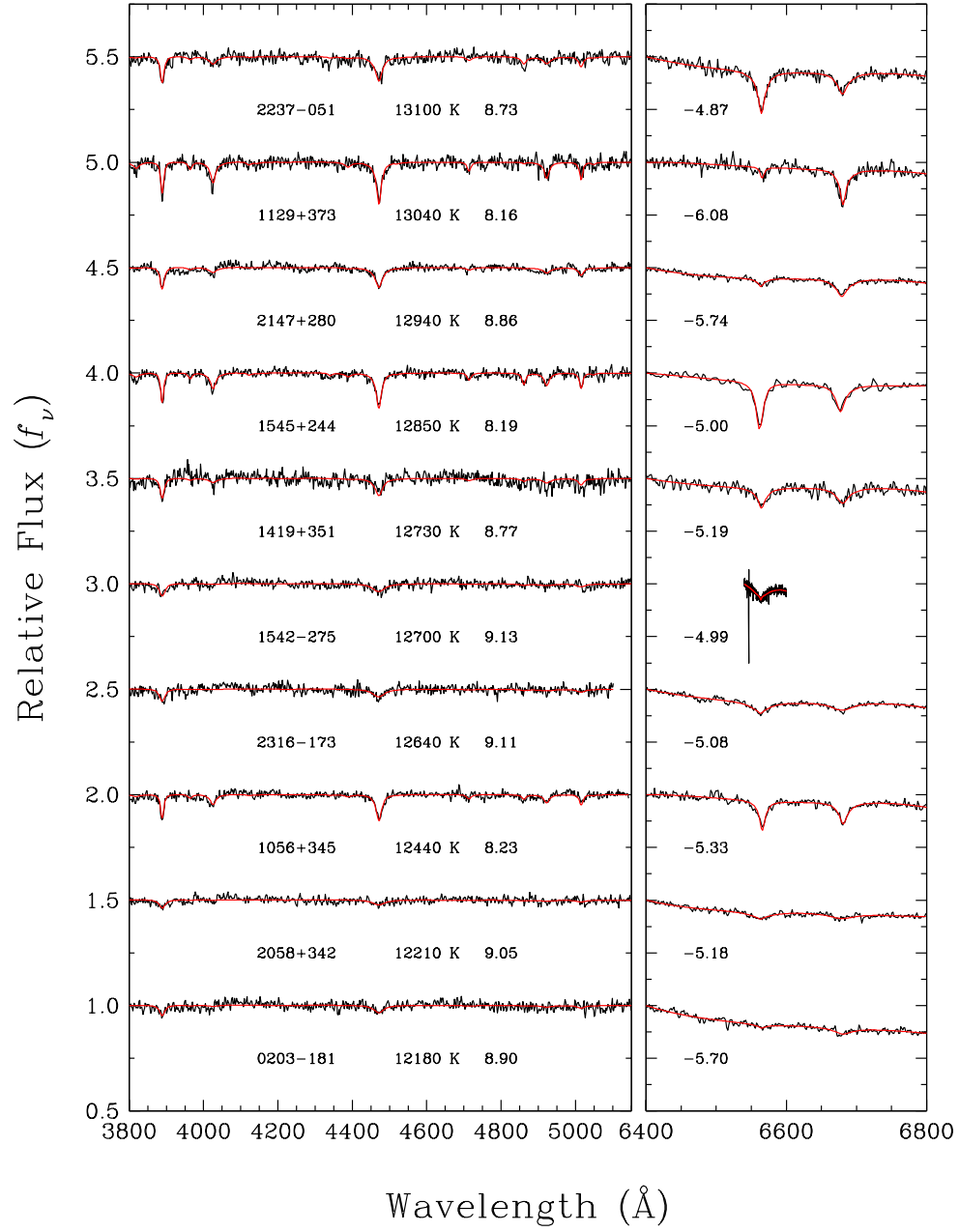


Fig. 18.— (Continued)